

University of Alberta

Comparison of Disinfection Effects of UV Light at 172, 222, 254 nm on *Bacillus subtilis* Spores

by

DING WANG



A thesis submitted to the Faculty of Graduate Studies and Research
in partial fulfillment of the requirements for the degree of

Master of Science

in

Environmental Engineering

Department of Civil and Environmental Engineering

Edmonton, Alberta

Fall 2008



Library and
Archives Canada

Bibliothèque et
Archives Canada

Published Heritage
Branch

Direction du
Patrimoine de l'édition

395 Wellington Street
Ottawa ON K1A 0N4
Canada

395, rue Wellington
Ottawa ON K1A 0N4
Canada

Your file Votre référence
ISBN: 978-0-494-47436-5
Our file Notre référence
ISBN: 978-0-494-47436-5

NOTICE:

The author has granted a non-exclusive license allowing Library and Archives Canada to reproduce, publish, archive, preserve, conserve, communicate to the public by telecommunication or on the Internet, loan, distribute and sell theses worldwide, for commercial or non-commercial purposes, in microform, paper, electronic and/or any other formats.

The author retains copyright ownership and moral rights in this thesis. Neither the thesis nor substantial extracts from it may be printed or otherwise reproduced without the author's permission.

AVIS:

L'auteur a accordé une licence non exclusive permettant à la Bibliothèque et Archives Canada de reproduire, publier, archiver, sauvegarder, conserver, transmettre au public par télécommunication ou par l'Internet, prêter, distribuer et vendre des thèses partout dans le monde, à des fins commerciales ou autres, sur support microforme, papier, électronique et/ou autres formats.

L'auteur conserve la propriété du droit d'auteur et des droits moraux qui protègent cette thèse. Ni la thèse ni des extraits substantiels de celle-ci ne doivent être imprimés ou autrement reproduits sans son autorisation.

In compliance with the Canadian Privacy Act some supporting forms may have been removed from this thesis.

Conformément à la loi canadienne sur la protection de la vie privée, quelques formulaires secondaires ont été enlevés de cette thèse.

While these forms may be included in the document page count, their removal does not represent any loss of content from the thesis.

Bien que ces formulaires aient inclus dans la pagination, il n'y aura aucun contenu manquant.


Canada

DEDICATION

This work is dedicated to my dearest parents, girlfriend and relatives

ABSTRACT

The efficacy of ultraviolet (UV) disinfection at wavelengths of 172, 222 and 254 nm of *Bacillus subtilis* spores was evaluated. A Xe₂^{*} excilamp, a KrCl^{*} excilamp and a low-pressure mercury lamp were used as the UV light sources at these three wavelengths, respectively. The first-order inactivation rate constants at 172, 222 and 254 nm were 0.0022, 0.122, 0.069 cm² mJ⁻¹, respectively, and, therefore, the 2 log reduction of *B. subtilis* spores required fluences of 909, 21.6, and 40.4 mJ cm⁻² at the above respective wavelengths. This means that UV exposure at 172 nm is much less efficient than the exposures at the other two wavelengths for the inactivation of *B. subtilis* spores, while UV exposure at 222 nm is more efficient than that at 254 nm. The results suggest possible applications of Xe₂^{*} and KrCl^{*} excilamps to microorganism disinfection.

ACKNOWLEDGEMENT

I would like to express my sincere gratitude to my supervisor Dr. James R. Bolton for his invaluable suggestion and directions for my research program. He is a very nice and warm-hearted professor, who usually answers my questions very patiently and gave many valuable recommendations about my thesis. Also, I'm very grateful for his continuous encouragement and support.

I extremely appreciate Dr. Mohamed Gamal El-Din who provided me with the equipment for my research and the financial support for the maintenance of GC and the orders for materials. At the same time, I would like to thank Dr. Thomas Oppenländer who greatly helped me for the experiments of my research and the writing of my thesis.

Furthermore, I would like to acknowledge Ms. Maria Demeter, Ms. Jody Yu and Ms. Jela Burkus, because of their tireless technical assistance for my lab work.

Finally, I would like to give my gratitude to my student fellows for their help and friendship.

TABLE OF CONTENTS

CHAPTER 1 INTRODUCTION	1
1.1 Background	1
1.2 Research Objectives	5
1.3 Organization of the Thesis	6
CHAPTER 2 LITERATURE REVIEW	7
2.1 Introduction to Ultraviolet (UV) Disinfection	7
2.1.1 Basic Concepts and Terminology of UV Technology	7
2.1.2 Measurement of UV Light	10
2.1.3 UV Inactivation or Disinfection	16
2.1.4 Sources of UV Light	22
2.2 Advanced Oxidation Processes (AOPs).....	28
2.2.1 Theory of Advanced Oxidation Processes (AOPs).....	28
2.2.2 Inactivation of Microorganisms Using Advanced Oxidation	30
2.3 Vacuum-ultraviolet (VUV) Photolysis of Aqueous System	32
2.3.1 VUV-induced Photochemistry	32
2.3.2 VUV photolysis of Oxygen and Organic Compounds.....	33
2.3.3 VUV-induced Photolysis of Liquid Water.....	34
2.3.4 VUV-induced Organic Compounds Removal in Aqueous Solution.....	35
2.4 Conclusions	38

CHAPTER 3 FLUENCE DETERMINATION OF THE XENON EXCILAMP AT 172

NM USING METHANOL AS AN ACTINOMETER.....	40
3.1 Introduction	40
3.2 Materials and Methods.....	43
3.2.1 Xe ₂ * Excilamp	43
3.2.2 Special Collimated Beam Apparatus for the Xe ₂ * Excilamp	44
3.2.3 Reagents and Deionized Water	49
3.2.4 Sample Preparation	49
3.2.5 UV Exposure Experiments.....	51
3.2.5 Sample Analyses	54
3.2.6 Calculation of Fluence Rate (Irradiance) at 172 nm	57
3.3 Results and Discussion.....	61
3.3.1 Kinetics of Rhodamine B Degradation in VUV-irradiated Solutions.....	61
3.3.2 Determination of a Methanol Calibration Curve for GC Analyses.....	66
3.3.3 Kinetics of Methanol Degradation in VUV-irradiated Solutions.....	68
3.4 Conclusions	73

CHAPTER 4 DISINFECTION EFFECT OF VACUUM-ULTRAVIOLET

(VUV)-INITIATED TREATMENT ON <i>BACILLUS SUBTILIS</i> SPORES IN AQUEOUS SUSPENSION	75
4.1 Introduction	75
4.2 Materials and Methods	77

4.2.1 <i>Bacillus subtilis</i> Methods	77
4.2.2 VUV Exposure Experiments	78
4.2.3 The Fluence Determination with VUV Light	79
4.2.4 Inactivation Kinetics	79
4.3 Results and Discussion.....	81
4.3.1 Fluence-response Curve of <i>B. subtilis</i> Spores using VUV Light.....	81
4.3.2 The Mechanisms of VUV Disinfection.....	82
4.3.3 Comparison of Disinfection Effect of VUV-induced AOP with Other AOPs	86
4.3.3 Comparison of Disinfection Effect of AOPs with Other Disinfection Methods.....	89
4.4 Conclusions	90
CHAPTER 5 DISINFECTION EFFECTS OF 254 NM AND 222 NM UV LIGHT ON <i>BACILLUS SUBTILIS</i> SPORES IN AQUEOUS SUSPENSION	
5.1 Introduction	92
5.2 Materials and Methods	94
5.2.1 UV Lamps and Collimated Beam Apparatus.....	94
5.2.2 The Fluence Determination at the wavelengths of 254 nm and 222 nm....	96
5.2.3 UV Exposure Experiments.....	98
5.2.4 Inactivation Kinetics	99
5.3 Results and Discussion.....	99

5.3.1 Fluence-response Curves of <i>B. subtilis</i> Spores at 254 nm and 222 nm	99
5.3.2 Shoulder and Tailing Regions in the Fluence-response Curves.....	101
5.3.3 Comparison of Inactivation Kinetics at 254 nm with Other Research Papers	103
5.3.4 Comparison of Disinfection Effects of UV Light at 254 nm, 222 nm and 172 nm.....	106
5.3.5 The Mechanisms of UVC Disinfection of <i>B. subtilis</i> Spores.....	107
5.4 Conclusions	111
CHAPTER 6 GENEAL CONCLUSIONS AND RECOMMENDATIONS	114
6.1 General Conclusions	114
6.2 Recommendations	116
REFERENCES.....	119
APPENDIX A DETAILED EXPERIMENTAL METHODS.....	139
Appendix A-1 <i>Bacillus subtilis</i> Spore Production, Purification and Enumeration..	139
APPENDIX B RAW DATA AND CALCULATIONS.....	143
Appendix B-1 Raw Data and Relative Calculations of Exposure Experiments on Rhodamine B Solutions and Methanol Solutions	143
Appendix B-2 CFU Enumeration of <i>Bacillus subtilis</i> Spores.....	162

LIST OF TABLES

Table 2.1 Emission wavelengths of excilamps.....	26
Table 4.1 Logs inactivation of microorganisms by AOPs reported by published papers .	87
Table 4.2 Disinfection doses of different disinfection processes required by 2 log inactivation of <i>B. subtilis</i> spores	89
Table 5.1 Calibration data of the detector	97
Table 5.2 Fluence required per log inactivation of <i>B. subtilis</i> spores at 254 nm	104
Table 5.3 The first-order inactivation rate constants of <i>B. subtilis</i> spores at different wavelengths determined in this research.....	106
Table B.1 Raw data and calculations for the exposure experiments on Rhodamine B solutions in the first collimated beam apparatus	143
Table B.2 Raw data and calculations for the exposure experiments on Rhodamine B solutions in the second collimated beam apparatus	146
Table B.3 Raw data and calculations for the calibration curves of methanol solutions used for GC analyses	147
Table B.4 Raw data and calculations for the concentrations of methanol solutions exposed to the VUV light.....	151
Table B.5 Calculations for the rate of methanol degradation versus UV exposure time	159
Table B.6 CFU enumeration of <i>B. subtilis</i> spores exposed to the VUV light at 172 nm .	162
Table B.7 CFU enumeration of <i>B. subtilis</i> spores exposed to the UV light at 254 nm...	164

Table B.8 Calculations of non-linear least-square regression for disinfection data at 254
nm..... 165

Table B.9 CFU enumeration of *B. subtilis* spores exposed to the UV light at 222 nm... 166

Table B.10 Calculations of non-linear least-square regression for disinfection data at 222
nm..... 167

LIST OF FIGURES

Figure 2.1 Schematic of a collimated beam apparatus.....	11
Figure 2.2 Absorption spectra of DNA and water.....	20
Figure 2.3 Photochemical dimerization of two thymine bases	21
Figure 3.1 Emission spectrum of a Xe ₂ * excilamp.....	41
Figure 3.2 View of the Xe ₂ * excilamp.....	44
Figure 3.3 The first collimated beam apparatus for the Xe ₂ * excilamp	46
Figure 3.4 The second collimated beam apparatus for Xe ₂ * excilamp.....	48
Figure 3.5 Sampling port with sample containers.....	49
Figure 3.6 Concentration changes of Rhodamine B solutions induced by the Xe ₂ * excilamp housed in the first collimated beam apparatus	62
Figure 3.7 Concentration changes of Rhodamine B solutions induced by the Xe ₂ * excilamp housed in the second collimated beam apparatus.....	65
Figure 3.8 The calibration curves for the GC internal standard method.....	67
Figure 3.9 Concentration changes of treated methanol solutions as a function of VUV exposure time at 172 nm	70
Figure 4.1 Fluence-response curves of <i>B. subtilis</i> spores with VUV light at 172 nm	82
Figure 5.1 Typical light emission spectrum of a KrCl* excilamp	94
Figure 5.2 View of the collimated beam apparatus.....	95
Figure 5.3 KrCl* excilamp	96

Figure 5.4 Fluence-response curve of *B. subtilis* spores with UV light at 254 nm..... 100

Figure 5.5 Fluence-response curve of *B. subtilis* spores with UV light at 222 nm..... 101

LIST OF ABBREVIATIONS

6-4PPs	Pyrimidine-(6-4)-pyrimidone photoproducts
AOPs	Advanced Oxidation Processes
ATCC	American Type Culture Collection
BPA	Bisphenol A
CD	Capacitive discharge
CFU	Colony forming units
CPDs	Cyclobutane-type pyrimidine dimers
DBD	Dielectric barrier discharge
DBPs	Disinfection by-products
DF	Divergence Factor
DI	Deionized
DO	Dissolved oxygen
DPA	Dipicolinic acid
EDCs	Endocrine disrupting compounds
FID	Flame ionization detector
GC	Gas chromatography
HDPE	High density polyethylene
LP	Low-pressure
LPHO	Low pressure high output

LT2ESWTR	Long-Term 2 Enhanced Surface Water Treatment Rule
MeOH	Methanol
MLD	Million gallons per day
MP	Medium-pressure
NER	Nucleotide excision repair
<i>p</i> CBA	<i>para</i> -chlorobenzoic acid
PF	Petri Factor
PRE	Photoreactivation enzyme
RED	Reduction equivalent dose
RF	Reflection Factor
RhB	Rhodamine B
SASP	Small acid-soluble proteins
SD	Surface discharged
SP	Spore photoproduct
TOC	Total organic carbon
USEPA	US Environmental Protection Agency
UV	Ultraviolet
VOCs	Volatile organic compounds
VUV	Vacuum Ultraviolet
WF	Water Factor

CHAPTER 1

INTRODUCTION

1.1 Background

Ultraviolet (UV) light is in the region of the electromagnetic spectrum lying between X-rays and visible light. It is usually divided into four sub-ranges: Vacuum UV (VUV) (100 to 200 nm), UVC (200 to 280 nm), UVB (280 to 315 nm) and UVA (315 to 400 nm) (Bolton, 2001).

Photons in the VUV region are absorbed by almost all substances including water and oxygen (Bolton, 2001). VUV-initiated photolysis of water is one of the Advanced Oxidation Processes (AOPs) to generate hydroxyl radicals ($\bullet\text{OH}$) in aqueous solution. This process has an advantage over other AOPs, since no addition of any chemical additives is required (Oppenländer *et al.*, 2005). Relying on non-specific reactions between hydroxyl radicals and target compounds at high reaction rates, AOPs are usually used to destroy refractory contaminants that cannot be oxidized by conventional oxidants, such as oxygen, chlorine or ozone, in water and wastewater treatment (Gültekin and Ince, 2007; Tchobanoglous *et al.*, 2003).

UVC is absorbed by some cellular components, such as proteins and nucleotides (DNA and RNA) of microorganisms, and leads to cell mutations, cancer and/or cell death.

Therefore UVC is used for disinfection in water and wastewater treatment (Bolton, 2001; Bolton and Linden, 2003; Hijnen *et al.*, 2006). In particular, in recent years the use of UV light for the disinfection of water and wastewater has become more and more important.

The reasons are as follows:

- (1) The conventional chemical water disinfection processes, such as chlorination and ozonation, usually generate disinfection by-products, which are toxic, mutagenic and/or carcinogenic to human health (Benabbou *et al.*, 2007; Jung *et al.*, 2008; Koivunen and Heinonen-Tanski, 2005). In contrast, with UV disinfection, no chemicals are added and no disinfection by-products (DBPs) or other chemical residues are generated (Betancourt and Rose, 2004).
- (2) UV disinfection was discovered to be highly efficient against *Cryptosporidium parvum* oocysts and *Giardia lamblia* cysts about ten years ago, in contrast to earlier research that incorrectly reported that UV light was inefficient in treating these two protozoan parasites (USEPA, 1996).
- (3) US Environmental Protection Agency (USEPA) issued the final form of Long-Term 2 Enhanced Surface Water Treatment Rule (LT2ESWTR) in January, 2006, designed to control *Cryptosporidium* and other microbial pathogens in drinking water for the enhanced protection of human health. The UV disinfection process was therefore given considerable encouragement.

Low-pressure (LP) mercury lamps, which generate primarily monochromatic UV light at 253.7 nm, are used most commonly to inactivate pathogens in water and

wastewater. A LP UV lamp is usually called a germicidal lamp, since its principal emission at 253.7 nm is close to the maximum of the DNA absorption wavelength at 260 nm (Bolton, 2001).

The disinfection of microorganisms by 254 nm UV light is primarily caused by the photoreaction of DNA, because the absorption of DNA at this wavelength is much higher than that of other cellular components. Pyrimidine dimers are the major photoproducts in UV-irradiated DNA of cells (Bolton, 2001). However, in *Bacillus subtilis* spores, which are derived from their vegetative cells, a species of aerobic and facultative Gram-positive bacteria with a rod shape, a novel photoproduct termed the spore photoproduct (SP) is formed. The formation of SP is the reason that spores are more resistant to UV light than the corresponding vegetative cells (Setlow, 2001).

Dielectric barrier discharge excilamps are a relatively new type of UV lamp with emission wavelengths ranging from the UV region (200 – 400 nm) to the VUV region (100 – 200 nm). A Xe₂^{*} and a KrCl^{*} excilamps with the emission maxima at 172 nm and 222 nm, respectively, were used in this research to evaluate the disinfection effects on *B. subtilis* spores at these wavelengths. These two lamps are considered to be essentially monochromatic lamps, since the half-widths of their emission bands are very narrow (Boyd and Zhang, 1997; Gellert and Kogelschatz, 1991; Sosnin *et al.*, 2006).

The disinfection effect of 172 nm VUV light derives from the oxidation of cell structures by hydroxyl radicals generated from the VUV-initiated photolysis of water. Therefore, the mechanism of disinfection by VUV light is very different from that by

UVC light (Mamane *et al.*, 2007; Rincón and Pulgarin, 2004). Although some studies have evaluated the disinfection effects of several AOPs, such as TiO₂/UV, UV/H₂O₂ and UV/O₃, the disinfection effect of VUV-initiated treatment on microorganisms in aqueous suspension has not been evaluated quantitatively.

The efficiency of UV disinfection of *B. subtilis* spores at 222 nm is probably not smaller than that at 254 nm, even though the absorption coefficient of DNA decreases at the wavelengths from 254 nm to 222 nm (Chen, 2007). This is because pyridine-2,6-dicarboxylic acid or dipicolinic acid (DPA) in the spore core appear to play the role of a photosensitizer in photochemical reactions of spore DNA. DPA can transfer triplet state energy derived from UV absorption to thymine bases in DNA (Douki *et al.*, 2005). The absorption coefficient of DPA at 222 nm is over twice that at 254 nm (Miller and Senkfor, 1982). Therefore, more photon flux at 222 nm than that at 254 nm is probably transferred from DPA to DNA.

Radiometry is a common method, by which a radiometer with a UV sensor is used to determine the fluence rate or irradiance in a collimated beam apparatus (Bolton, 2001; Bolton and Linden, 2003). However, a regular radiometer cannot be used for the determination of the fluence rate at 172 nm, since the sensor available has almost no sensitivity below 200 nm. Oppenländer and Schwarzwälder (2002) used an actinometry method, in which methanol was utilized as an actinometer in aqueous solution to determine the fluence rate at this wavelength.

1.2 Research Objectives

A LP UV lamp with an emission maximum at 253.7 nm is commonly studied and used in UV disinfection processes. However, fewer studies have focused on the disinfection effect of excilamps, which also emit narrow wavelength bands, but not at 253.7 nm. In addition, the mechanisms of UV disinfection at 172 and 222 nm UV light emitted by Xe_2^* and KrCl^* excilamps, respectively, probably differ from that at 254 nm. As a result, disinfection effects at these wavelengths, compared with 254 nm, are not clear. Therefore, this research was concentrated on a comparison of the disinfection effects of UV light at 172, 222 and 254 nm, using the same batch of *B. subtilis* spores in aqueous suspension. Specifically, the objectives of this research were:

- (1) to determine the fluence rate (irradiance) of 172 nm light emitted by a Xe_2^* excilamp in a collimated beam apparatus using an actinometry method;
- (2) to evaluate quantitatively the disinfection effect of VUV light at 172 nm on *B. subtilis* spores in aqueous suspension;
- (3) to evaluate quantitatively the disinfection effect of 222 nm UV light emitted by a KrCl^* excilamp on the same batch of *B. subtilis* spores in aqueous suspension;
- (4) to evaluate quantitatively the disinfection effect of 254 nm UV light emitted by a LP UV lamp on the same batch of *B. subtilis* spores in aqueous suspension;

- (5) to compare the disinfection effects at these three wavelengths;
- (6) to speculate on the probable disinfection mechanisms with UV light at 172 nm and 222 nm.

1.3 Organization of the Thesis

This thesis is organized into six chapters. Chapter 1 presents the general background of the UV disinfection process and the mechanisms. At the same time, it briefly proposes the research problems and study objectives. Chapter 2 reviews the literature related to this research. Chapter 3 describes the actinometry method and the results to determine the fluence rate (irradiance) at 172 nm. Chapter 4 describes the disinfection results of *B. subtilis* spores exposed to 172 nm VUV light, and discusses the probable disinfection mechanisms. Chapter 5 is similar to Chapter 4, but relates to the wavelengths of 222 nm and 254 nm. Chapter 6 summarizes the discussions in previous chapters, and proposes recommendations for future studies.

CHAPTER 2

LITERATURE REVIEW

2.1 Introduction to Ultraviolet (UV) Disinfection

2.1.1 Basic Concepts and Terminology of UV Technology

UV light spans the wavelength range from 100 to 400 nm and lies between the X-ray and visible regions. It is usually divided into four sub-ranges: Vacuum Ultraviolet (VUV) (100 – 200 nm), UVC (200 – 280 nm), UVB (280 – 315 nm) and UVA (315 – 400 nm) (Bolton, 2001; Chen, 2007; Hargreaves *et al.*, 2007; Moore and Ferreira, 2006).

VUV is absorbed by almost all substances including water and oxygen in the air, which means that it can be only transmitted in a vacuum (Bolton, 2001). However, the long wavelength part of the VUV light ($\lambda > 160$ nm) can be utilized by applying transparent media, for example synthetic quartz material (SUPRASIL[®]) or nitrogen or argon atmosphere.

UVC is absorbed by some cellular components, such as proteins and nucleotides (DNA and RNA), and therefore can lead to cell mutations, cancer and/or cell death. The UVC range is sometimes called the germicidal range because it is highly effective in inactivating bacteria and viruses; hence, it is used for disinfection in water and wastewater treatment (Bolton, 2001; Bolton and Linden, 2003; Hijnen *et al.*, 2006).

UVB light can cause sun burning and eventually induce skin cancer, since it can be

directly absorbed by DNA (Geng *et al.*, 2008; Cadet *et al.*, 2005). It has been reported that human skin cancers, especially basal and squamous carcinomas, are closely related to the UV component of sunlight with wavelengths less than 320 nm (Setlow, 1974). UVB also influences the expression of genes in plants (Kalbin *et al.*, 2005).

UVA leads to sun tanning, and it is far less photobiologically active (Bolton, 2001; Moore and Ferreira, 2006). The stratospheric ozone layer in the atmosphere absorbs almost all the UVC light and most of the UVB; therefore, the exposure of living cells to sunlight in the outdoor environment includes 95% of UVA and 5% of UVB light (Hargreaves *et al.*, 2007; Moore and Ferreira, 2006).

There are some important and easily confused concepts that apply to photochemical studies, and were introduced and discussed clearly in Bolton (2000, 2001), Bolton and Stefan (2002) and Bolton and Linden (2003).

Irradiance (symbol E ; units W m^{-2}) is defined as the total radiant power incident from all upward directions on an infinitesimal element of surface of area dA containing the point under consideration divided by dA . The *irradiance* is the appropriate term when the UV light is coming from all directions above the surface irradiated by the UV source. In addition, the units mW cm^{-2} ($= 10 \text{ W m}^{-2}$) are often (in North America) used in the place of W m^{-2} .

Fluence rate (symbol E_0 ; units W m^{-2}) is defined as the total radiant power incident from all directions onto an infinitesimally small sphere of cross-sectional area dA , divided by dA . The *fluence rate* is the appropriate term when an entity, such as a microorganism,

is being exposed to UV light coming from many different directions. *Fluence rate* has the same units as *irradiance* (W m^{-2} or mW cm^{-2}). Also, the units of $\mu\text{W cm}^{-2}$ are in use as well.

Fluence (symbol F ; units J m^{-2}) (also called UV Dose) is defined as the total radiant energy of all wavelengths passing from all directions through an infinitesimally small sphere of cross-sectional area dA , divided by dA . The units mJ cm^{-2} are also often used for *fluence* (UV dose) in North America. When the *fluence rate* is constant over time, the *fluence* (UV dose) is given by the *fluence rate* times the exposure time (in seconds). For the application of UV light to microorganism reduction, *fluence* is more appropriate than UV dose because the term ‘dose’ is used to describe the total absorbed energy, while *fluence* is related to the ‘incident’ UV energy. In most cases only a small fraction (about 1%) of the radiant energy is absorbed by a microorganism.

Quantum yield (unitless) Φ is defined as the number of moles of product formed or the number of moles of reactant removed (P) per einstein of photons absorbed. One einstein of photons is one mole (6.022×10^{23}) of photons. The *quantum yield* is a measure of the photon efficiency in a given photochemical reaction.

Transmittance (symbol T_λ ; unitless) is defined as the ratio of the transmitted irradiance to the incident irradiance for monochromatic light with a wavelength λ . When the light beam passes through the solution, the light is attenuated because of absorbing substances in the solution and also from the reflection from the suspended particles and the interface between different media.

Absorbance (symbol A_λ ; unitless) is defined as the logarithm to the base 10 of the ratio of the incident irradiance to the irradiance of the transmitted light for the monochromatic light with wavelength λ . Normally absorbance does not include the effect of light scattered by particles suspended in the medium.

Absorption coefficient (symbol a ; units cm^{-1}) is the *absorbance* for a 1 cm path length for the light beam.

2.1.2 Measurement of UV Light

The fluence rate (irradiance) is best determined in a collimated beam apparatus, which is often used at the bench scale to perform the photochemical studies. The UV lamp is placed in the top chamber of the collimated beam apparatus. The beam of UV light passes through a collimating tube and finally impinges on a solution in a Petri dish or other suitable container. Because of the substantial distance between the lamp and the solution exposed, the beam can be considered quasi collimated. A schematic of a collimated beam apparatus is shown in Figure 2.1 (Bolton, 2001; Bolton and Stefan, 2002; Bolton and Linden, 2003). The collimated beam apparatus is always constituted of several important components, including a UV lamp, a shutter, a UV transparent window, a collimating tube (collimator), a power supply system, a fan, and a platform (on which the Petri dish and magnetic stirrer are placed) (Bolton and Stefan, 2002; Bolton and Linden, 2003).

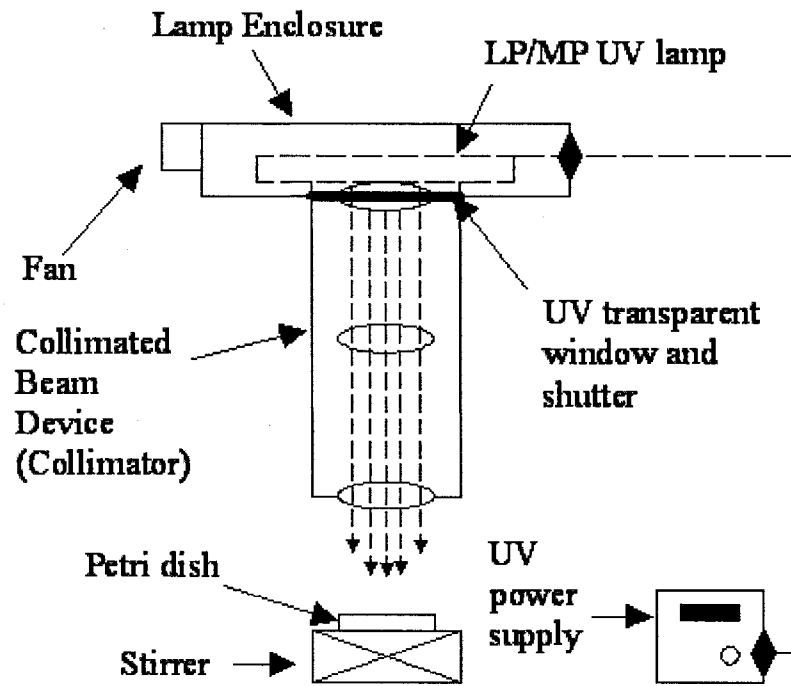


Figure 2.1 Schematic of a collimated beam apparatus

There are several methods to calculate or measure the fluence rate or irradiance:

Mathematical Modeling

Different mathematical models can be used to calculate the fluence rate distribution in a given volume. With the method reported by Blatchley III E.R. (1997), a numerical model termed line source integration was used to calculate the intensity field as a function of collimator geometry. Giese and Darby (2000) used mathematical modeling with a radiometer to determine the fluence rate distribution around a medium-pressure (MP) lamp. Bolton (2000) derived a mathematical model based on the multiple point source summation approximation, which assumes that the emission of a linear lamp is equivalent to n point sources, to calculate the fluence rate distribution and the average

fluence rate in annular reactors. Mathematical modeling was also used to predict the performance of UV reactor in different operational situations (Feng, 2007). Sometimes, it is combined with other methods to calculate the complex distribution of fluence rate in the UV reactor with multiple UV lamps inside (Jin *et al.*, 2005).

Radiometry

Radiometry is a typical method by which a radiometer is used to determine the fluence rate or irradiance in a collimated beam setup (Bolton, 2001; Bolton and Linden, 2003). A radiometer consists of a UV sensor, which produces a tiny current proportional to the incident irradiance, which can be detected by a very sensitive electronic ammeter (Bolton and Linden, 2003). The sensitivity of the detector can decrease due to ageing effects and possible surface damage; therefore, periodic calibration of the detector against a standard is required (Zhang *et al.*, 1999). Chemical actinometry, which is introduced later, can be used for the calibration of detectors (Bolton and Linden, 2003). When using a radiometer to determine the fluence rate (irradiance) in a collimated beam apparatus, there are some corrections to be considered (Bolton and Linden, 2003):

Reflection Factor (RF): When the beam of light passes from one medium to another with a different refractive index, a small fraction of beam is reflected at the interface between the two media. The average refractive indices of water and air in the 200 – 300 nm region are 1.372 and 1.002 respectively. Using the Fresnel Law, the Reflection Factor is 0.975 in the case of the beam of light with wavelengths between 200 and 300 nm passing from air to water.

Petri Factor (PF): The irradiance across the surface area of the irradiated solution in the Petri dish is usually non-uniform. The PF is the ratio of the average incident irradiance over the area of the Petri dish to the incident irradiance at the centre of the Petri dish. The PF should be more than 0.9 in a well designed collimated beam apparatus.

Water Factor (WF): The WF corrects for the attenuation of the incident irradiance because of the absorption of light by components in the water. The mathematical equation to calculate the WF is:

$$[2.1] \quad WF = \frac{1-10^{-al}}{al \ln(10)}$$

where a is the absorption coefficient (cm^{-1}), and l is the vertical path length (cm) of the water in the Petri dish.

Divergence Factor (DF): The DF stems from the imperfectly collimated beam. It is defined as

$$[2.2] \quad DF = \frac{L}{L+l}$$

where L is the distance from the UV lamp to the surface of the solution to be irradiated and l is the depth of the water.

For a monochromatic light source in a collimated beam, the average irradiance [$E(\text{avg})$] is calculated by multiplying the radiometer reading at the centre of the Petri dish (E^0) by the above four corrections, that is

$$[2.3] \quad E(\text{avg}) = E^0 \times \text{RF} \times \text{PF} \times \text{WF} \times \text{DF}$$

The fluence (UV dose) is then calculated as the product of average fluence rate (irradiance) in the water and the exposure time. The detailed procedures to calculate the fluence (UV dose) have been developed by Bolton (2004) in an Excel spreadsheet.

Biodosimetry

Biodosimetry is the most reliable and widely applied method to determine the fluence (UV dose) in a UV reactor (Sommer *et al.*, 1999; Bolton, 2001; Feng, 2007). The method is performed as follows: first, a non-pathogenic surrogate is injected as a challenge microorganism (usually, MS2 coliphage, *Bacillus subtilis* spores or *E. Coli* bacteria) into the influent water of the UV reactor to be tested; second, the influent and effluent are sampled and enumerated from which one can calculate the log inactivation of this surrogate; third, the fluence-response curve of the same microorganism in the same water matrix is determined using a collimated beam apparatus; finally, the corresponding UV dose [called the *reduction equivalent dose* (RED)] for the same log inactivation value is calculated from the fluence-response curve determined by the collimated beam apparatus (Bolton, 2001; Feng, 2007). Although biodosimetry is dependable, it is only used effectively with flow rates less than 80 MLD (million gallons per day), since it is difficult to produce enough microorganisms to utilize in the determination of the UV dose in a larger UV reactor. Furthermore, the microorganisms from the different culture batches have different sensitivity to UV, which will influence the results of UV dose (Mamane-Gravetz and Linden, 2004).

Chemical Actinometry

Chemical actinometry is another method extensively used to measure the fluence (UV dose) (Jin *et al.*, 2006). A chemical actinometer involves a photochemical reactant (inorganic or organic), for which the quantum yield is known accurately. The fluence (UV dose) is determined by following the yield of the actinometer after exposure to UV light (Bolton, 2001; Zhang *et al.*, 1999). Ideally, the quantum yield of the actinometer should be constant regardless of the different concentrations of the actinometer, temperature of solution and the wavelengths of UV over a reasonable range (Zhang *et al.*, 1999). The ferrioxalate actinometer is the most commonly used actinometric standard (Araya-Hernández and Morales, 2006; Goldstein and Rabani, 2008; Zhang *et al.*, 1999). The detailed protocol to measure the fluence using ferrioxalate actinometer is described by Bolton (2006). The disadvantage of the ferrioxalate actinometer is that it needs complex and time-consuming analytical procedures. Hence, a large number of methods in place of it have been proposed (Zhang *et al.*, 1999). The potassium iodide/potassium iodate (KI/KIO₃) actinometer is another choice that can be applied (Jin *et al.*, 2005). The detailed steps of the reaction of iodide ion (I⁻) oxidized to triiodide ion (I₃⁻) have been given by Rahn *et al.* (2002). Bolton and Stefan (2004) presented an experimental protocol to apply the KI/KIO₃ actinometer for fluence measurements. The advantage of the iodide-iodate actinometer is that this actinometer absorbs wavelengths only from 200 – 300 nm, and does not absorb wavelengths above 310 nm. This means that this actinometer can easily be used in room light. In contrast, the ferrioxalate actinometer

must be used in a red light environment, because it has a significant quantum yield at wavelengths up to 500 nm (Bolton, 2001; Bolton and Stefan, 2004; Goldstein and Rabani, 2008; Rahn *et al.*, 2003).

The applications of some other actinometers have also been reported. In the research reported by Zhang *et al.* (1999), an organic chemical 3,4-dimethoxynitrobenzene was used to measure the fluence of 308 nm UV light emitted by a XeCl* excilamp. Oppenländer and Schwarzwälder (2002) applied actinometry with methanol as the actinometer for VUV measurements at 172 nm. Brandi *et al.* (2003) used 1,4-dioxane and phenol as actinometers to measure the fluence at wavelengths of 313 nm and 365 nm, respectively. Jin *et al.* (2006) tried to use the uridine actinometer integrated with the mathematical modeling to estimate the germicidal fluence using MP UV lamps, since uridine has an absorbance spectrum similar to that of microbial DNA. Zhang *et al.* (1996) also proposed uridine could be applied to measure the fluence of a KrCl* excilamp. Feng *et al.* (2007) reported the use of free chlorine (OCI⁻ and HOCl) as an actinometer to validate the performance of a UV reactor.

2.1.3 UV Inactivation or Disinfection

In recent years, the use of UV light for the disinfection of water and wastewater has become an important physical procedure (Koivunen and Heinonen-Tanski, 2005). For example, since the 1980s UV disinfection has been widely used in water treatment plants in Europe (Hijnen *et al.*, 2006), and over 2000 wastewater treatment plants in the world are now using low- or medium pressure UV technology as the disinfection process

(Macauley *et al.*, 2006).

There has been a long history in the use of UV technology in microorganism reduction. The first application of using UV light as the process of disinfection in drinking water treatment was in 1910 in Marseille, France after the invention of the mercury lamp and quartz tubes. Afterwards, interest in UV application decreased since chlorination was introduced. At that time UV disinfection involved high operating costs, low reliability and some maintenance problems. On the other hand, chlorination was a cheaper and more reliable method, and also left a disinfectant residual after treatment (Hijnen *et al.*, 2006). However, over the last several years, the conventional chemical water disinfection processes like chlorination and ozonation have incurred anxiety about disinfection by-products (DBPs). Some of them are toxic, mutagenic and/or carcinogenic such as trihalomethanes and haloacetic acids (Benabbou *et al.*, 2007; Jung *et al.*, 2008; Koivunen and Heinonen-Tanski, 2005). Therefore, the application of UV disinfection has come back into favour, since no chemicals are added and no DBPs or other chemical residues are generated (Betancourt and Rose, 2004). However, considerable breakthrough of UV disinfection arose from two factors: first, the discovery of its high efficacy against *Cryptosporidium parvum* oocysts and *Giardia lamblia* cysts about ten years ago, in contrast to earlier research that incorrectly reported UV light was inefficient to treat these two protozoan parasites and that protozoan (oo)cysts were the most resistant to UV irradiation (USEPA,1996); second, the US Environmental Protection Agency (USEPA) issued the final form of Long-Term 2 Enhanced Surface Water Treatment Rule

(LT2ESWTR) in January, 2006 to control *Cryptosporidium* and other microbial pathogens in drinking water for enhanced protection of human health.

Cryptosporidium is a protozoan parasite that lives and reproduces in one host and causes a gastrointestinal disease called cryptosporidiosis (USEPA, 2006a). It is one of the most resistant microorganisms against chlorination. It was reported that there was no disinfection effect for *Cryptosporidium* even when contacted with high concentrations of chlorine for 18 h (Betancourt and Rose, 2004). However, it is very sensitive to UV irradiation. In fact, protozoa (such as *Cryptosporidium* and *Giardia*) have a similar susceptibility as do bacteria, whereas viruses are the least sensitive (Hijnen *et al.*, 2006). In the report of Kim *et al.* (2002), a 5 log reduction of *Legionella* bacteria was obtained with a UV dose of 30 mJ cm⁻². Craik *et al.* (2000) indicated that two and three log inactivation of *Cryptosporidium parvum* oocysts could be achieved at UV doses of 10 and 25 mJ cm⁻², respectively. Campbell and Wallis (2002) found that a UV dose of 10 mJ cm⁻² at 254 nm could result in a 2 log reduction of *Giardia lamblia* cysts, and 20 mJ cm⁻² achieved between 2 and 3 logs reduction.

The application of UV technology for disinfection does not involve addition of chemicals to the water. As a result, it will neither change the chemical properties of the treated water nor induce UV disinfection by-products. It is much more effective than chlorine in the inactivation of protozoa. However, it has no lasting residual disinfection effect, which means that bacterial growth can occur in drinking water distribution systems (Pozos *et al.*, 2004). In addition, the design and installation of a UV reactor is not

very easy, because the performance of the reactor is dependent on hydraulic distribution of the reactor (Betancourt and Rose, 2004, Tchobanoglous *et al.*, 2003).

UV light is absorbed by DNA, RNA and proteins of microorganisms. The absorption spectrum of DNA in microorganisms peaks at about 260 nm, which is close to 253.7 nm, the principal emission of the low pressure mercury lamp. The absorption spectrum of DNA and of drinking water is illustrated in Figure 2.2. Therefore, it is possible for UV light to be transmitted through an aqueous solution and expose the microorganisms directly to the UV light. Although UV light is absorbed by proteins (below about 230 nm) in the membranes of microorganisms, the inactivation of these proteins does not readily occur, since the quantum yield of this process is about 0.01. Hence, the degradation of membrane proteins, which ultimately induces the disruption of the membranes themselves, requires a much higher fluence (UV dose) than that required to inactivate the DNA (or RNA in some species of viruses) (Bolton, 2001; Setlow, 2002). In the UV range of 230 – 290 nm, DNA (or RNA) has a much higher absorption coefficient than do other cellular components (Kovács *et al.*, 2007). Therefore, the mechanism of UV disinfection of microorganisms is primarily related to the absorption and photoreaction of DNA (Jagger and Setlow, 1964).

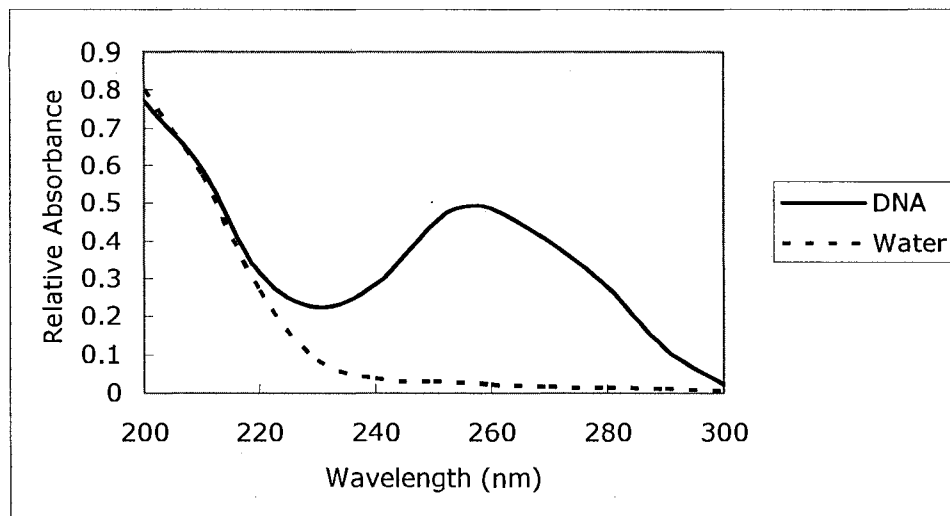


Figure 2.2 Absorption spectra of DNA and water

DNA is a nucleic acid polymer that usually has a double-stranded helix and is stabilized by hydrogen bonds between the bases attached to the two strands. There are four bases found in DNA, adenine (A), cytosine (C), guanine (G) and thymine (T). They form 'base pairs', that is, A with T and C with G. It is reported that the photochemical changes in DNA by UV exposure comprise chain breakage, cross-linking of strands, hydration of the pyrimidines (thymine and cytosine), and formation of dimers between thymine residues in the polynucleotide chains (Setlow and Setlow, 1962). Two major photoproducts in UV-exposed DNA of cells are cyclobutane-type pyrimidine dimers (CPDs) (the quantum yields of purines are much lower than that of pyrimidines) and pyrimidine-(6-4)-pyrimidone photoproducts (6-4PPs) (Douki et al., 2005; Kamiya et al., 1998; LeClerc et al., 1991). The pyrimidine dimers are primarily constituted of thymine-thymine dimers, with small amounts of cytosine-thymine dimers and cytosine-cytosine dimers (Nicholson *et al.*, 1991; Setlow, 1960; Setlow and Setlow, 1987),

since the absorbance of thymine is higher than that of cytosine, and the quantum yield for the formation of thymine dimers is also higher than that for cytosine-thymine dimers and cytosine-cytosine dimers (Giese and Darby, 2000). Thymine dimers form between adjacent thymines in polynucleotide chains. The reaction is illustrated in Figure 2.3 (Bolton, 2001; Siede *et al.*, 2006). The thymine dimers inhibit the ability of DNA to replicate itself, and therefore the microorganism is not able to reproduce (Setlow *et al.*, 1963, Setlow and Carrier, 1964). It was reported that the thymine dimers block DNA replication more strongly than 6-4PPs, whereas the latter is more mutagenic than the former (Kamiya *et al.*, 1998; LeClerc *et al.*, 1991).

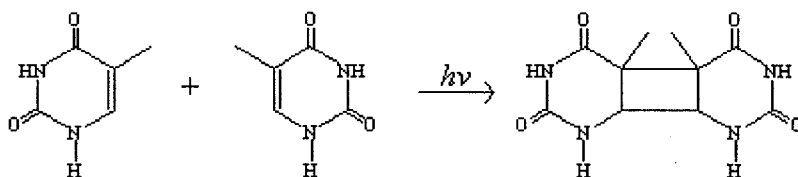


Figure 2.3 Photochemical dimerization of two thymine bases

Some microorganisms have mechanisms to remove or repair the UV-induced DNA lesions in order to restore DNA functionality after exposure to UV. This phenomenon is a potential disadvantage of UV disinfection. Two major pathways of repair are dark repair and photoreactivation.

Dark repair is a multi-enzyme repair process that does not need light and has been discovered in almost all bacteria, with mechanisms including nucleotide excision repair, postreplication recombinational and error-prone repair (Hijnen *et al.*, 2006; Trombert *et al.*, 2007; Zimmer *et al.*, 2003). RecA protein, which is a multifunctional protein involved

in homologous recombination, DNA repair and coordination of cell division, plays an important role in dark repair (Jungfer *et al.*, 2007).

Photoreactivation occurs in presence of UVA and visible light (310 – 480 nm) exposure after DNA damage (Sanz *et al.*, 2007). It can be subdivided into two categories: indirect and direct photoreactivation. Indirect photoreactivation is not related to the splitting of thymine dimers, but causes a delay of cells in growth and division in order to obtain a longer time for nucleic acid repair and therefore diminish the lethal effect of UV light (Setlow, 1966). It is reported that the two steps for direct photoreactivation mechanisms are as follows. First, a photoreactivation enzyme (PRE) combines with the dimer to be repaired and forms a complex. This step does not need light exposure but depends on temperature, pH and the ionic strength in aqueous solution. Second, with the absorption of light energy the dimer is decomposed followed by the release of the PRE and repaired DNA (Sanz *et al.*, 2007).

2.1.4 Sources of UV Light

The **Low-pressure (LP) mercury lamp** is the most commonly used UV source in UV disinfection. UV light is emitted by the excitation of the mercury vapour contained in the lamp (Tchobanoglous *et al.*, 2003). In this type of lamp, the internal mercury gas pressure is low, usually 0.007 mm Hg (about 1 Pa), and output power is also low (e.g., 40 – 80 W). The LP UV lamp provides primarily two lines in the UV region at the wavelengths of 184.9 nm and 253.7 nm, as well as several weak lines in the visible region. The emission at 253.7 nm is the principal output, which accounts for about 85% of the

total output power. A LP UV lamp covered by a commercial quartz sleeve is considered to be a monochromatic and germicidal lamp, because 184.9 nm light, in the VUV region, is absorbed by the quartz sleeve, and 253.7 nm is close to the maximum DNA absorption wavelength at 260 nm (Alapi and Dombi, 2007; Bolton, 2001; Wang *et al.*, 2005; Zimmer *et al.*, 2003).

The **Low pressure high output (LPHO) lamp** is a modified type of LP lamp. It is similar to the LP lamp with a monochromatic output at 253.7 nm. The advantage of LPHO lamps is that there is a mercury amalgam inside in place of mercury, which allows 2 – 4 times the output of LP lamps and longer lifetime (Bolton, 2001; Tchobanoglous *et al.*, 2003).

The **Medium-pressure (MP) mercury lamp** is an alternative to LP lamps. Compared to the LP lamp, the internal mercury gas pressure and output power of the MP lamp are much higher, which can reach up to hundreds of kPa and 30 kW respectively. This type of lamp is polychromatic with wavelengths ranging from the far UV (185 nm) to the infrared (1367 nm). As a result, MP lamps have a lower efficiency in the UVC range, but have a high intensity at germicidal wavelengths (50 to 100 times higher than a LP lamp) (Bolton, 2001; Summerfelt, 2003; Tchobanoglous *et al.*, 2003; Wang *et al.*, 2005; Zimmer *et al.*, 2003).

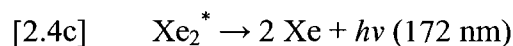
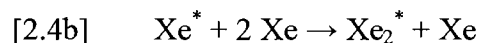
The **Pulsed UV lamp** is a relatively new lamp and mercury-free (filled with a rare gas, e.g., xenon). The electric energy of direct current is stored in a capacitor and released through a high-speed switch (in several microseconds). Each time the switch closes, the

lamp is fired with the production of a plasma that has a very high temperature (10,000 – 15,000 K) and with a very intense broad-band spectrum including UV, visible and infrared wavelengths. There are two types of pulsed UV lamp: surface discharged (SD) type and flashlamp type (Bolton, 2001; Bohrerova *et al.*, 2008; Tchobanoglous *et al.*, 2003). It has been reported that the inactivation of microorganisms, such as *Escherichia coli*, is similar or faster using pulsed UV lamp compared with LP and MP lamp at the equivalent fluence (Bohrerova *et al.*, 2008; Wang *et al.*, 2005). In addition, the pulsed UV lamp has suppressive effect on photoreactivation, but no tailing phenomena (Otaki *et al.*, 2003).

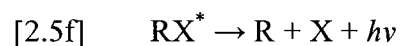
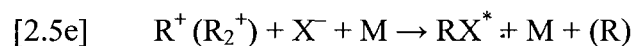
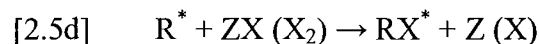
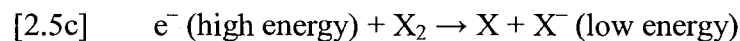
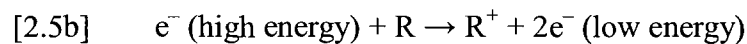
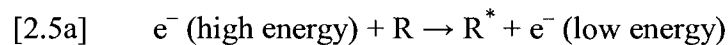
Excilamps (also called excimer lamps or exciplex lamps) are the most recently developed type of UV lamp. They are based on the generation of rare gas excited dimers (excimers), halogen excited dimers or rare gas halide excited complexes. The emission of excilamps is incoherent usually at wavelengths in the UV region (200 – 400 nm or the VUV region (100 – 200 nm). Compared with the traditional lamps, the emission band of excilamps is very narrow (no more than 10 – 20 nm at half height) which results in a high concentration of radiant flux and high efficiency at a certain emission band (Boyd and Zhang, 1997; Gellert and Kogelschatz, 1991; Sosnin *et al.*, 2006).

An excimer is a dimer which is only stable in the excited states and easily dissociates to the ground state with emission of light. The mechanism of UV light emitted from rare gas excimers is described as follows (taking a xenon excimer for example). First, with collision of a high energy electron, a Xe atom in the ground state is transferred

to the electronically excited state. Second, the excited state Xe atom collides with other Xe atoms in the ground state to generate a Xe excimer. Finally, the Xe excimer dissociates into two Xe atoms and emits a 172 nm photon. The reactions are indicated in [2.4a] – [2.4c] (Heit *et al.*, 1998; Sosnin *et al.*, 2006).



For rare gas halogen exciplex molecules, it is more complex. The primary reactions are shown in [2.5a] – [2.5f]:



where, R and X represent a rare gas atom and a halogen atom, respectively; ZX means a halogen containing molecule; M is a third particle. The series of reactions starts with the generation of excited rare gas atoms and positive rare gas ions, as well as negative halogen ions, from the collisions of high energy electrons with rare gas atoms and halogen molecules ([2.5a], [2.5b] and [2.5c]). Then an exciplex molecule RX^* is created by the so-called harpoon reaction ([2.5d]), which is caused by the transfer of a loosely

bound electron from an excited rare gas atom to a halogen containing molecule or halogen molecule. RX^* is also produced by three body recombination of a positive atomic or molecular rare gas ion with a negative halogen ion and a third particle ([2.5e]). At last, the exciplex molecule RX^* rapidly decomposes and emits a photon ([2.5f]) (Boyd and Zhang, 1997; Sosnin *et al.*, 2006).

The primary emission wavelengths of excilamps containing different substances are displayed in Table 2.1 (Boyd and Zhang, 1997; Sosnin *et al.*, 2006).

Table 2.1 Emission wavelengths of excilamps

Elements	----	Ne	Ar	Kr	Xe
----			126 nm	146 nm	172 nm
F	158 nm	106 nm	193 nm	248 nm	351 nm
Cl	259 nm		175 nm	222 nm	308 nm
Br	289 nm		165 nm	207 nm	282 nm
I	342 nm			190 nm	253 nm

Excilamps can be driven by capacitive discharge (CD) or dielectric barrier discharge (DBD) (also known as silent discharge). The electrodes of both types are covered by a dielectric. A classical CD works in the situation of lower gas pressure (10^{-3} – 100 torr) and higher excitation field frequency (several MHz), compared with DBD, which usually works at pressures above 100 torr and tens to hundreds of kHz, respectively. For the DBD device, many microdischarges (also called filaments) are formed on the surface of the dielectric. These filaments can exist only for a few

nanoseconds, but usually quasi-simultaneously, randomly covering the whole surface of the dielectric (Boyd and Zhang, 1997; Sosnin *et al.*, 2006).

The advantages of excilamps include: (1) high photon flux (can be tuned), (2) absence of mercury; (3) changeable geometry (such as cylindrical, coaxial and planar, as well as optional), which is the first time it has been possible to change the lamp shape for optimization in application; (4) short response time to ignite and full radiant power after ignition (Sosnin *et al.*, 2006).

Excilamps can be used in copiers and scanners, as well as plasma displays (Sosnin *et al.*, 2006). Some other applications are shown below: low temperature material deposition (UV induced metal deposition, photo-deposition of insulating layers) (Kogelschatz *et al.*, 2000), UV assisted oxidation of Si, Ge and SiGe at low temperature (Kogelschatz *et al.*, 2000), photo-etching, microstructuring and surface modification of various polymers (Chen *et al.*, 2004; Kogelschatz *et al.*, 2000; Periyasamy *et al.*, 2007; Zhang *et al.*, 1993), UV curing of paints, varnishes, coating and adhesives (Boyd and Zhang, 1997; Zhang *et al.*, 2002), photochemically induced grafting on polymers (Zhu and Kelley, 2005), photodegradation of pollutants in water and air (Boyd and Zhang, 1997; Li *et al.*, 2006), advanced oxidation processes (AOPs) assisted by excilamps (Ikematsu *et al.*, 2004; Matafonova *et al.*, 2008), and UV inactivation of microorganisms (Clauß *et al.*, 2005; Sosnin, *et al.*, 2004).

2.2 Advanced Oxidation Processes (AOPs)

2.2.1 Theory of Advanced Oxidation Processes (AOPs)

Advanced Oxidation Processes (AOPs) involve the generation and application of the hydroxyl free radical ($\bullet\text{OH}$), which is the second strongest oxidant after fluorine with an oxidation potential of 2.80 V, to destroy refractory contaminants that cannot be oxidized by conventional oxidants, such as oxygen, chlorine or ozone (Gültekin and Ince, 2007; Tchobanoglous *et al.*, 2003). For example, Chen *et al.* (2006) found that an AOP was effective in removing bisphenol A (BPA), one of the endocrine disrupting compounds (EDCs), which is difficult to treat by conventional water treatment processes.

The short-lived hydroxyl radical is generally non-selective and can react with almost all reduced materials including a large group of organic chemicals at normal temperature and pressure, regardless of the specific classes or groups of compounds. It is usually used for removal of trace amounts of refractory organic compounds via electrophilic radical addition, hydrogen abstraction, and electron transfer (Tchobanoglous *et al.*, 2003). With a series of degradative oxidation reactions (involving molecular oxygen), the compounds convert to less complex and less harmful intermediate products and eventually are mineralized to produce CO_2 with sufficient contact time and enough hydroxyl radicals. Unlike other chemical and biological treatment, AOPs are environmentally friendly because they neither transfer pollutants from one phase to another nor generate a large amount of sludge (Gültekin and Ince, 2007; Tchobanoglous

et al., 2003).

At the present, there are many methods to produce hydroxyl radicals. Several are exemplified as follows (Gültekin and Ince, 2007; Pera-Titus *et al.*, 2004; Tchobanoglous *et al.*, 2003):

1. Photochemical processes

- VUV photolysis
- $O_3 + UV$
- $UV + H_2O_2$
- $O_3 + UV + H_2O_2$
- $UV + \text{ultrasound}$
- Photo-Fenton ($H_2O_2 + Fe^{2+}/Fe^{3+} + UV$)
- Photocatalysis ($UV + TiO_2$)

2. Non-photochemical processes

- Ozonation (O_3)
- $O_3 + H_2O_2$
- Fenton: $H_2O_2 + Fe^{2+}/Fe^{3+}$
- $O_3 + Fe^{2+}/Fe^{3+}$
- $O_3 + TiO_2$
- $O_3 + TiO_2 + H_2O_2$
- Ultrasound
- $O_3 + \text{ultrasound}$

2.2.2 Inactivation of Microorganisms Using Advanced Oxidation

In addition to high efficiency of AOPs for the destruction of refractory contaminants in aqueous solution, the inactivation of microorganisms with hydroxyl radicals has been investigated (Mamane *et al.*, 2007; Rincón and Pulgarin, 2004). Unlike UVC disinfection, which relies on the disruption of nucleic acids (such as DNA and RNA), hydroxyl radicals mainly oxidize and disrupt the cell wall and cell membranes (resulting in lipid peroxidation) and therefore disintegrate the cell. On the other hand, some hydroxyl radicals may penetrate into the interior of the microorganism to react with enzymes and other intracellular components and also lead to inactivation of the microorganisms (Mamane *et al.*, 2007; Rincón and Pulgarin, 2004).

Rajala-Mustonen and Heinonen-Tanski (1995) compared the disinfection effects of UV light at 254 nm, ozonation and the UV/H₂O₂ AOP, based on two types of coliphages, and indicated that ozonation was the most effective method, followed by UV disinfection. The AOP (UV/H₂O₂) was the least effective. Mamane *et al.* (2007) investigated inactivation of different microorganisms using an AOP involving generation of OH radicals by H₂O₂ and UV light with the wavelengths higher than 295 nm. In their research, they found that hydroxyl radicals have almost no effect on the inactivation of T4 phage and *B. subtilis* spores. For T7 phage and MS2, 1 and 2 logs reduction respectively were reached for a UV exposure for 15 min and a H₂O₂ concentration of 25 mg L⁻¹. For *E. coli*, a 1 log reduction was reached for the same length of UV exposure, but at a 10 mg L⁻¹ as H₂O₂ concentration. However, Sharrer and Summerfelt (2007) argued the AOP involving

the combination of ozone and UV (at 254 nm) was more efficient for the inactivation of total heterotrophic bacteria than ozonation or UV exposure alone. For ozone a CT (the concentration of the disinfectant C times the exposure time t) value of about 0.42 min mg/L and a fluence (UV dose) of 47 mJ cm^{-2} produced a log reduction of about 1.77.

In the past several years, semiconductor photocatalysis has attracted more attention concerning its effect on the disinfection of microorganisms. Most papers studying disinfection effect of AOPs related to the photocatalytic technology. As one of the AOPs, TiO_2 particles suspended in aqueous solution combined with UV exposure is a process that is commonly used because TiO_2 is an economical photocatalyst. TiO_2 exposed to UV light with wavelengths lower than 385 nm produces hydroxyl radicals on its surface (Rincón, and Pulgarin, 2005). When a water sample with suspended TiO_2 is exposed to UV light, rapid microorganism death has been observed (Herrera Melián *et al.*, 2000). Watts *et al.* (1995) obtained a 2 log reduction of coliform bacteria and poliovirus treated in a 250 mg/L TiO_2 suspension for 150 min and 30 min, respectively, under their laboratory lights (with an emission spectrum from about 285 nm to above 400 nm). Paleologou *et al.* (2007) found more than a 2 log reduction of *Escherichia coli* under the conditions of 20 min contact time and 0.5 g/L TiO_2 powder and exposure to 350 – 400 nm UVA light. Benabbou *et al.* (2007) indicated that bacterial inactivation was influenced by the TiO_2 concentration in suspension and the UVA fluence (UV dose). Rincón and Pulgarin (2005) reported that *E. coli* was more sensitive to TiO_2 photocatalysis than *Bacillus subtilis* spores. In the following year, they compared several AOPs, such as

UV-vis/TiO₂, UV-vis/TiO₂/H₂O₂, UV-vis/H₂O₂, and UV-vis/Fe³⁺/H₂O₂ (Photo-Fenton) and found that the UV-vis/TiO₂/H₂O₂ process was more efficient than UV-vis/TiO₂, based on the results that the reduction of *E. coli* obtained from an initial concentration of 1×10^7 CFU mL⁻¹ to a final concentration of less than 1 CFU mL⁻¹ for ~20 min contact time under 1000 W m⁻² solar irradiation with 0.5 mg/L TiO₂ and 10 mg/L H₂O₂ (Rincón and Pulgarin, 2006).

Sun *et al.*, (2003) improved the photocatalysis processes. A novel TiO₂ – Fe₂O₃ membrane photocatalytic oxidation reactor was used to get a 2 log reduction of *E. coli* for 60 s contact time at a dissolved oxygen (DO) concentration of 21.3 mg/L and 10⁹ CFU mL⁻¹ initial concentration of *E. coli*. After their research, Choi *et al.* (2007) fabricated novel nanostructured crystalline TiO₂ films to carry out disinfection experiments on *E. coli*. They considered the TiO₂/UV process to be a fast method for microorganism reduction, since their results indicated 4 log removal of *E. coli* for a 1.5 h contact time at a TiO₂ concentration of 77.8 µg/mL and a UV irradiance of 3.48 mW cm⁻² at 365 nm.

2.3 Vacuum-ultraviolet (VUV) Photolysis of Aqueous System

2.3.1 VUV-induced Photochemistry

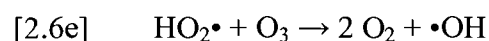
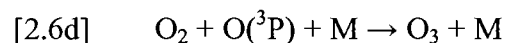
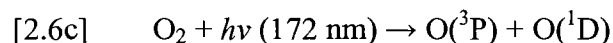
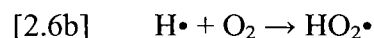
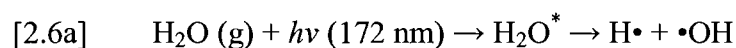
Vacuum UV (VUV) encompasses UV light with wavelengths between 100 and 200 nm. Absorption of water increases sharply as the wavelength decreases from 190 to 120 nm. This absorption also generates hydroxyl radicals, which are used in an AOP to

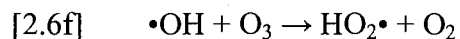
degrade aqueous refractory contaminants. As a result, this VUV region plays an important role in photochemistry (Azrague *et al.*, 2005). In addition, VUV also initiates gas phase photooxidations. For example, it can dissociate molecular oxygen, methanol, as well as other organic compounds in the gas phase (Alapi and Dombi, 2007).

The Xe excilamp, with an emission maximum at 172 nm and half-width of less than 14 nm (Heit *et al.*, 1998), is an important VUV source and also it is used in this research. Bench-scale experiments using the Xe excilamp have indicated that the VUV photolysis of water has an important potential for cleaning up contaminated water (USEPA, 1998). The following sections will discuss some typical reactions induced by the Xe excilamp.

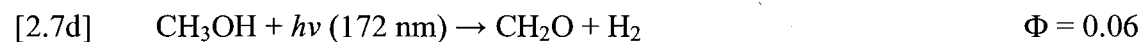
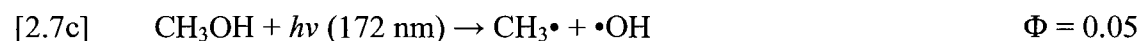
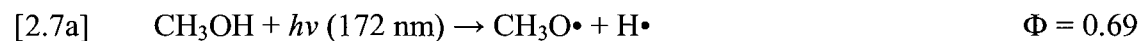
2.3.2 VUV photolysis of Oxygen and Organic Compounds

VUV light is absorbed significantly by water vapour and oxygen in the air. The penetration depths of 172 nm UV light into the air saturated by water vapour and pure dry oxygen at a gas pressure of 10^4 Pa are 6 mm and 28.5 mm, respectively (Sosnin *et al.*, 2006). Oxygen in the gas phase exposed to 172 nm produces ozone. The reactions of an air system containing oxygen and gaseous water exposed to 172 nm light are shown below in Reactions [2.6a] to [2.6f] (Sosnin *et al.*, 2006):





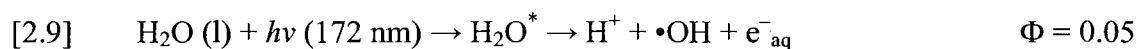
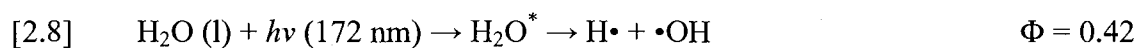
VUV light can be applied to the oxidation and photolysis of volatile organic compounds (VOCs) in the gas phase (Sosnin *et al.*, 2006), since they can be oxidized by hydroxyl radicals initiated by VUV irradiation (the reactions are similar to that of the organic compounds oxidized in aqueous solution, which will be discussed later in Section 2.2.2.3) or destroyed by direct absorption of VUV (Alapi and Dombi, 2007; Skurat, 2003). For example, methanol (CH_3OH , MeOH) molecules absorb strongly in the VUV region with a very high absorption coefficient of 4000 cm^{-1} at 172 nm. These molecules photolyze to form methoxyl- and hydroxymethyl radicals (Reaction [2.7a] and [2.7b]) or produce methyl radicals, formaldehyde and hydrogen (Reaction [2.7c] and [2.7d]) with the sum of the quantum yields (Φ) being 0.88 at 172 nm (Heit *et al.*, 1998).



2.3.3 VUV-induced Photolysis of Liquid Water

Water intensively absorbs VUV light ($< 190 \text{ nm}$) with a high absorption coefficient (approximately 20 cm^{-1} at 184.9 nm and 550 cm^{-1} at 172 nm). Thus for an absorbance of VUV light of $A > 2$ by water, the penetration depths at 184.9 nm and 172 nm are about 0.1 and 0.0036 cm, respectively (Oppenländer *et al.*, 2005). The photochemically induced homolysis of water molecules is the principal reaction of water exposed to VUV light. It

generates hydroxyl radicals, which can be used as a method for hydroxyl radical production in AOPs with the advantage over other methods of no addition of any chemical additives (Reaction [2.8]) (Oppenländer *et al.*, 2005). The quantum yields of homolysis of water are dependent on the wavelengths of VUV light, for example, 0.33 at 184.9 nm, 0.42 ± 0.04 at 172 nm, 0.7 at 147.9 nm, and about 1 at 123.6 nm (Gonzalez *et al.*, 2004; Quici *et al.*, 2008). In addition to water homolysis, there is a heterolytic reaction of water, which is a minor reaction with a lower quantum yield of 0.05 ± 0.01 at 172 nm, generating hydrated electrons (e^-_{aq}) (Reaction [2.9]) (Oppenländer *et al.*, 2005).



Hydrogen peroxide (H_2O_2) generated by the VUV-induced photolysis of water was investigated by Azrague *et al.* (2005). They discovered that in pure water, in presence of dissolved O_2 , a quasi-stationary concentration of H_2O_2 was reached at 1.1×10^{-4} M, which is almost twice of that in pure water without dissolved O_2 (6×10^{-5} M).

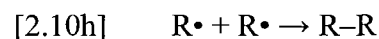
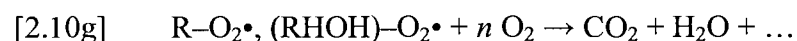
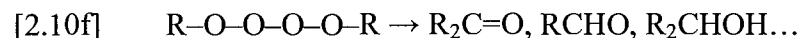
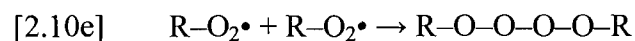
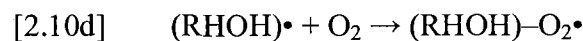
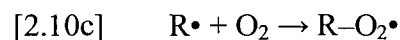
2.3.4 VUV-induced Organic Compounds Removal in Aqueous Solution

Although the absorption coefficients of most organic compounds (such as MeOH) are higher than water molecules, for organic compounds in aqueous solution, it is assumed that the photons are absorbed almost exclusively by water molecules and result in water photolysis, because the concentrations of organic compounds in dilute aqueous solution are much lower than the concentration of water (55 M) in aqueous solution (Heit *et al.*, 1998).

There are many papers reporting VUV photolysis applications, especially using Xe excilamps, for the oxidation and mineralization of organic compounds in aqueous solution. Oppenländer *et al.* (2005) used a VUV flow-through photoreactor containing a cylindrical xenon excilamp with coaxial geometry to perform their research on the photomineralization of 1-heptanol and benzoic acid and found that the reactor system equipped with an internal tubular ceramic air diffuser for supply of air or oxygen bubbles to VUV-initiated AOPs led to an enhanced rate of mineralization. They accordingly drew the conclusion that the rate of TOC reduction was strongly dependent on the concentration of dissolved O₂ in the exposed solution. The same type of photoreactor was used earlier by Baum and Oppenländer (1995) for examining the VUV oxidation of volatile chloroorganic compounds (1,2-dichloroethene, trichloroethene, and tetrachloroethene) and non-volatile chloroorganic compounds (2,4-dichlorophenol) in aqueous solution. After 60 min irradiation at 172 nm, almost all of the above compounds were oxidized. The mineralization of various organic micropollutants, such as C₁ – C₈ homologous alcohols and phenols, in aqueous solution by VUV were also investigated. These workers found that the efficiency of total organic carbon (TOC) reduction was dependent on the molecular structure of the organic compounds (Oppenländer and Gliese, 2000; Han *et al.*, 2004).

A series of photochemical reactions and thermal reactions is involved in the VUV-induced oxidation and mineralization of organic containing water (Reactions [2.10a] to [2.10g]). The degradations of saturated organic compounds (RH_{saturated}) and unsaturated

compounds ($\text{RH}_{\text{unsaturated}}$), such as aromatic hydrocarbons, are dependent on the concentration of dissolved molecular oxygen. In the presence of dissolved oxygen, aliphatic peroxy radicals ($\text{R-O}_2\cdot$) and cyclohexadienyl-type peroxy radicals $[(\text{RHOH})\text{-O}_2\cdot]$ are important intermediates in the degradation of $\text{RH}_{\text{saturated}}$ and $\text{RH}_{\text{unsaturated}}$ compounds, respectively (Reactions [2.10c] and [2.10d]). Moreover, with sufficient dissolved oxygen these intermediates undergo some subsequent reactions and eventually are oxidized to CO_2 and H_2O (Reactions [2.10e] to [2.10g]). However, under conditions of oxygen deficiency, these intermediates may recombine to produce new molecules with more carbon atoms and higher molecular weights (Reaction [2.10h]) (Sosnin *et al.*, 2006; Oppenländer *et al.*, 2005).



Oppenländer and Schwarzwälder (2002) investigated the degradation of methanol in aqueous solution by use of a Xe_2^* excilamp. The overall reaction kinetics in their research was dependent on the initial concentration of methanol. At lower initial

methanol concentrations (< 75 mM), pseudo first-order rate behaviour prevailed. Whereas, in a higher concentration domain (from 75 to 400 mM), pseudo zero-order rate behaviour was found. In addition, the rate constant was almost invariant over the initial concentration range from 75 to 250 mM. As a result, in this concentration range, a methanol solution can be used as an actinometer for VUV fluence rate measurements (Heit *et al.*, 1998). In fact, the fluence rate at 172 nm has been determined by this method in this study. In addition, according to results concerning the degradation of dissolved Rhodamine B (RhB) and methanol in water, the rate of VUV-initiated oxidation and mineralization of organic compounds in aqueous solution is independent of water temperature from 20 to 50°C (Oppenländer and Xu, 2008).

2.4 Conclusions

In the UV wavelength region, UVC light is mainly used for disinfection in water and wastewater treatment. Photons in VUV range have an energy high enough to break chemical bonds in most molecules, and consequently VUV light can be used in photochemistry, such as photolysis of water and organic compounds in aqueous solution.

A collimated beam apparatus is used in bench-scale photochemical studies. The fluence rate or irradiance can be determined by mathematical modeling, radiometry, biosimetry or chemical actinometry.

UV disinfection technology is attracting more attention these years, since the discovery of its high efficacy against *Cryptosporidium parvum* oocysts, which are considered very dangerous to human health in drinking water. On the other hand, UV disinfection does not need to add any chemicals into the treated water. Compared to other disinfection processes, it is environmentally friendly. The mechanism of UV disinfection is principally the disruption of the DNA or RNA in microorganisms.

Plentiful UV sources are commercially available, such as LP lamps, LPHO lamps, MP lamps, pulsed UV lamps, and excilamps. The excilamp is a mercury-free lamp with a narrow emission band, based on the generation of rare gas excited dimers (excimers), halogen excited dimers or rare gas halide excited complexes.

Advanced oxidation processes (AOPs) involve the generation and application of a very strong oxidant, hydroxyl radical ($\bullet\text{OH}$) used for the removal of refractory compounds in aqueous solution, which are difficult to remove by conventional treatment processes. In addition, its effect on microorganism disinfection has been also investigated. Compared with other hydroxyl generation technologies, the VUV-induced photolysis of aqueous solution has an advantage of no chemical addition into the water matrix. The complex reactions of VUV-induced photolysis of organic solutions have been investigated by several groups.

CHAPTER 3

FLUENCE DETERMINATION OF THE XENON EXCILAMP AT 172 NM USING METHANOL AS AN ACTINOMETER

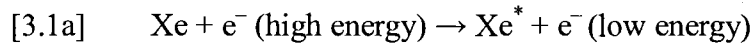
3.1 Introduction

Dielectric barrier discharge excilamps are a relatively new type of UV lamps with emission wavelengths ranging from the UV region (200 – 400 nm) to the VUV region (100 – 200 nm). Excilamps usually contain rare gas molecules and/or halogen molecules in the discharge gaps. Rare gas excited dimers (R_2^*), halogen excited dimers (X_2^*) or rare gas halide excited complexes (RX^*) are generated by the collision between the molecules in the discharge gaps and the high energy electrons that are released from the high voltage electrodes. Photons are then emitted by decomposition of the excimers into ground state atoms (Sosnin *et al.*, 2006). Excilamps have some important applications, such as photodecomposition techniques of metal, dielectric and semiconductor layers, surface modification of polymers, as well as patterned material removal from polymer surfaces (Kogelschatz, 1992).

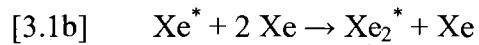
In this research, a xenon excilamp was used. The emission band of this lamp is relatively narrow with an emission maximum at 172 nm and the half-width of no more than 14 nm. A typical emission spectrum of a Xe_2^* excilamp is illustrated in Figure 3.1

(Heit *et al.*, 1998). The mechanism of emitting 172 nm UV light by a Xe_2^* excilamp is described by the following reactions (Heit *et al.*, 1998).

(1) An excited state Xe atom is created by collision of a Xe atom in the ground state with a high energy electron:



(2) The Xe atom in the excited state continues to collide with other Xe atoms in the ground state and then generates a Xe excimer (Xe_2^*):



(3) A photon at 172 nm is emitted by the dissociation of the Xe excimer into Xe atoms in the ground state.

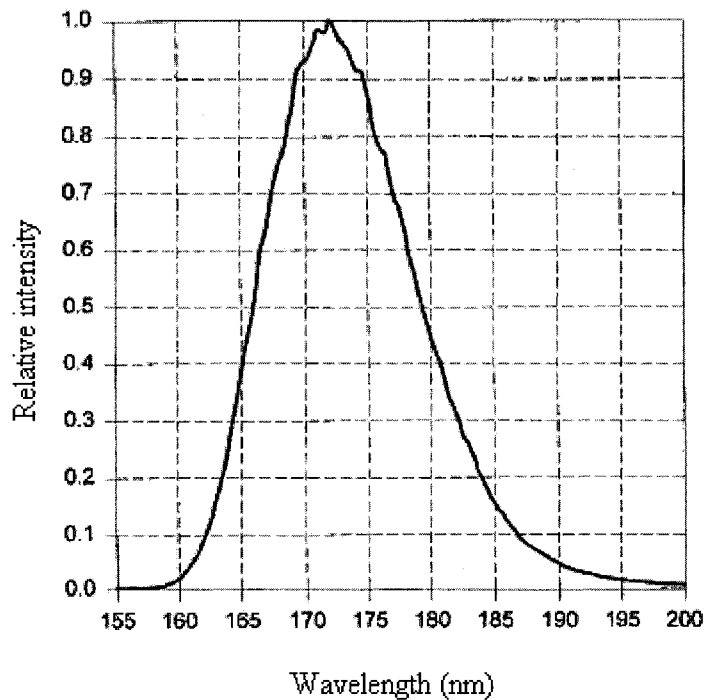
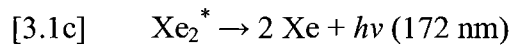
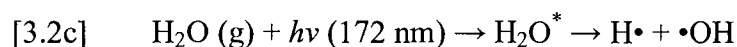
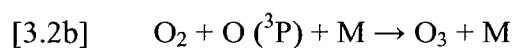
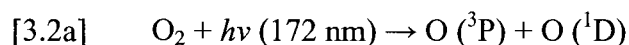


Figure 3.1 Emission spectrum of a Xe_2^* excilamp

Photons emitted by Xe_2^* excilamps are in the VUV region. They are absorbed intensively by gaseous oxygen to produce ozone (Reactions [3.2a] and [3.2b]). In addition, the VUV light is absorbed by liquid water to produce hydroxyl radicals ($\bullet\text{OH}$). This process is called the VUV-induced photolysis of water (Reaction [3.2c]) (Sosnin *et al.*, 2006).



where M is another molecule which serves to remove the excess kinetic energy.

Hydroxyl radicals play a decisive role in Advanced Oxidation Processes (AOPs). Since hydroxyl radicals non-specifically oxidize target compounds at high reaction rates, AOPs are extensively used to remove refractory contaminants in water (Tchobanoglous *et al.*, 2003).

Because of a high absorption of 172 nm VUV by air, Xe_2^* excilamps cannot impinge on the aqueous solution to be treated across an air gap. Some research papers reported the application of a xenon-excimer flow-through photoreactor, which pumped water solution flowing through the inner quartz tube of the lamp without the air gap (Baum and Oppenländer, 1995; Oppenländer and Gliese, 2000; Oppenländer and Schwarzwälder, 2002; Oppenländer, *et al.*, 2005; Oppenländer and Xu, 2007; Sosnin *et al.*, 2006). But the disadvantage of this design is that the VUV light beam is not quasi-collimated, which means that the determination of the fluence rate or irradiance at

172 nm from this photoreactor is inaccurate, and the disinfection effect cannot be compared with the results of other lamps housed in a collimated beam apparatus. Therefore, a new collimated beam apparatus was constructed, especially for the Xe₂^{*} excilamp, with an atmosphere of ultra high purity nitrogen. On the other hand, a regular radiometer cannot be used for the determination of the fluence rate at 172 nm, since there is almost no sensitivity of radiometer detectors below 200 nm, and the calibration curves do not cover the VUV region. As a result, an actinometry method reported by Oppenländer and Schwarzwälder (2002), using methanol as an actinometer in aqueous solution, was used to determine the fluence rate (irradiance) of the Xe₂^{*} excilamp. The initial and final concentrations of methanol were determined by the internal standard method using gas chromatography (GC). In addition, Anagnostopoulos *et al.*, (2006) reported that the internal standard method was better than the external standard method, based on analysis results for 21 pesticides. Better repeatability and reproducibility were observed with the internal standard method.

The objective of the study in this chapter is to determine the fluence rate (irradiance) of a Xe₂^{*} excilamp in a special collimated beam apparatus.

3.2 Materials and Methods

3.2.1 Xe₂^{*} Excilamp

A dielectric barrier discharge Xe₂^{*} excilamp (Model: BD_P – barrier discharge,

portable, Institute of High Current Electronics, Russia) was used (Figure 3.2). The dimensions of this lamp were $26.5 \times 7.7 \times 77$ cm (Length \times Width \times Height) including an air-cooling fan. The output window dimensions were 10 cm \times 6 cm. The emission maximum was 172 nm with the half-width of less than 14 nm. The input power of the lamp was 35 W.

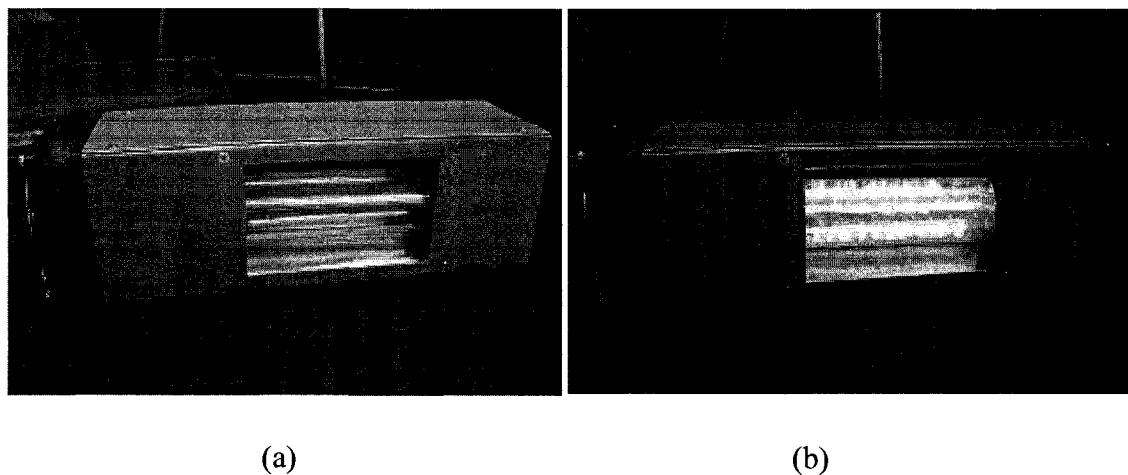
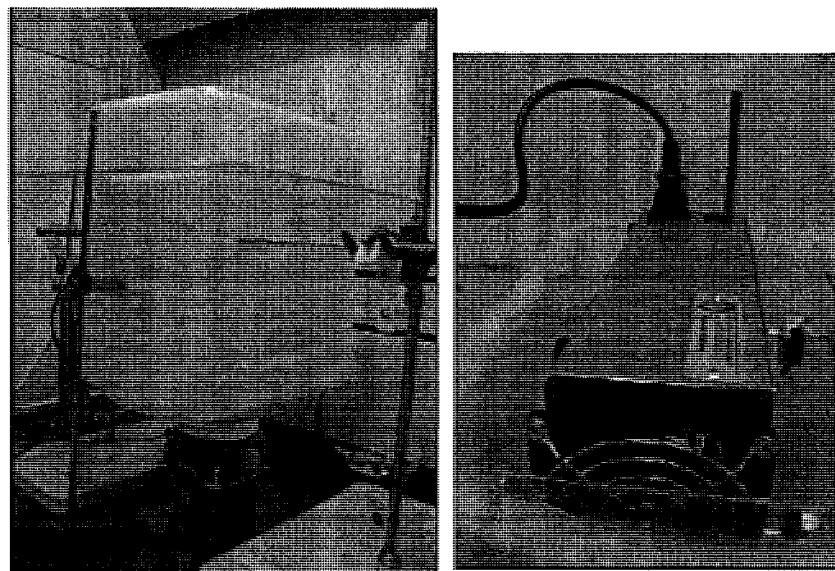


Figure 3.2 View of the Xe_2^* excilamp: (a) Off; (b) On

3.2.2 Special Collimated Beam Apparatus for the Xe_2^* Excilamp

The 172 nm photons emitted by a Xe_2^* excilamp cannot be used in a regular collimated beam apparatus, since oxygen in the air absorbs VUV photons and therefore prevents them from impinging on the water solution to be treated. A special collimated beam apparatus separated from the air was required. Figure 3.3 illustrates the first collimated beam apparatus for this research. Since, in the presence of oxygen, the Xe_2^* excilamp produces ozone that is harmful to human health, the collimated beam apparatus was placed in a fume hood. It was converted from a 20 L Nalgene high density

polyethylene (HDPE) carboy, cut into two parts, and positioned upside down. Holes were drilled in the walls in order to make two steel rods cross it. The lamp was put on the rods and fixed with clamps. The steel rods were also used to connect the apparatus with outside supporting structures. A 22 cm collimating tube (inner diameter = 6.2 cm, outer diameter = 7.3 cm) was fixed vertically under the lamp. The total path length of the light beam from the window of the lamp to the surface of the sample was 24 cm. The upper part of the apparatus that was the bottom of the carboy was glued with the lower part by silicone. The plexiglass sheet between the two parts was used to connect them more smoothly. Two holes were drilled on the top of the apparatus to allow the power cable and the nitrogen tube to go inside. The apparatus was supplied with ultra high purity nitrogen (Praxair Canada Inc.) through a thick plastic tube, and a thin-tube tributary diverged from the main flow to purge the air from the collimating tube. The main flow rate of nitrogen was controlled by a flow controller (Cole-Palmer Instrument Company, USA). The cap of the carboy was used as sampling port. Several fine holes were drilled near it in order to discharge the nitrogen outside. Silicone was used to seal leaks of the joints between the apparatus and external supporting structures to make sure there were no influents of air into the apparatus.



(a)

(b)

Figure 3.3 The first collimated beam apparatus for the Xe_2^* excilamp: (a) View of this apparatus; (b) The Xe_2^* excilamp placed inside before sealing the upper part of the apparatus

After this first apparatus was used for about two months, it was opened because a shorter collimating tube was needed to replace the initial one. However, when the apparatus was opened, yellow dust was found covering everything inside the apparatus. It was assumed that this yellow dust was from the degradation of polyethylene (the principal material of the apparatus) exposed to the VUV light. It was harmful to the Xe_2^* excilamp and also significantly influenced the intensity of the lamp. Therefore a second collimated beam apparatus was constructed using acrylic plexiglass sheets with a thickness of 6 mm (Figure 3.4a). This material is more stable than polyethylene under

exposure to the UV light. The design of the second apparatus (Figure 3.4b) was similar to that of the first one. The main body of the apparatus was like a box, enclosed by six plexiglass sheets. The dimensions of the main body were 40 cm × 15 cm × 22 cm. Several holes were drilled in the walls to fix steel rods that were used to support the lamp and to connect the power cable and the nitrogen tubes. The sampling port was cut from the old apparatus and was glued with the bottom surface of the new apparatus. For preventing the apparatus against the UV exposure, aluminum foil was used to cover the inside walls of the apparatus. Several areas without aluminum foil were positioned for inspection of the situations of the lamp in the apparatus. A 7 cm long collimating tube was placed in the second apparatus. The total path length of the light beam from the window of the lamp to the surface of the sample was 8 cm. A thin tube supplying nitrogen was also connected to the collimating tube to purge the air out of it. Other instruments and materials were the same as those used for the first collimated beam apparatus.

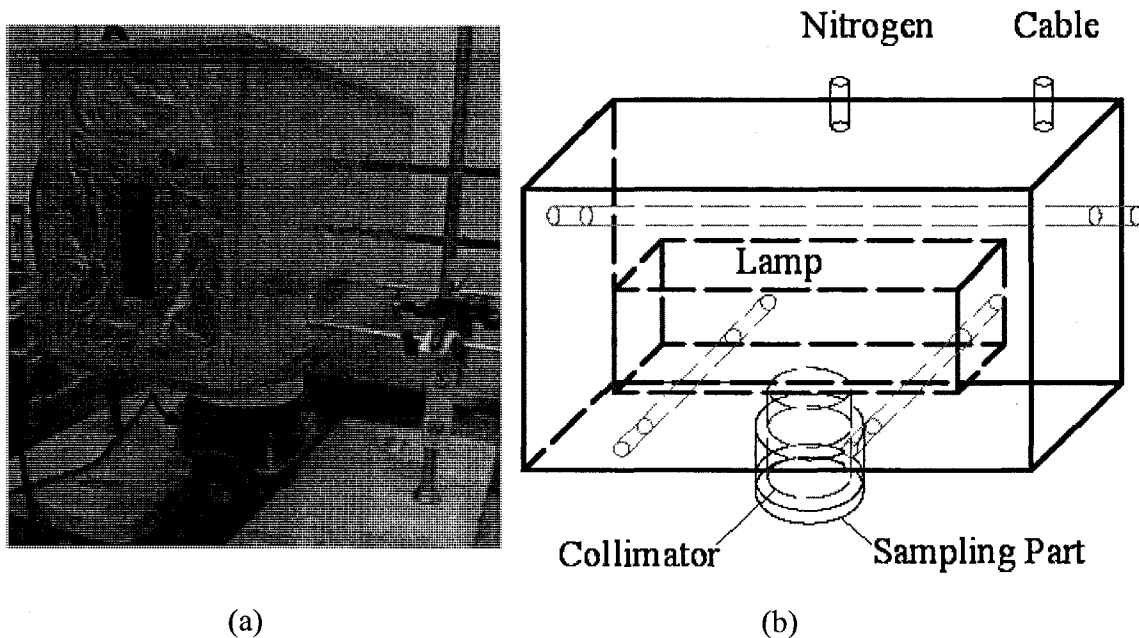


Figure 3.4 The second collimated beam apparatus for Xe_2^* excilamp: (a) Photo; (b)

Design of this apparatus

The sampling port constituted the cap of the carboy and a frame, which was glued into the cap, to fix the sample containers. Pyrex[®] Petri dishes with 5.8 cm inner diameter and two 10 mm path length spectrophotometer cuvettes (volume = 3.5 mL for each) made of SUPRASIL[®] Quartz with stoppers (Hellma Canada, Ltd.) were used as containers. The inner surface of the cap was covered by black paint to decrease the reflection of the VUV light when cuvettes were used. The sampling port with a Petri dish or cuvettes is shown in Figure 3.5. Teflon-coated micro stirring bars with the size of 8 mm × 2 mm were used to mix the sample being exposed.

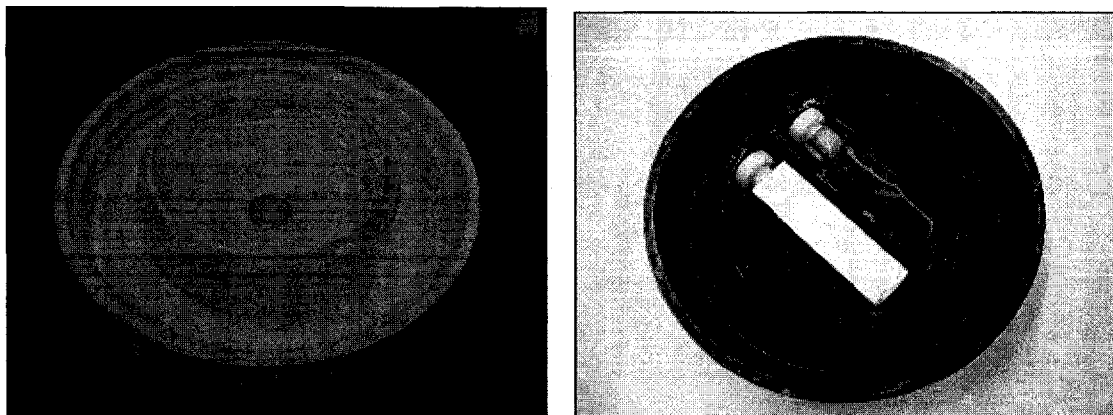


Figure 3.5 Sampling port with sample containers: (a) With a Petri dish; (b) With cuvettes

3.2.3 Reagents and Deionized Water

Rhodamine B (Fisher Scientific Co., Canada), methanol (HPLC grade, Fisher Scientific Co., Canada), and 1,4-dioxane (standard for GC, Sigma-Aldrich Canada, Ltd.) were used in this research. Rhodamine B is a dye with a red colour in aqueous solution. Deionized water (DI water) with the resistivity of 18.2 M Ω cm at 25°C (processed by a Milli-Q Academic A10 – Millipore Corporation, USA) was extensively used as the general solvent for solutions.

3.2.4 Sample Preparation

Rhodamine B solutions

A 10 mg L⁻¹ Rhodamine B aqueous solution was used to evaluate the relative performance of the Xe₂* excilamp. 1 L of Rhodamine B solution at a concentration of 1 g L⁻¹ was first prepared by adding 1.00 g of Rhomanine B powder weighed by an electronic balance (Model: EP613C, Ohaus Corporation, USA) to a 1000 mL volumetric

flask. Then the 10 mg L^{-1} solution was prepared by transferring a 10 mL aliquot of 1 g L^{-1} solution using a volumetric transfer pipette into another 1000 mL volumetric flask. Finally, this 1 L stock at 10 mg L^{-1} was stored in an amber narrow-mouth glass bottle for the UV exposure experiments.

Methanol Solutions

Methanol in aqueous solution was used as an actinometer to determine the fluence rate (irradiance) of the Xe_2^* excilamp. Methanol stock solutions at concentrations of 5.015, 10.03, 15.04 and 20.06 mM with a volume of 100 mL for each experiment were prepared.

First, 1 L of methanol solution at a concentration of 100.3 mM was prepared by the following method. Based on the methanol molecular weight of 32.04 g mol^{-1} , the mass of pure methanol needed for 1 L of a 100 mM solution was 3.204 g. From the pure methanol density of 0.7915 g cm^{-3} , the volume of pure methanol needed was 4.405 mL. However, since methanol is very volatile, a very accurate methanol concentration cannot be prepared. The mass of liquid methanol loses very quickly when it is exposed to the air during transfer. Therefore, a micropipette was used to transfer approximately 4.408 mL of pure methanol into a 1000 mL volumetric flask that had been put on the electronic balance. The flask was covered with its stopper as soon as the transfer was completed. The exact mass of methanol transferred was determined by the increase in weight of the flask combined with the stopper as read from the balance. The actual mass transferred was 3.214 g. Therefore the corresponding concentration of this 1 L methanol solution was

100.3 mM.

Second, a series of methanol solutions at concentrations of 5.015, 10.03, 15.04 and 20.06 mM was prepared by diluting the 100.3 mM solution, by transferring exact volumes of the 100.3 mM solution calculated beforehand into 100 mL volumetric flasks by volumetric transfer pipettes and adding DI water to the mark of the flasks. Each solution at different concentrations was stored in an amber narrow-mouth glass bottle.

1,4-Dioxane Solutions

A 1,4-dioxane solution was required as an internal standard for the determination of the methanol concentration in GC analyses. Two solutions at concentrations of 99.33 mM and 9.933 mM with volumes of 500 mL and 50 mL, respectively, were prepared and stored in amber narrow-mouth glass bottles. The method of preparation was the same as that for preparing the methanol solutions, based on the molecular weight of 1,4-dioxane (88.11 g mol^{-1}) and its density (1.034 g cm^{-3}).

3.2.5 UV Exposure Experiments

The first series of UV exposure experiments on Rhodamine B were carried out in the first collimated beam apparatus. First of all, it was important to determine how long a time was required to supply the apparatus with nitrogen gas before igniting the lamp, in order to remove the air from the apparatus and to ensure that the lamp worked in an oxygen-free environment. The reason is that in the presence of oxygen, the VUV light is absorbed, which results in a highly diminished irradiance onto the surface of the sample. On the other hand, ozone is produced from the oxidation of oxygen molecules exposed to

the VUV light, which is harmful to the components of the lamp and decreases the lifetime of the lamp. Potassium iodide-starch test paper (Fisher Scientific Co., Canada) was used to determine the required length of time for nitrogen purging, based on the phenomenon that the paper changes colour from white to blue in the presence of ozone. It was thus determined that 30 min at the maximum flow rate of nitrogen regulated by the flow controller was required to purge the apparatus of oxygen. During the UV exposure experiments, nitrogen had to be supplied all the time at a lower flow rate of 1,674 mL min⁻¹, which was equivalent to “100” displayed on the flow controller.

Petri dishes were used to contain Rhodamine B solutions for treatment. Each sample was exposed to UV once for the desired length of exposure time. The detailed procedures for the experiments are described as follows:

1. 10 mL of the Rhodamine B stock solution at a concentration of 10 mg L⁻¹ was transferred using a volumetric transfer pipette from the 1 L stock solution to a Pyrex[®] Petri dish that contained an 8 mm × 2 mm Teflon-coated micro stirring bar.
2. The Petri dish was placed in the sampling port of the apparatus (Figure 3.5a), which was then screwed on tightly.
3. The collimated beam apparatus was supplied with nitrogen gas for 30 min at the maximum flow rate, which was achieved by turning on the flow controller to the maximum.
4. After 30 min, the flow rate of nitrogen was turned down to 1,674 mL min⁻¹,

which was “100” displayed on the flow controller.

5. The lamp was switched on, and the start of the exposure time was indicated by starting a stopwatch (Fisher Scientific Co., Canada) as soon as the lamp was lit. There was usually a delay of about several minutes between turning on the switch and igniting the lamp.
6. The lamp was turned off as soon as the desired exposure time was completed. A series of exposure times (from 1 to 10 min, at intervals of 1 min) was carried out. Triplicate runs for each exposure time were carried out.
7. The nitrogen cylinder was closed.
8. The treated sample was analyzed by a spectrophotometer and a new sample was prepared for the next run.

After the first series of UV exposure experiments on Rhodamine B, the second collimated beam apparatus replaced the first one. 30 min was also enough as the required time for supplying nitrogen before starting the lamp, since the second apparatus had a smaller volume than that of the first apparatus. At the same time, two SUPRASIL[®] Quartz cuvettes with stoppers were used to contain samples being exposed in place of Petri dishes. An 8 mm × 2 mm Teflon-coated micro stirring bar in each cuvette was used to mix the sample completely.

For the exposure experiments on Rhodamine B solutions at the same concentration (10 mg L⁻¹), two cuvettes were filled completely with samples (without air bubbles inside) and were exposed to the 172 nm UV light simultaneously under identical conditions. In

this way, duplicate runs were realized at the same time. A series of exposure times (5, 10, 15, 20 min) was carried out. Each sample was exposed to the UV light once.

For the exposure experiments on methanol solutions, 1.5 mL of methanol solution (15.04 mM) was transferred to both cuvettes with a 1 mL glass syringe. Then the outlet of a thin plastic tube was put above the surface of the samples (not submerged into the samples) to supply ultra high purity nitrogen to the cuvettes for 2 min to remove air from the cuvettes. A stopper closed the cuvette immediately after the purge was completed. One of the cuvettes was covered with aluminum foil as the blank (Figure 3.5b). The samples were exposed to the 172 nm UV light for 0.5, 1.0, 1.5, 2.0, and 2.5 h, respectively. Each exposure time was duplicated, and each sample was exposed to the UV light once. The procedures of the exposure experiments using the second apparatus were the same as that used in the first apparatus.

3.2.5 Sample Analyses

Rhodamine B solutions

Absorbances at a wavelength of 554 nm (the absorption maximum) of the exposed Rhodamine B solutions for different exposure times (A_t) were determined by an Ultraspec 2000 UV/visible spectrophotometer (Pharmacia Biotech, Fisher Scientific Co., Canada) in a 10 mm path length quartz cell (Fisher Scientific Co., Canada). Triplicate measurements for each sample were recorded. In addition, the absorbance of the initial stock solution (A_0) was also analyzed.

The degradation of Rhodamine B should follow first-order reaction kinetics

(Oppenländer and Xu, 2008). The model is (Equation [3.3]):

$$[3.3] \quad \ln \frac{C_t}{C_0} = -kt$$

where, C_t and C_0 represent the final and initial concentrations (M), respectively, of a Rhodamine B solution exposed to the VUV light for a length of time t (min); k is the first-order reaction rate constant (min^{-1}). The absorbance in a Rhodamine B solution at 554 nm follows the Beer-Lambert Law, in which the absorbance is proportional to the concentration and the path length. That is

$$[3.4] \quad A = \varepsilon \cdot C \cdot l$$

where, A is the net absorbance of a Rhodamine B solution at 554 nm (where the absorbance of a solvent blank has been subtracted); ε is the molar absorption coefficient of Rhodamine B in this solution ($\text{M}^{-1} \text{cm}^{-1}$); C represents the concentration of Rhodamine B in this solution; l is the path length (cm) (in this case, $l = 1$ cm). The $\ln [A_t / A_0]$ versus the corresponding exposure time was plotted, and the first-order reaction rate constant of the degradation of Rhodamine B was determined from the slope of the straight line.

Methanol solutions

The gas chromatography (GC) analyses of the UV exposed methanol solutions were performed with a GC (Model: CP-3800, Varian, Inc., USA) equipped with an autosampler (Model: CP-8410, Varian, Inc., USA). A CP-FFAP CB for free fatty acids capillary GC column (Varian, Inc., USA) was isothermally used at 60°C. The column size was 25 m × 0.32 mm × 0.45 mm (length × inner diameter × outer diameter). A 10 μL

glass syringe was used to inject 1.0 μL sample to the column at a split ratio of 10:1 for each measurement. A flame ionization detector (FID) was used to analyze the samples. The column flow (H_2 as a carrier gas) was 5 mL min^{-1} , and both the injector and the detector temperatures were 250°C . The molar concentrations of the methanol solutions were quantitatively determined by introducing a 1,4-dioxane solution at a concentration of 9.933 mM as an internal standard. For each methanol sample to be analyzed, one crimp top vial (National Scientific, USA) containing a mixture of 1 mL of the methanol sample and 0.5 mL of the 1,4-dioxane solution at a concentration of 9.933 mM transferred by a 1 mL glass syringe was measured three times by GC.

The calibration curve was plotted first before determining the sample concentrations. The mixtures of 1 mL of methanol solutions at each known concentrations (symbol: C_{MeOH}), which were 5.015, 10.03, 15.04, and 20.06 mM, with 0.5 mL of the 1,4-dioxane solution at 9.933 mM (symbol: C_{standard}) were prepared. The solutions were transferred using 1 mL glass syringes. For each methanol concentration, three mixtures were used, and each mixture was measured in triplicate by GC. The peak areas of methanol and 1,4-dioxane in each mixture were obtained from the results of GC chromatograms. The averages of peak areas of methanol and 1,4-dioxane at each methanol concentration, denoted by A_{MeOH} and A_{standard} , respectively, were calculated. Then a calibration curve of $C_{\text{MeOH}} / C_{\text{standard}}$ versus $A_{\text{MeOH}} / A_{\text{standard}}$ was plotted. The slope of this curve represented the calibration factor (F), which is represented by:

$$[3.5] \quad F = \frac{C_{\text{MeOH}} \cdot A_{\text{standard}}}{C_{\text{standard}} \cdot A_{\text{MeOH}}}$$

In the following UV exposure experiments, 1 mL of methanol sample exposed to the UV light was analyzed by GC using a mixture of 0.5 mL 1,4-dioxane solution at 9.933 mM. As a result, the methanol and 1,4-dioxane solutions were diluted by each other in the mixture. The concentration of methanol in the mixture was only 2/3 of that in the actual methanol sample, at the same time, the concentration of 1,4-dioxane in the mixture was 1/3 of 9.933 mM. Therefore, the actual concentration of a treated methanol sample was determined by Equation [3.6]:

$$[3.6] \quad C_{\text{MeOH}} = F \cdot \frac{A_{\text{MeOH}}}{A_{\text{standard}}} \cdot 9.933 / 2$$

3.2.6 Calculation of Fluence Rate (Irradiance) at 172 nm

According to Oppenländer and Schwarzwälder (2002), the first step of the actinometry method for calculating the fluence rate or irradiance of the 172 nm UV light is to determine the zero-order reaction rate constant (k_0) of methanol degradation in the aqueous solution exposed to the 172 nm UV light. Based on their conclusion, the degradation kinetics was dependent only on the initial concentration of the methanol solution. Zero-order kinetics was observed at the initial concentrations ranging from 75 to 250 mM.

After determining k_0 , the photon flow rate at 172 nm absorbed by the methanol solution was calculated in Equation [3.7].

$$[3.7] \quad P_{\text{abs}} = \frac{1}{0.946} \cdot k_0 \cdot \frac{V_R}{\Phi_{\text{H}_2\text{O}} \cdot \zeta_{\text{H}_2\text{O}} + \Phi_{\text{MeOH}} \cdot \zeta_{\text{MeOH}}}$$

where, P_{abs} : the absorbed photon flow rate, einstein s^{-1} ,

k_0 : the zero-order reaction rate constant, M s^{-1}

V_R : the total exposed volume (L), $V_R = 1.5 \text{ mL} = 0.0015 \text{ L}$,

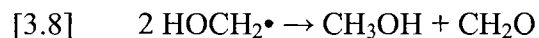
$\Phi_{\text{H}_2\text{O}}$: the total quantum yield of hydroxyl radical production, $\Phi_{\text{OH}} = 0.42$,

$\zeta_{\text{H}_2\text{O}}$: the fraction of photons absorbed by water,

Φ_{MeOH} : the total quantum yield of methanol photolysis, $\Phi_{\text{MeOH}} = 0.88$,

ζ_{MeOH} : the fraction of photons absorbed by methanol.

The factor of 0.946 in Equation [3.7] is related to the production of methanol by the disproportionation reaction of hydroxymethyl radicals ($\text{HOCH}_2\bullet$) (reaction [3.8]), which are intermediates during VUV-induced methanol mineralization in the aqueous solution. Hydroxymethyl radicals decrease the degradation rate of methanol. This contribution of 5.4% methanol production to the VUV photolysis of methanol was reported by Heit *et al.* (1998).



In addition,

$$[3.9] \quad \zeta_{\text{H}_2\text{O}} = k_{\text{H}_2\text{O}} / (k_{\text{H}_2\text{O}} + \varepsilon_{\text{MeOH}}^{172} \cdot [\text{MeOH}]_0)$$

$$[3.10] \quad \zeta_{\text{MeOH}} = \varepsilon_{\text{MeOH}}^{172} \cdot [\text{MeOH}]_0 / (\varepsilon_{\text{MeOH}}^{172} \cdot [\text{MeOH}]_0 + k_{\text{H}_2\text{O}})$$

where, $k_{\text{H}_2\text{O}}$: the linear absorption coefficient of pure water, cm^{-1} ,

$$k_{\text{H}_2\text{O}} (\text{at } \lambda = 172 \text{ nm}) = 550 \text{ cm}^{-1},$$

$\varepsilon_{\text{MeOH}}^{172}$: the molar absorption coefficient of methanol at 172 nm, $\text{M}^{-1} \text{cm}^{-1}$,

$$\varepsilon_{\text{MeOH}}^{172} = 162 \text{ M}^{-1} \text{cm}^{-1},$$

$[\text{MeOH}]_0$: the initial concentration of methanol, M.

$\zeta_{\text{H}_2\text{O}}$ and ζ_{MeOH} in Equations [3.9] and [3.10] were determined after substituting the known value for $[\text{MeOH}]_0$. Based on k_0 from the UV exposure experiments, P_{abs} was then determined.

On the other hand, the energy of photons per einstein at 172 nm [one einstein of photons is one mole (6.022×10^{23}) of photons] is:

$$[3.11] \quad U_{172} = N_A \cdot h \cdot \frac{c}{\lambda}$$

where, U_{172} : the energy of photons per einstein at 172 nm, J einstein^{-1} ,

N_A : the Avogadro number, mol^{-1} , $N_A = 6.0221 \times 10^{23} \text{ mol}^{-1}$,

h : the Planck constant, J s , $6.6261 \times 10^{-34} \text{ J s}$,

c : the speed of light, m s^{-1} , $2.9979 \times 10^8 \text{ m s}^{-1}$,

λ : the wavelength of light, m, at 172 nm, $\lambda = 172 \times 10^{-9} \text{ m}$.

Therefore,

$$\begin{aligned} U_{172} &= 6.0221 \times 10^{23} \text{ mol}^{-1} \times 6.6261 \times 10^{-34} \text{ J s} \times 2.9979 \times 10^8 \text{ m s}^{-1} / (172 \times 10^{-9} \text{ m}) \\ &= 695,496 \text{ J einstein}^{-1}. \end{aligned}$$

Finally, the fluence rate or irradiance on the surface of the sample was determined by:

$$[3.12] \quad E_0 = \frac{P_{\text{abs}} \cdot U_{172}}{\text{the surface area of the sample}} \cdot \frac{1}{1-R}$$

where, E_0 : the fluence rate or irradiance on the surface of the methanol sample, W cm^{-2} ,

the surface area of the sample: $3.8 \text{ cm} \times 0.95 \text{ cm}$, since the sample was contained

in the cuvette,

$(1 - R)$: the reflection factor,

R : the reflection coefficient, which is defined as:

$$[3.13] \quad R = \frac{(n_1 - n_2)^2}{(n_1 + n_2)^2}$$

where, n_1 and n_2 are the refractive indices of the two media, which are water and air in this case.

At the VUV wavelength of 172 nm, the refractive index of air is 1.002. The refractive index of water was determined by a model related to the Lorentz-Lorenz function (LL), which is expressed in detail by Equations [3.14] and [3.15] (Huibers, 1997):

$$[3.14] \quad LL = 0.233225 + 8.35872 \cdot 10^{-10} \cdot \lambda^2 + \frac{552.261}{\lambda^2} + \frac{852.502}{\lambda^2 - 18225.0} + \frac{311354}{\lambda^2 - 1.02400 \cdot 10^7}$$

where, λ : the wavelength of the light, nm.

$$[3.15] \quad LL = \left(\frac{n_1^2 - 1}{n_1^2 + 2} \right) \cdot \frac{1}{\rho}$$

where, n_1 : the refractive index of water,

ρ : the normalized density of water, at 25°C , $\rho = 0.99705$.

LL was calculated by substituting $\lambda = 172 \text{ nm}$ in Equation [3.14], then n_1 was determined by Equation [3.15], that is, 1.503. Therefore, $R = 0.040$, according to Equation [3.13].

3.3 Results and Discussion

3.3.1 Kinetics of Rhodamine B Degradation in VUV-irradiated Solutions

Rhodamine B molecules are oxidized and mineralized by hydroxyl radicals generated from the VUV-induced homolysis of water. Along with the degradation of Rhodamine B molecules, the red colour of the exposed Rhodamine B solution faded out. Therefore, the final absorbance at 554 nm was less than the initial absorbance.

The first-order reaction rate constants of Rhodamine B degradation in triplicate runs and their overall analysis are shown in Figure 3.6. The results in Figure 3.6 were obtained from experiments carried out in the first collimated beam apparatus with a 22 cm collimating tube. A_0 and A_t stand for the initial and final absorbances of an exposed sample at 554 nm. The detailed raw data and calculations are tabulated in Table B.1. Since the absorbance of a Rhodamine B solution is proportional to concentration, the decreasing rate of the absorbance is equal to that of the concentration. The error bars shown in Figure 3.6d represent the standard deviations of results in triplicate runs for each exposure time.

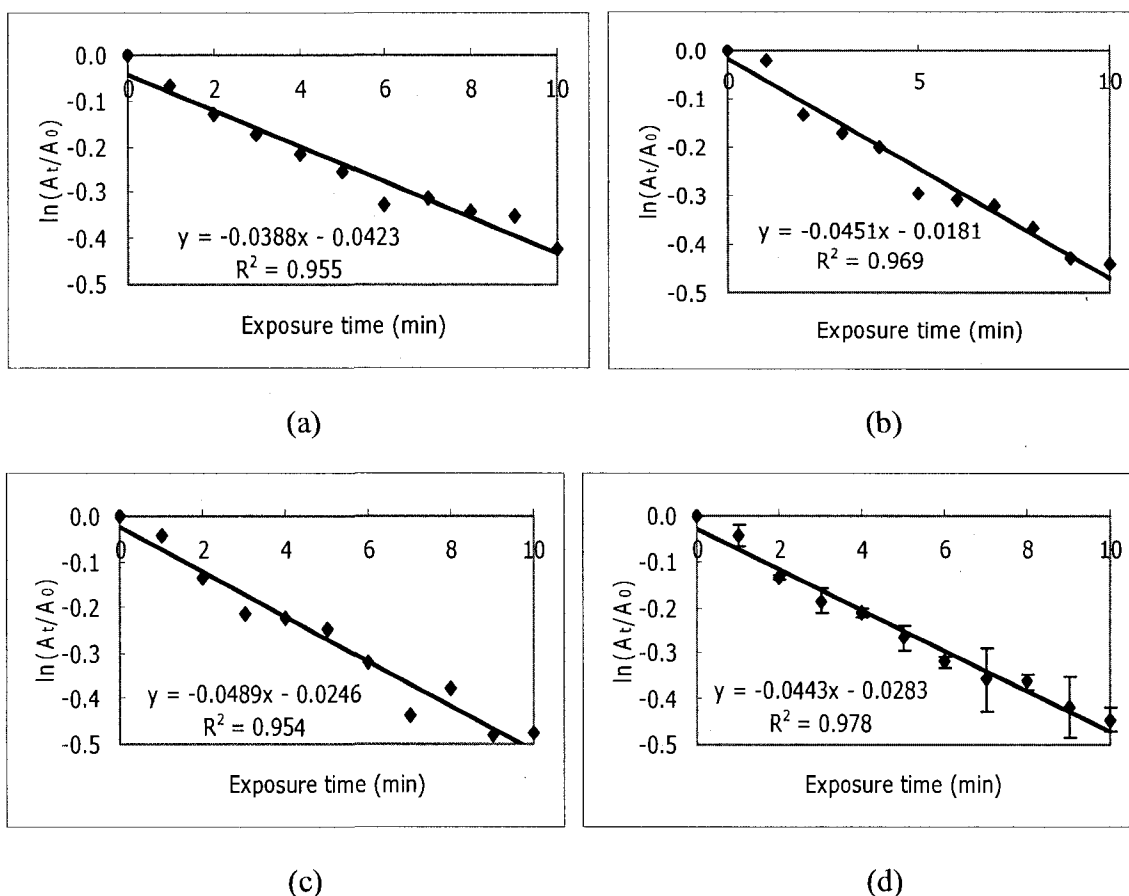


Figure 3.6 Concentration changes of Rhodamine B solutions induced by the Xe_2^* excilamp housed in the first collimated beam apparatus: (a) The first run; (b) The second run; (c) The third run; (d) The overall analysis of three runs

From Figure 3.6d, the average first-order reaction rate constant is 0.0443 min^{-1} . Compared with the results of Oppenländer and Xu (2007), which reported that the rate constant of Rhodamine B degradation was 0.852 min^{-1} in a Xe_2^* excimer flow-through photoreactor, the rate of degradation was 20 times lower. One of the probable reasons is the different setups of the experimental instruments, based on the following estimation.

The flow-through system consisted of a cylindrical Xe_2^* excilamp with an

irradiation length of 25 cm and an irradiation efficiency of about 10%. According to the electric input power of 140 W, the radiant power was about 14 W. Since the inner diameter of the lamp was 1.7 cm, which was approximately equal to the diameter of the flow channel containing the exposed sample, the irradiated surface area of the sample was 133.5 cm^2 ($3.14 \times 1.7 \text{ cm} \times 25 \text{ cm} = 133.5 \text{ cm}^2$). Thus, the approximate irradiance over the surface of the sample was 105 mW cm^{-2} ($14 \text{ W} / 133.5 \text{ cm}^2 \times 1000 \text{ mW W}^{-1} \approx 105 \text{ mW cm}^{-2}$). However, the lamp used here was operated at an input power of 35 W. Assuming that the irradiation efficiency was also 10%, the radiant power of this lamp was 3.5 W. The length of the lamp output window was 10 cm. The inner diameter of the collimating tube was 6.2 cm. Therefore about 60% of radiant power was captured by the collimating tube, which was about 2.1 W. Supposing that this 2.1 W as the radiant power was emitted by a point source, and the distance from the point source to the sample in the Petri dish was 24 cm, the irradiance over the surface of the sample was 0.29 mW cm^{-2} ($2.1 \text{ W} / [4 \times 3.14 \times (24 \text{ cm})^2] \times 1000 \text{ mW W}^{-1} = 0.29 \text{ mW cm}^{-2}$), which was about 360 times lower than that in the flow-through system. Considering the treated volume was 10 mL, 100 times lower than that in the flow-through system, the irradiance obtained per unit volume of the sample was 3.6 times lower than that in the reported system.

From the above estimation, the degradation rate of Rhodamine B should be about 3.6 times lower than that in the flow-through reactor, but the actual result is about 20 times. The reasons are probably that the actual irradiation efficiency of the lamp is lower than 10%, and the calculation hypotheses are not accurately consistent with the actual

conditions. For example, simplifying the lamp as a point source may not be accurate for this system. In addition, yellow dust, which was introduced in Section 3.2.2, is probably the primary reason. A significant proportion of radiant power may be attenuated by the absorption of yellow dust covering the quartz tube of the lamp.

Because of the unexpectedly low degradation rate of Rhodamine B, based on the results of Oppenländer and Xu (2007), the reaction rate of methanol in an aqueous solution in the first collimated beam apparatus was considered to be much lower, which would require an impractically long exposure time to achieve a detectable change of concentration. Therefore, it was determined to open the collimated beam apparatus and shorten the collimating tube, in order to increase the irradiance through the sample. However, the yellow dust was found and it eventually resulted in the replacement with the second collimated beam apparatus.

A 7 cm collimating tube was equipped in the second apparatus. The total path length of the beam from the lamp window to the surface of the sample solution was now only 8 cm. Two spectrophotometer cuvettes made of SUPRASIL[®] quartz were used. In this series of experiments, the cuvettes were completely filled with the Rhodamine B solution without any air bubbles inside. The reason is that the air in the bubble absorbs the VUV light and produces ozone. As a result, the sample cannot obtain the identical irradiance over the surface, and ozone, as another strong oxidant, probably contributes to the degradation of Rhodamine B and influences the accuracy of the results. Cuvette #1 and cuvette #2 were exposed to the UV light simultaneously to achieve duplicate runs. The

calculated first-order rate constants of duplicate runs and the overall analysis with the error bars are illustrated in the following plots. The detailed raw data and calculations are tabulated in Table B.2.

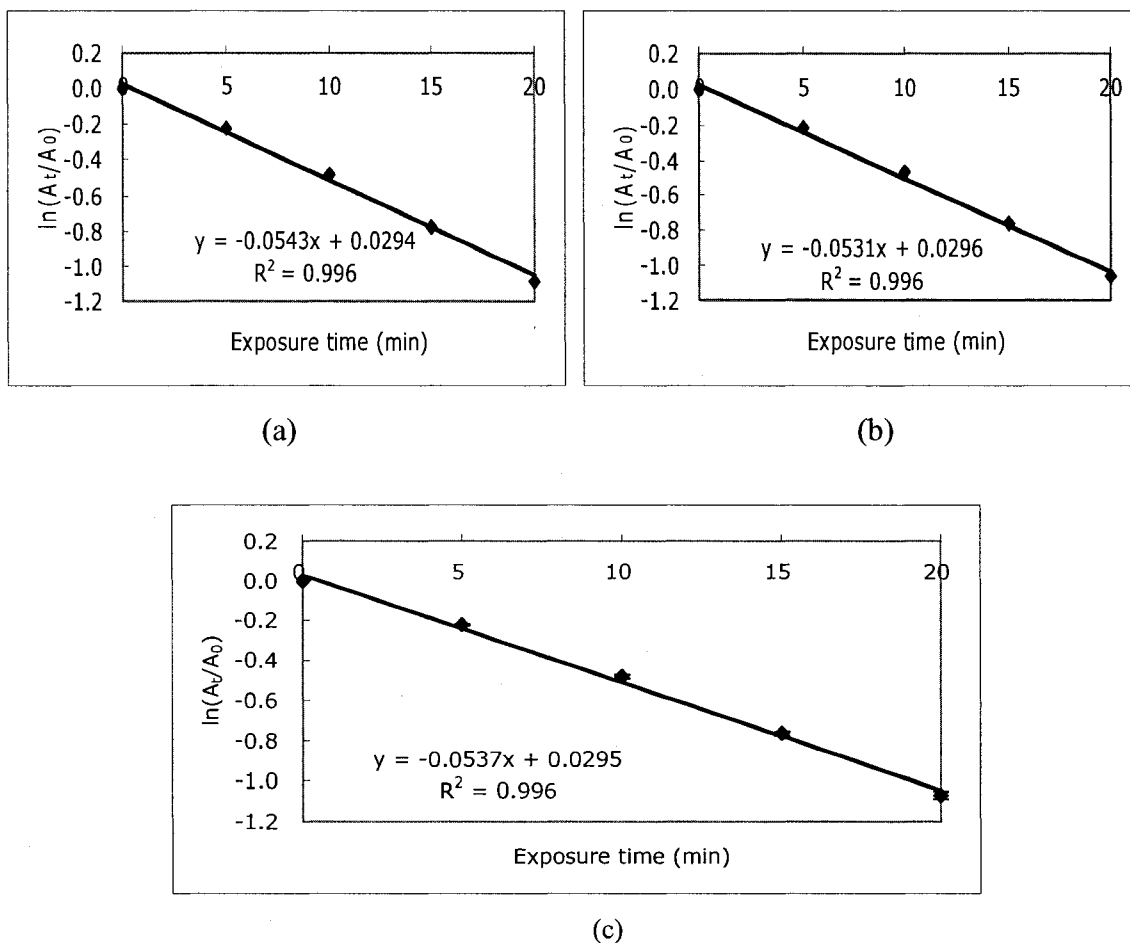


Figure 3.7 Concentration changes of Rhodamine B solutions induced by the Xe_2^* excilamp housed in the second collimated beam apparatus: (a) The first run (cuvette #1); (b) The second run (cuvette #2); (c) The overall analysis of 2 runs

Compared with the error bars in Figure 3.6, the reproducibility of the second series of Rhodamine B experiments was higher, since the cuvettes were used to contain the

exposed sample. With the stoppers, the cuvettes can effectively prevent the evaporation of the aqueous samples. This was very important in the following exposure experiments on methanol solutions, since methanol is a volatile compound. However, the rate of Rhodamine B degradation was not increased significantly, although the path length of the UV light decreased from 24 cm to 8 cm. This is partially because not 100% of radiant power can pass through the walls of the cuvettes. The transmission of a wall made of SUPRASIL[®] Quartz with the thickness of 1.5 mm was about 80% at 172 nm (Franke *et al.*, 2006; Hellma, 2007; Heraeus, 2008). The other reason is probably that the ratio of the surface area to the sample volume in cuvettes was much less than that in Petri dishes. In a Petri dish, a 10 mL treated sample spread over a surface area of 26.4 cm² with a depth of only about 3.8 mm. In contrast, in the cuvettes, the surface area of a 3.5 mL treated sample was about 3.6 cm² with a depth of 10 mm. Mixing tends to be incomplete at a larger depth, since, the penetration depth of the 172 nm UV light is very small (less than 0.1 mm). As a result, the lower ratio of the surface area to the volume in cuvettes caused the lower efficiency of UV photolysis. The aqueous sample with a smaller surface area receives a lower irradiance per volume. It gives rise to an inefficient treatment for the bottom part of the sample, and therefore brings about slower degradation.

3.3.2 Determination of a Methanol Calibration Curve for GC Analyses

Before determining an unknown concentration of a methanol solution exposed to the VUV light, a calibration curve for the internal standard method in GC was required. Mixtures of the methanol solutions and the 1,4-dioxane solution at known concentrations

and with known volumes were used. The triplicate and the overall calibration curves for the GC internal standard method are shown in Figure 3.8, summarized from the GC chromatograms. The detailed information has been introduced in Section 3.2.5. Raw data and calculations are tabulated in Table B.3.

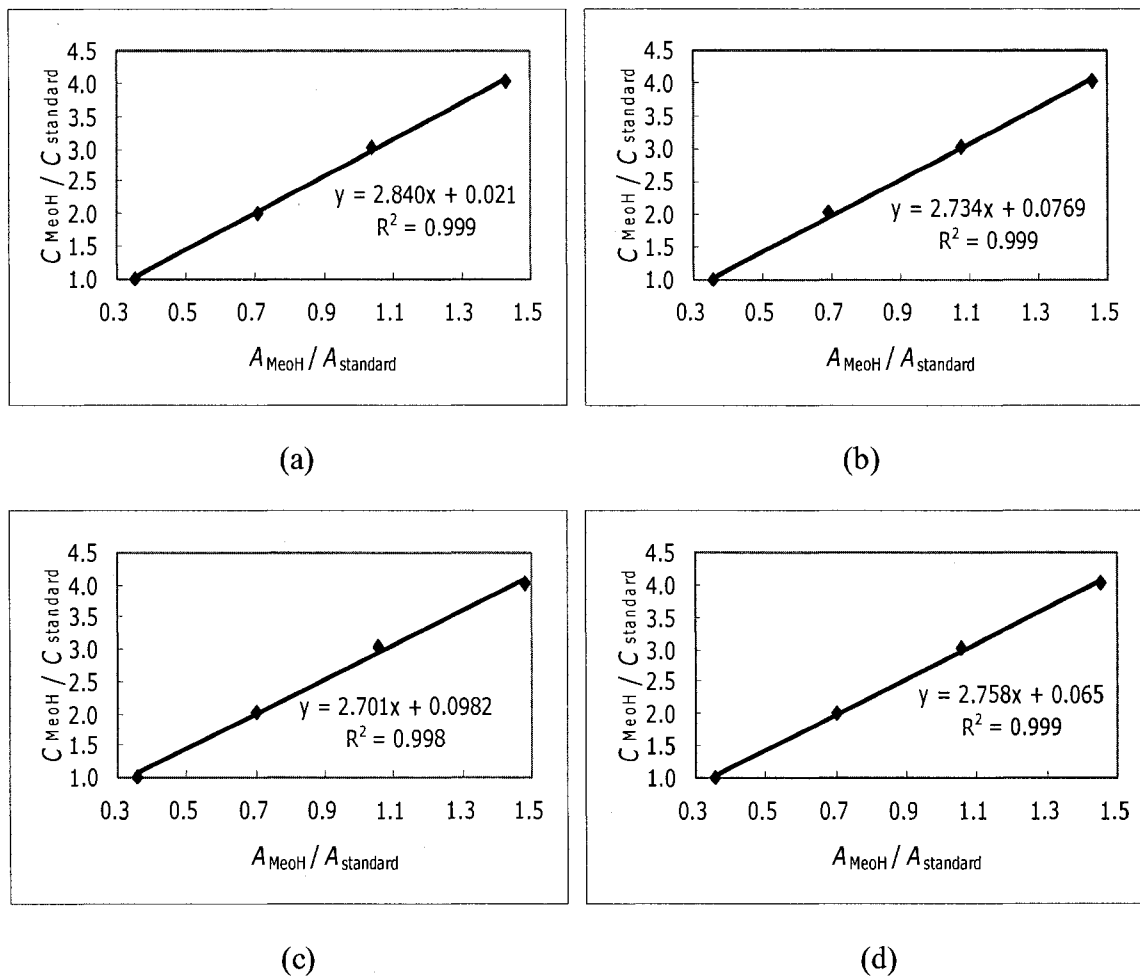


Figure 3.8 The calibration curves for the GC internal standard method: (a) Run 1; (2) Run 2; (3) Run 3; (4) The overall calibration curve based on the three runs

From Figure 3.8, it is clear that the ratio of A_{MeOH} to A_{standard} was proportional to the ratio of C_{MeOH} to C_{standard} in each run, with a high R^2 value (almost up to 1). The

percentage errors of three measurements for each mixture and three mixtures of triplicate runs at each concentration level were less than 2%, which are shown in Table B.3. This indicates that the analyses of methanol concentrations by GC were accurate and reliable. From Figure 3.8d, the overall calibration curve for triplicate runs was expressed by a mathematical model, which is highlighted in Equation [3.16].

$$[3.16] \quad C_{\text{MeOH}} / C_{\text{standard}} = 2.7582 \times A_{\text{MeOH}} / A_{\text{standard}} + 0.065$$

Equation [3.16] was used to determine unknown concentrations of the methanol solutions exposed to the VUV light in the following exposure experiments on methanol solutions at an initial concentration of 15.04 mM. The slope of the curve in Figure 3.8d was equivalent to the calibration factor (F) in Equation [3.5]. According to Equation [3.6], the actual concentration of a treated methanol sample was determined from:

$$[3.17] \quad C_{\text{MeOH}} = (2.7582 \times A_{\text{MeOH}} / A_{\text{standard}} + 0.065) \times (9.933 \times 1/3) / (2/3).$$

3.3.3 Kinetics of Methanol Degradation in VUV-irradiated Solutions

For the UV exposure experiments on the methanol solutions, a 1.5 mL sample volume in each cuvette was exposed. The reasons for using 1.5 mL as a volume of a treated sample are explained as follows. First, the smaller sample volume is shallower, which allows more intense mixing by the stirring bar and results in a higher efficiency of UV treatment. With a smaller volume, the degradation rate should increase. Second, this setup should increase the experimental accuracy. The exposure experiments were carried out with cuvettes fully filled with a methanol solution. But gas bubbles arose after UV exposure. The bubbles may be hydrogen produced from Reaction [2.7d]. These bubbles

caused a variation in irradiance over the sample surface. Hence, the sample to be treated with a volume of 1.5 mL was applied. The rest of space in a cuvette was occupied by nitrogen gas, which acts as a buffer zone. The hydrogen produced was able to migrate into the gas phase. The irradiance on the surface of the sample was not influenced, since hydrogen is transparent in this wavelength range.

Two cuvettes containing 1.5 mL of methanol stock solution at 15.04 mM were exposed to the UV light simultaneously, but cuvette #1 was always covered by aluminum foil during the exposure as a blank run. The final concentration of a treated solution in cuvette #2 was compared with that in cuvette #1, in order to determine the corrected decrease of the methanol concentration. The decrease of methanol concentration versus exposure time in duplicate runs and the overall analysis are illustrated below in Figure 3.9, with the raw data and detailed calculations attached in Table B.4 and Table B.5.

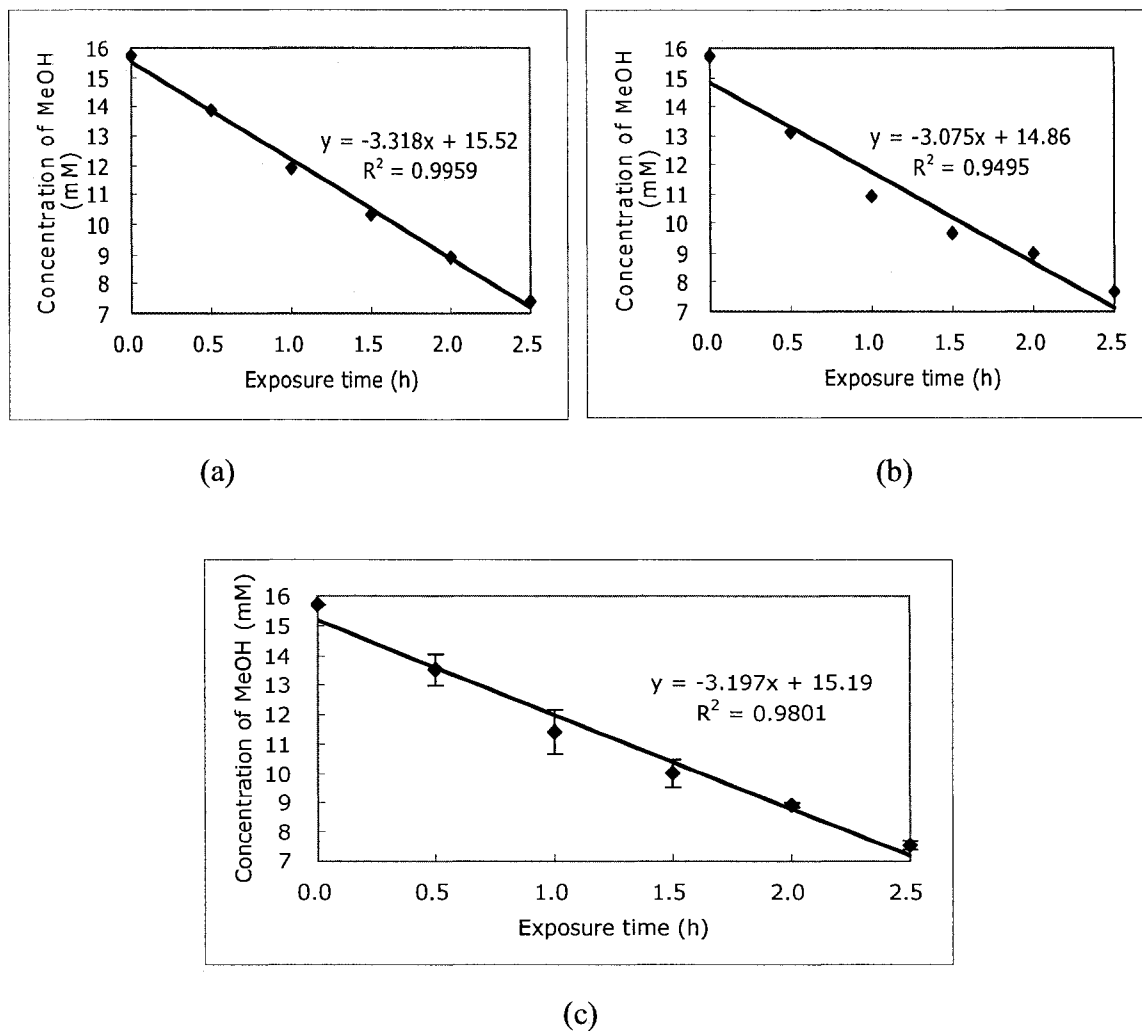


Figure 3.9 Concentration changes of treated methanol solutions as a function of VUV exposure time at 172 nm: (a) Run 1; (2) Run 2; (3) The overall degradation curve with error bars

According to Figure 3.9, the degradation of methanol followed zero-order reaction kinetics at the initial methanol concentration of about 15 mM. The average zero-order reaction rate constant (k_0) based on the duplicate runs was 3.20 mM h^{-1} , with the percentage error of 5.4% (i.e., $k_0 = 3.03$ to 3.37 mM h^{-1}), which equals to $8.88 \times 10^{-7} \pm$

5.4% M s^{-1} (i.e., $k_0 = 8.40 \times 10^{-7}$ to $9.36 \times 10^{-7} \text{ M s}^{-1}$). This result was different from that reported in Oppenländer and Schwarzwälder (2002), which indicated that first-order kinetics was observed at initial concentrations below 75 mM, whereas zero-order kinetics was observed at the initial concentrations from 75 to 150 mM. Based on this reported conclusion, the methanol solution at 15 mM should follow the first-order kinetics. But here, it followed zero-order kinetics. This may be because the operational conditions of UV exposure experiments were different. After all, the flow-through reactor used by Oppenländer and Schwarzwälder (2002) was very distinct from the collimated beam apparatus used here. The degradation of the methanol solution at an initial concentration of about 100 mM exposed to the VUV light for 3 h showed that the concentration changed less than the standard deviation of GC analyses at that concentration level, which means that the degradation was too low to be detected by GC (data not shown).

The average concentration of the stock solution in duplicate runs analyzed by GC was 15.72 mM, shown in Table B.5, which was a little higher than the theoretical concentration (15.04 mM). The transfer of samples to be treated from the stock solution may have caused the evaporation of two components in this solution (water molecules and methanol molecules), and hence led to the change of the methanol molar concentration. However, the difference between the concentrations measured by GC and theoretical concentration of the stock solution was not large. In addition, the percentage errors of measurements for stock solution concentration was only 1.06% and 0.55% in the first run and the second run, respectively (shown in Table B.5), which means that the

reliability of GC measurements was satisfactory.

It was obvious that the methanol concentration in cuvette #1 was less than the stock solution concentration, and along with the longer exposure time, the concentration in cuvette #1 tended to decrease further. In theory, the concentration of the solution that was not exposed to UV (i.e., covered with aluminum foil) should not change. But perhaps the foil could not intercept 100% of the UV light, therefore, a small portion of the UV light impinged on the solution and led to the concentration decrease. Consequently, the corrected concentration of a treated solution in cuvette #2 needed to be determined by subtracting the difference between the concentrations of stock solution and the concentration in cuvette #1 from the concentration in cuvette #2.

Since the initial concentration of methanol in stock solution was 15.72×10^{-3} M, substituting this value for $[\text{MeOH}]_0$ in Equations [3.9] and [3.10], $\zeta_{\text{H}_2\text{O}}$ and ζ_{MeOH} were calculated, as shown in Equations [3.18] and [3.19], respectively.

$$[3.18] \quad \zeta_{\text{H}_2\text{O}} = 550 \text{ cm}^{-1} / (550 \text{ cm}^{-1} + 162 \text{ M}^{-1} \text{ cm}^{-1} \times 15.72 \times 10^{-3} \text{ M}) = 0.9954$$

$$[3.19] \quad \zeta_{\text{MeOH}} = 162 \text{ M}^{-1} \text{ cm}^{-1} \times 15.72 \times 10^{-3} \text{ M} / (162 \text{ M}^{-1} \text{ cm}^{-1} \times 15.72 \times 10^{-3} \text{ M} + 550 \text{ cm}^{-1}) = 0.0046$$

Then, the absorbed photon flow (P_{abs}) was determined by Equation [3.20], derived from Equation [3.7]:

$$[3.20] \quad P_{\text{abs}} = \frac{1}{0.946} \times 8.88 \times 10^{-7} \text{ M s}^{-1} \times \frac{0.0015 \text{ L}}{0.42 \times 0.9954 + 0.88 \times 0.0046} \\ = 3.34 \times 10^{-9} \text{ einstein s}^{-1}$$

Based on Equation [3.12], the fluence rate or irradiance on the surface of the sample was

determined from:

$$\begin{aligned} [3.21] \quad E_0 &= \frac{3.34 \times 10^{-9} \text{ einstein s}^{-1} \cdot 695496 \text{ J einstein}^{-1}}{3.8 \text{ cm} \times 0.95 \text{ cm}} \cdot \frac{1}{1 - 0.040} \\ &= 0.000669 \text{ W cm}^{-2} = 0.669 \text{ mW cm}^{-2}. \end{aligned}$$

Considering the percentage error, the fluence rate was $0.669 \pm 5.4\% \text{ mW cm}^{-2}$ (i.e., $E_0 = 0.633$ to 0.705 mW cm^{-2}). This result was used in future experiments discussed in the next chapter on disinfection of *Bacillus subtilis* spores by the UV light at 172 nm emitted by the Xe₂* excilamp.

3.4 Conclusions

In this research, two collimated beam apparatuses, specially constructed for a Xe₂* excilamp with an emission maximum at 172 nm, were used. The second apparatus, used for most of the VUV exposure experiments, was an improved model based on the inadequacies of the first apparatus.

The VUV exposure experiments on Rhodamine B solutions, at a concentration of 10 mg L⁻¹ contained in a Petri dish or in spectrophotometer cuvettes were carried out in the first and the second collimated beam apparatus, respectively. Compared with the flow-through reactor used by Oppenländer and Schwarzwälder (2002), the degradation rate of Rhodamine B was lower than expected. The reasons were multiple, including a low irradiation efficiency, the production of yellow dust in the first apparatus from the VUV-induced degradation of the apparatus material, the absorption of the irradiance by

the walls of cuvettes, and the lower ratios of surface area to volume of the samples in cuvettes, which decreased the efficiency of VUV photolysis of the samples under incomplete mixing.

The VUV fluence rate or irradiance of the Xe₂* excilamp onto the sample was determined by an actinometry method with methanol in the aqueous solution as an actinometer. The degradation of methanol at an initial concentration of 15.04 mM followed zero-order reaction kinetics. Based on the degradation rate constant of methanol, the fluence rate or irradiance was calculated, which was $0.669 \pm 5.4\%$ mW cm⁻² (i.e., $E_0 = 0.633$ to 0.705 mW cm⁻²). This value was used in future experiments on the disinfection of *Bacillus subtilis* spores induced by VUV exposure.

CHAPTER 4

DISINFECTION EFFECT OF VACUUM-ULTRAVIOLET (VUV)-INITIATED TREATMENT ON *BACILLUS SUBTILIS* SPORES IN AQUEOUS SUSPENSION

4.1 Introduction

Vacuum-ultraviolet (VUV) photolysis of liquid water is one of the methods to produce hydroxyl radicals ($\bullet\text{OH}$), which play an important role in Advanced Oxidation Processes (AOPs). Relying on a high oxidation potential of hydroxyl radicals, AOPs are usually used to remove aqueous refractory contaminants (Tchobanoglous *et al.*, 2003). In addition, the inactivation of microorganisms with hydroxyl radicals has been investigated in some research papers. But most of the papers are limited to TiO_2 photocatalysis (TiO_2/UV). A few papers are related to AOPs involving the combination of UV and hydrogen peroxide ($\text{UV}/\text{H}_2\text{O}_2$), as well as the combination of UV and ozone (UV/O_3). A detailed introduction was given in Section 2.2.2. However, the disinfection effect of VUV-initiated treatment on microorganisms in aqueous suspension has not been quantitatively evaluated.

The disinfection mechanism by UVC exposure in the 220 – 290 nm germicidal range is quite different from that by hydroxyl radicals. The UVC light in that region disrupts the nucleic acids (such as DNA and RNA) of microorganisms, whereas hydroxyl

radicals primarily oxidize and disrupt the cell wall and membranes (resulting in lipid peroxidation) and therefore induce the disintegration of the cell walls. The inactivation of the microorganisms by hydroxyl radicals may also be partially caused by their penetration into the interior of the microorganism to react with enzymes and other intracellular components (Mamane *et al.*, 2007; Rincón and Pulgarin, 2004).

Bacillus subtilis spores are derived from their vegetative cells (i.e. growing cells), which are aerobic and facultative Gram-positive bacteria with a rod shape. The dormant endospores are formed in sporulation, a process induced by starvation for one or more nutrients. Without detectable metabolism, the spores lack most common high-energy compounds, including ATP and other nucleoside triphosphates (Douki *et al.*, 2005; Setlow, 1992a). The spores can survive for a very long period of time even in a hydrated state. For example, at least 50% survival of spores stored in water at 6 to 10°C for at least one year is commonly observed (Setlow, 1992a). Spores are also extremely resistant to various harsh treatments, such as heat, desiccation and toxic chemicals. At the same time, they have 10- to 50-fold more resistance to UV light than the corresponding vegetative cells (Setlow, 2001; Setlow and Setlow, 1993a).

The structure of a spore surrounded by several layers is very different from that of a vegetative cell. From the outside in, these layers include the exosporium, the proteinaceous spore coat, the cortex composed of peptidoglycan, and the central core containing normal cell structures, such as spore enzymes, ribosomes, and spore DNA (Setlow, 1995). Whether an exosporium of the *B. subtilis* spore exists or not is debatable.

But it is certain that a *Bacillus anthracis* spore, which is closely related genetically to *B. subtilis*, contains exosporium, which is mainly constituted of different proteins (Liu *et al.*, 2007; Mehta *et al.*, 2006). Waller *et al.* (2004), using the ruthenium red staining, observed an external glycoprotein layer surrounding a spore of *B. subtilis*, and therefore deduced the existence of the exosporium of *B. subtilis* spores, which consists of glycoproteins.

B. subtilis spores are used extensively as a surrogate in UV disinfection studies. The reasons are as follows, since the spores:

- (1) are highly resistant to UV exposure;
- (2) survive for a long period of time;
- (3) are easy and inexpensive to culture;
- (4) can be enumerated using standard microbiological techniques;
- (5) cause little or no human health or environmental risk (Craik *et al.*, 2002; Kang, 2008).

The objective of this chapter is to evaluate quantitatively the disinfection effect of the VUV-initiated treatment on *B. subtilis* spores.

4.2 Materials and Methods

4.2.1 *Bacillus subtilis* Methods

A stock suspension of *B. subtilis* (ATCC 6633, American Type Culture Collection, Manassas, VA.) at a concentration of about 3×10^8 CFU mL⁻¹ was produced by using the

modified Shaeffer Medium method. Spores in the stock suspension and experimental samples were enumerated by using a pour plate method. All of the sterile media, reagents and materials were sterilized by autoclaving at 121°C for 15 min or were purchased pre-sterilized. All experimental steps involving exposing *B. subtilis* spores to air (except the UV exposure experiments in the collimated beam apparatus) were performed in a biological safety cabinet (Model 1284 Class II A/B3, Forma Scientific Co., Marietta OH.), in order to avoid accidental contamination. In addition, the cabinet was started 20 min before use, and the LP UV lamp in it was turned on during this period of time.

The details of *B. subtilis* spores production, purification and enumeration are given in Appendix A, according to a guidance manual compiled by Guest (2004) and the thesis of Uvbiama (2006).

4.2.2 VUV Exposure Experiments

The second collimated beam apparatus for the Xe₂* excilamp (shown in Chapter 3) was used in the disinfection experiments on *B. subtilis* spores. The procedure was similar to that of the experiments on methanol solutions discussed in the previous chapter. The approximate 10⁻² diluted spore suspension to be exposed by Xe₂* excilamp at a concentration of about 3.5 × 10⁶ CFU mL⁻¹ was prepared by transferring 1 mL aliquot of spore stock suspension into 100 mL sterile DI water. A sample of 1.5 mL of this 10⁻² diluted spore suspension was transferred into each of two SUPRASIL[®] Quartz cuvettes using a 1 mL glass syringe. Ultra high purity nitrogen was supplied for 2 min to remove the air from the cuvettes, in the same manner as was described in the methanol exposure

experiments. The cuvette #1 was always covered by aluminum foil as a blank run. Before adding the cell suspensions, the dry cuvettes were sterilized by the exposure to UV light emitted by a LP UV lamp in the biological safety cabinet for 15 min. The samples were exposed to the 172 nm VUV light for 5, 10, 15, 30, 60 min, respectively. Each exposure time was carried out in triplicate, and each sample was exposed only once.

4.2.3 The Fluence Determination with VUV Light

The average fluence rate E_0 (mW cm^{-2}) of the Xe_2^* excilamp in the collimated beam apparatus was constant over time, which was calculated in the previous chapter using the actinometry method. It was determined to be 0.669 mW cm^{-2} . Therefore, the fluence F (mJ cm^{-2}) is given by the fluence rate times the exposure time t (s), which is described in Equation [4.1].

$$[4.1] \quad F = E_0 \times t$$

4.2.4 Inactivation Kinetics

The initial concentration N_0 (CFU mL^{-1}) of *B. subtilis* spores before exposure to VUV was determined from enumeration of the 10^{-2} diluted spore suspension, and the final concentration, N , (CFU mL^{-1}) of viable spores after a given VUV exposure was determined from enumeration of an exposed sample in cuvette #2. Both N and N_0 were calculated from the geometric mean of the colony forming units (CFU) of the triplicate Petri dishes, and the log inactivation was calculated by Equation [4.2].

$$[4.2] \quad \text{Log Inactivation} = \log_{10} \frac{N_0}{N}$$

The fluence-response curve was then obtained from the plot of the log inactivation versus the fluence (USEPA, 2006b). The shape of the fluence-response curve typically has three regions: a shoulder region at a low fluence, where little inactivation occurs; a log-linear region at a mid-range fluence, where the first-order inactivation is observed; and a tailing region at a high fluence, where the slope of the curve decreases with increasing fluence (Mamane-Gravetz and Linden, 2005; USEPA, 2006b).

The fluence-inactivation relationship with the shoulder phenomenon was properly described using the target theory, which states that there are a finite number of critical targets on every individual cell, and these targets are vulnerable and randomly attain the hits. Because the spores have double-stranded DNA, several targets n_c require one hit (multi-target) or one target requires a series of hits n_c (multi-hit) before a full inactivation of the microorganism occurs (Severin *et al.*, 1983; Uvbiama, 2006). Since both multi-target and multi-hit kinetics models can predict the fluence-inactivation relationship appropriately in a batch reactor (Severin *et al.*, 1983), the multi-target model was used here, which is described by Equation [4.3] (Cabaj *et al.*, 2002).

$$[4.3] \quad \frac{N}{N_0} = 1 - (1 - 10^{-kF})^{n_c}$$

where, N_0 is the initial concentration of the *B. subtilis* spore suspension before exposure, CFU mL⁻¹; N is the final concentration of viable spores in a UV exposed sample, CFU mL⁻¹; k is the first-order inactivation rate constant, which is equal to the slope of the

fluence-response curve in the log-linear region, $\text{cm}^2 \text{mJ}^{-1}$; F is the fluence, mJ cm^{-2} ; and n_c represents the number of critical targets, which is closely related to the shoulder.

The multi-target model was used to describe the inactivation kinetics of *B. subtilis* spores exposed to the UVC light at the wavelengths of 222 and 254 nm, which will be introduced in the next chapter. For this chapter, since no shoulders were observed, a simple model, the Chick-Watson model (Equation [4.4]) was used to describe the disinfection kinetics of spores exposed to the VUV light.

$$[4.4] \quad \log_{10} \frac{N_0}{N} = kF$$

4.3 Results and Discussion

4.3.1 Fluence-response Curve of *B. subtilis* Spores using VUV Light

Spore enumeration data are tabulated in Table B.6, Appendix B-2. The log inactivation of *B. subtilis* spores as a function of the fluence is presented in Figure 4.1. The error bars represent the standard deviations. From Figure 4.1, the fluence-response curve shows a log-linear region at fluences varying from approximately 0 to 600 mJ cm^{-2} , and a tailing region at higher fluences. A shoulder region is not apparent. Therefore, the Chick-Watson model, which is able to predict the log-linear model, was used to simulate the relationship between the log inactivation and the fluences from 0 to 600 mJ cm^{-2} . Since the log inactivations at about 1200 and 2400 mJ cm^{-2} deviate from the log-linear region,

these points were ignored. Hence, the mathematical model of the fluence-response curve of *B. subtilis* spores with VUV light is shown in Equation [4.5]:

$$[4.5] \quad y = 0.0022x$$

where, y represents the value of log inactivation, which is $\log(N_0/N)$; x represents the fluences from 0 to 600 mJ cm^{-2} at 172 nm, which were determined by the actinometry method described in detail in Chapter 3; 0.0022 represents the first-order inactivation rate constant, $\text{cm}^2 \text{ mJ}^{-1}$, in which the regression line was forced through zero.

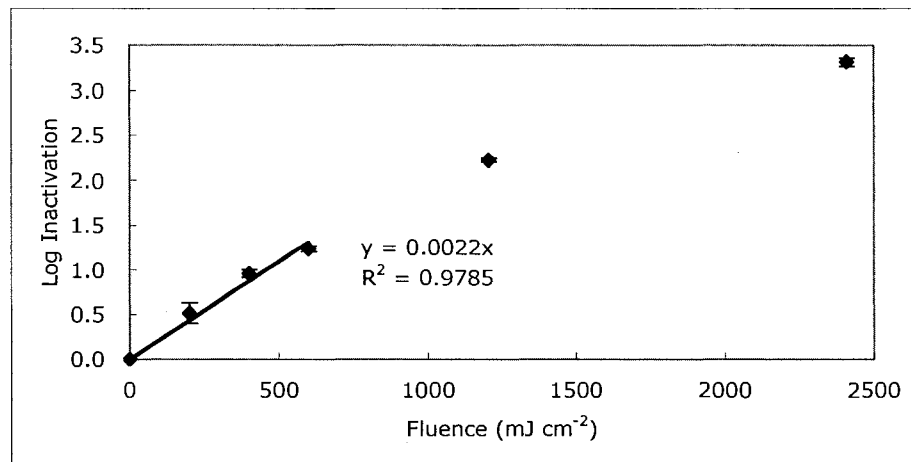


Figure 4.1 Fluence-response curve of *B. subtilis* spores with VUV light at 172 nm

From Figure 4.1, the 2 log reduction of *B. subtilis* spores required the fluence of 909 mJ cm^{-2} . The corresponding exposure time was about 23 min in terms of the collimated beam apparatus used here.

4.3.2 The Mechanisms of VUV Disinfection

The disinfection efficacy of the VUV light relies on the presence of hydroxyl

radicals ($\bullet\text{OH}$), which are generated by the VUV-initiated photolysis of water. Few research papers have related the VUV disinfection of *B. subtilis* spores, but many papers have discussed the probable mechanisms of disinfection of *Escherichia coli* or viruses using other AOPs. The mechanisms of VUV disinfection of *B. subtilis* spores can be deduced from these publications.

Most of the papers related to $\bullet\text{OH}$ radical induced disinfection focused on the photocatalysis (i.e. UV + TiO_2). The UV light used for photocatalytic TiO_2 reaction is usually in the UVB and the UVA regions. Some of them proposed the probable mechanisms of photocatalysis disinfection of microorganisms. Actually, the mechanism of the photocatalytic cell death has not been clearly elucidated and is still being discussed (Rincón and Pulgarin, 2006). However, other oxidizing agents, such as chlorine and ozone have been studied extensively. Chlorine can alter the bacterial cell permeability, which leads to leakage of the cytoplasm, and subsequently other chlorine molecules can diffuse into the cell to oxidize nucleic acids and proteins. Ozone can disrupt the function of the cell membrane to inactivate the cell metabolism (Watts *et al.*, 1995). Therefore, when hydroxyl radicals, which have a higher oxidation potential than do chlorine and ozone molecules, contact a cell, they probably induce surface oxidations (presumably by hydrogen abstractions or electrophilic additions to C=C double bonds) of the cell wall and cell membrane molecules that result in disruption of the cell membrane and subsequently disintegration of the cell. Saito *et al.* (1992) found leakage of intracellular potassium ions induced by hydroxyl radicals, which represents the significant disorder of

the cell membrane. At the same time, since the phenomenon that hydroxyl radicals react with most biological molecules at diffusion-control rates, they may diffuse into the cell to inactivate the enzymes, damage the intracellular components and interfere with the protein synthesis (Watts *et al.*, 1995; Mamane *et al.*, 2007). Consequently, Watts *et al.* (1995) proposed that the disinfection of hydroxyl radicals may be limited by mass transfer through the cell wall or cell membrane.

Maness *et al.* (1999) proposed for the first time that hydroxyl radicals attack the polyunsaturated phospholipids of the cell membrane of *E. coli* and cause lipid peroxidation reactions. These reactions subsequently result in alternations of the membrane architecture and conformational changes in many membrane-bound proteins and electron mediators. These changes can cause a breakdown of the cell membrane structure and membrane functions and therefore induce cell death. As a result, they pointed out that the disorder of the cell membrane was the root of the killing effect by hydroxyl radicals.

Sunada *et al.* (2003) found that the outer membrane of the cell wall of an *E. coli* cell acts as a barrier to the photocatalysis disinfection process. They also proposed that the peptidoglycan layer of the cell wall did not have such a barrier function, since the concentration of peptidoglycan did not change during the reaction. *E. coli*, as a species of Gram-negative bacteria, has a thin cell wall consisting of a layer of peptidoglycan surrounded by an outer lipid membrane containing phospholipids, lipopolysaccharides and lipoproteins. When hydroxyl radicals encounter the outer surface of the cell, reactions

start with a partial decomposition of the outer membrane. During this process, the cell viability is not lost significantly, but the permeability of the outer membrane is changed. This change enables hydroxyl radicals to penetrate through the peptidoglycan layer and arrive at the inner membrane (i.e., the cytoplasmic membrane) of the cell. Subsequently, the cytoplasmic membrane is attacked by hydroxyl radicals leading to the peroxidation of membrane lipids, which eventually causes cell death.

In contrast, Du and Gebicki (2004) proposed that the proteins were the initial cell targets of hydroxyl radicals, prior to cell lipids and DNA. They found a significant formation of protein peroxides before the lipid peroxidation or DNA damage when cells were exposed to hydroxyl radicals.

A hypothesis of the mechanism of *B. subtilis* spores inactivation by hydroxyl radicals can be deduced from the above discussions. Presumably, the disinfection of *B. subtilis* spores is primarily caused by the oxidation and disruption of the cell membrane. The breakdown of the cell membrane perhaps results from the peroxidation of polyunsaturated phospholipids or the peroxidation of proteins. In addition, a minor disinfection effect may be attributed to the reactions between hydroxyl radicals that have penetrated into the spore core and the intracellular components. Before the reaction of hydroxyl radicals with the cell membrane, the outer structure of a spore, which consists of the exosporium, the spore coat and the cortex, is probably destroyed by hydroxyl radicals in turn. Since the exosporium and spore coats are constituted of proteins (Setlow, 1995; Martins *et al.*, 2002), they tend to be oxidized easily. However, since the primary

component of the cortex is peptidoglycan, hydroxyl radicals can perhaps penetrate through it to oxidize the cell membrane without the destruction of the cortex.

4.3.3 Comparison of Disinfection Effect of VUV-induced AOP with Other AOPs

Many research papers reported the disinfection results of microorganisms (primarily for *E. coli*) by AOPs (especially photocatalysis, i.e., UV + TiO₂). The results varied very largely, which are shown in Table 4.1. The variation of the results is maybe related to the different initial concentrations of microorganism samples, the different light sources and fluences, the different disinfectant concentrations, and the different temperatures, etc.

Table 4.1 Logs inactivation of microorganisms by AOPs reported by published papers

Log Inactivation	Kind of Microorganism	Disinfection Method	Disinfection time	Reference
1.5	<i>E. coli</i>	TiO ₂ (1 g L ⁻¹) + UVA (265 nm, 0.8 mW cm ⁻²)	30 min	Maness <i>et al.</i> (1999)
2	<i>E. coli</i>	TiO ₂ film + UVA (0.8 mW cm ⁻²)	50 min	Sunada <i>et al.</i> (2003)
3	<i>E. coli</i>	TiO ₂ (1 g L ⁻¹) + simulated solar irradiation	30 min	Rincón and Pulgarin (2004)
2	<i>E. coli</i>	TiO ₂ (1 g L ⁻¹) + UVA	120 min	Cho <i>et al.</i> (2004)
4	<i>E. coli</i>	TiO ₂ (0.5 g L ⁻¹) + UVA + H ₂ O ₂ (25 mg L ⁻¹)	10 min	Paleologou <i>et al.</i> (2007)
1.5	<i>E. coli</i>	H ₂ O ₂ (25 mg L ⁻¹) + UV (> 295 nm)	7.5 min	Mamane <i>et al.</i> (2007)
1	Total coliform	TiO ₂ (250 mg L ⁻¹) + UVA	75 min	Watts <i>et al.</i> (1995)
2	Poliovirus	TiO ₂ (250 mg L ⁻¹) + UVA	30 min	Watts <i>et al.</i> (1995)
0.4	<i>B. subtilis</i> spores	O ₃ (2.5 mg L ⁻¹) + H ₂ O ₂ (1.5 mg L ⁻¹)	10 min	Sommer <i>et al.</i> (2004)

This research showed that the hydroxyl radicals can inactivate *B. subtilis* spores. This is consistent with the conclusion of Cho *et al.* (2002). On the other hand, the spores are more resistant to hydroxyl radicals than *E. coli*. This was shown by Mamane *et al.* (2007), who found 1 log inactivation of *E. coli* after exposure to hydroxyl radicals for 15 min, but no inactivation of *B. subtilis* spores was observed even when exposed for longer times using the UV/H₂O₂ AOP. Therefore, compared with the results enumerated in Table

4.1, the concentration of hydroxyl radicals generated by VUV-initiated photolysis of water should be higher than that in most of the previously published papers, since 2 log inactivation of *B. subtilis* spores was obtained after VUV exposure for 23 min. This means VUV-initiated photolysis of water is more efficient in generating hydroxyl radicals and more effective for the inactivation of microorganisms, compared with other AOPs, such as TiO₂/UV, H₂O₂/UV and O₃/H₂O₂.

Moreover, this conclusion can be supported by quantitative estimation. According to Mamane *et al.* (2007) and Cho *et al.* (2004), the hydroxyl radical concentration in aqueous solution can be indirectly determined by the rate of consumption of a probe compound, *para*-chlorobenzoic acid (*p*CBA). In the TiO₂ photocatalytic system with 1 g L⁻¹ TiO₂ established by Cho *et al.* (2004), the hydroxyl radical concentration was approximately 6.8×10^{-8} mg L⁻¹. Based on the disinfection results of Mamane *et al.* (2007), this value was about 5.2×10^{-10} mg L⁻¹. In addition, Cho *et al.* (2003) pointed out that 2 log inactivation of *B. subtilis* spores probably require a CT (the concentration of the disinfectant *C* times the exposure time *t*) value of hydroxyl radicals at 1.7×10^{-4} mg min L⁻¹. In this sense, if the difference of *B. subtilis* spores resistance to oxidation between this research and Cho *et al.* (2003) is overlooked, the hydroxyl radical concentration here was about 7.4×10^{-6} mg L⁻¹ (1.7×10^{-4} mg min L⁻¹ / 23 min = 7.4×10^{-6} mg L⁻¹), which is much higher than that generated by the other AOPs. Although this estimation is very inaccurate, the trend of higher hydroxyl radical concentration generated by 172 nm photolysis of water should be viable.

4.3.3 Comparison of Disinfection Effect of AOPs with Other Disinfection Methods

The disinfection effect of VUV-initiated AOP on *B. subtilis* spores is also compared with other disinfection methods using different disinfectants. Table 4.2 shows the doses of some disinfectants required by 2 log inactivation of *B. subtilis* spores published in research papers.

Table 4.2 Disinfection doses of different disinfection processes required by 2 log inactivation of *B. subtilis* spores

Disinfection Process	Disinfection Dose	Reference
Ozone	CT = 3.5 mg min L ⁻¹ (pH = 7.4)	Dow <i>et al.</i> (2006)
Ozone	CT = 4.9 mg min L ⁻¹ (pH = 7)	Jung <i>et al.</i> (2008)
Ozone	CT = 3.2 mg min L ⁻¹ (pH = 5.6)	Cho <i>et al.</i> (2006)
Free chlorine	CT = 410 mg min L ⁻¹ (pH = 8.2)	Son <i>et al.</i> (2005)
Free chlorine	CT = 370 min L ⁻¹ (pH = 8.2)	Cho <i>et al.</i> (2006)
Chlorine dioxide	CT = 34 mg min L ⁻¹ (pH = 8.2)	Cho <i>et al.</i> (2006)
UV at 254 nm	Fluence = 30 mJ cm ⁻²	Jung <i>et al.</i> (2008)
UV at 254 nm	Fluence = 22 mJ cm ⁻²	Cho <i>et al.</i> (2006)

According to Table 4.2, the CT value of hydroxyl radicals for achieving 2 log inactivation of *B. subtilis* spores (1.7×10^{-4} mg min L⁻¹) is much lower than that of other disinfectants. This means hydroxyl radicals are extremely efficient and fast in inactivating the spores. However, the concentration of hydroxyl radicals generated by AOPs is also extremely low, which is only 10^{-6} to 10^{-10} mg L⁻¹. In contrast, other disinfectants can achieve high concentrations, such as tens to hundreds mg L⁻¹. Therefore, the disinfection

time required by AOPs is still very long, which means AOPs are not an efficient method used for the disinfection of microorganisms.

4.4 Conclusions

In this chapter, the fluence-response curve of *Bacillus subtilis* spores exposed to hydroxyl radicals of VUV-initiated AOP was plotted. From the curve, a mathematical model was determined to describe the relationship between the fluence at 172 nm and the log inactivation of spores. Finally, the fluence required by a 2 log inactivation of the spores was calculated, which was 909 mJ cm^{-2} .

The mechanisms of disinfection of *B. subtilis* spores by hydroxyl radicals are not clear yet. The hypothesis of the mechanisms is that the disinfection is primarily caused by the oxidation and disruption of the cell membrane by hydroxyl radicals. Breakdown of the cell membrane may result from the peroxidation of polyunsaturated phospholipids or the peroxidation of proteins. Before destruction of the cell membrane, the outer structure of the spores, which consists of the exosporium, the spore coats and the cortex, is destroyed by hydroxyl radicals. Or perhaps hydroxyl radicals can penetrate through the cortex to oxidize the cell membrane without the destruction of the cortex.

Compared with the data published in previous papers, the concentration of hydroxyl radicals generated by VUV-initiated photolysis of water here is probably higher than with other AOPs, which means that the VUV-initiated AOP is an efficient method. However,

compared with the data of other disinfection methods, AOPs are not an effective and practicable process for the use of microorganism inactivation in water treatment.

CHAPTER 5

DISINFECTION EFFECTS OF 254 NM AND 222 NM UV LIGHT ON *BACILLUS SUBTILIS* SPORES IN AQUEOUS SUSPENSION

5.1 Introduction

UV treatment has been used for water and wastewater disinfection for many years. This technology is becoming popular as an alternative disinfection technology to chlorination, due to its ability to inactivate pathogenic microorganisms without forming regulated disinfection by-products. The practical germicidal wavelength of UV light is defined as the range between 200 and 280 nm, which lies in the UVC range, since it is more effective in inactivating bacteria and viruses than other ranges. In this range, UV light is absorbed by DNA, RNA and proteins of microorganisms.

A low-pressure (LP) mercury lamp used in this research is the most common lamp utilized in UV disinfection processes. Since the output of a LP UV lamp is primarily at 253.7 nm, the LP UV lamp is considered to be the monochromatic lamp in the germicidal UV region. In addition, 253.7 nm is close to the maximum DNA absorption wavelength of 260 nm; also at this wavelength the absorbance of proteins is much lower than that of DNA. Therefore, the photons at 253.7 nm are primarily absorbed by the DNA of microorganisms resulting in the damage of DNA by altering nucleotide base pairing,

especially the formation of thymine dimers. As a result, the LP UV lamp is also called a germicidal lamp.

A dielectric barrier discharge KrCl* excilamp with the emission maximum at 222 nm was also used. It is a monochromatic lamp, since the half-width of its emission band is only about 4.5 nm (Tarasenko *et al.*, 1998). The typical emission spectrum of a KrCl* excilamp is illustrated in Figure 5.1 (Ikematsu *et al.*, 2004). The absorbance of DNA at 222 nm is lower than that at 253.7 nm, but the absorption coefficient of proteins increases sharply as the wavelength decreases from 240 nm (Kirschenbaum, 1972). For example, trypsin, a kind of enzyme, which is used to degrade proteins in the digestive system, has an absorption coefficient at 222 nm over 10 times higher than that at 253.7 nm (Setlow, 1960). However, Bolton (2001) indicated that the disruption of DNA, which inhibits the ability of the replication of microorganisms, requires much lower fluence than the disruption of cell membranes, which is caused by the absorption of UV by proteins. But it is not certain that the efficiency of disinfection of *B. subtilis* spores with UV light at 222 nm is lower than that at 254 nm, since pyridine-2,6-dicarboxylic acid or dipicolinic acid (DPA) in spores, which has a higher absorption coefficient at 222 nm than that at 254 nm, plays an important role in photochemical reactions of spore DNA (Setlow and Setlow, 1993a).

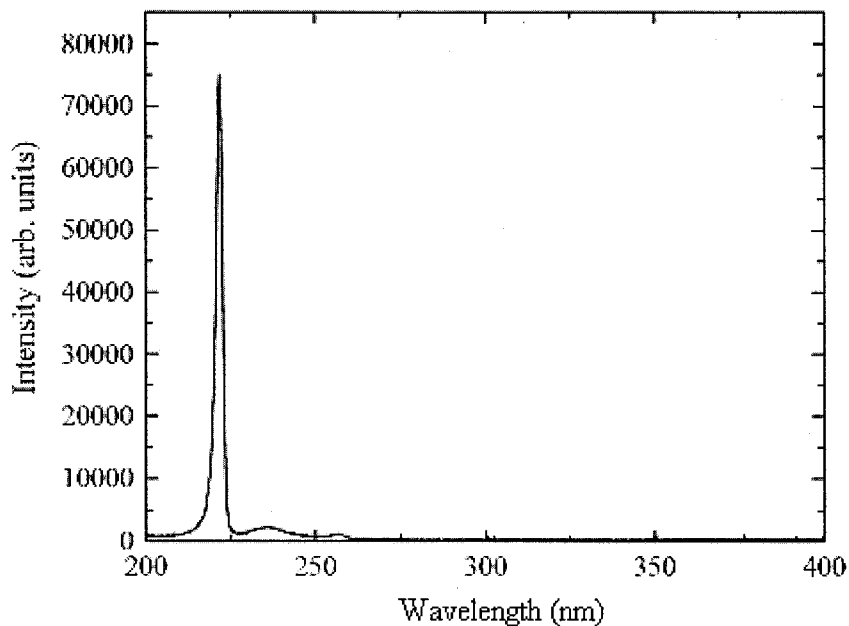


Figure 5.1 Typical light emission spectrum of a KrCl* excilamp

The objective of this chapter is to determine fluence-response curves of *Bacillus subtilis* spores at 254 nm and 222 nm and to compare them with each other, as well as with the result of 172 nm that has been given in Chapter 4.

5.2 Materials and Methods

5.2.1 UV Lamps and Collimated Beam Apparatus

UV exposure experiments were carried out using a collimated beam apparatus (Model: PSI-1-120, Calgon Carbon Corporation, USA) (Figure 5.2). A 10 W LP UV lamp (Ster-L-Ray Germicidal Lamp, Model: G12T6L 15114, Atlantic Ultraviolet Corporation, USA) was used for UV exposure experiments on *B. subtilis* spores at 254 nm. For 222

nm UV experiments, a dielectric barrier discharge KrCl* excilamp (Model: BD_P – barrier discharge, portable, Institute of High Current Electronics, Russia) was used, which was housed in the top compartment of the collimated beam apparatus (Figure 5.3). The dimensions of this lamp were $26.5 \times 7.7 \times 77$ cm (Length \times Width \times Height) including an air-cooling fan and an individual power cable. The output window dimensions were 10 cm \times 6 cm. The input power of the lamp was 35 W. The distances from the LP lamp and the KrCl* excilamp to the surface of the sample, which was contained in a Pyrex® Petri dish with 5.8 cm inner diameter, were 41.2 cm and 40.8 cm, respectively. The sample was mixed by a magnetic stirrer during exposure.

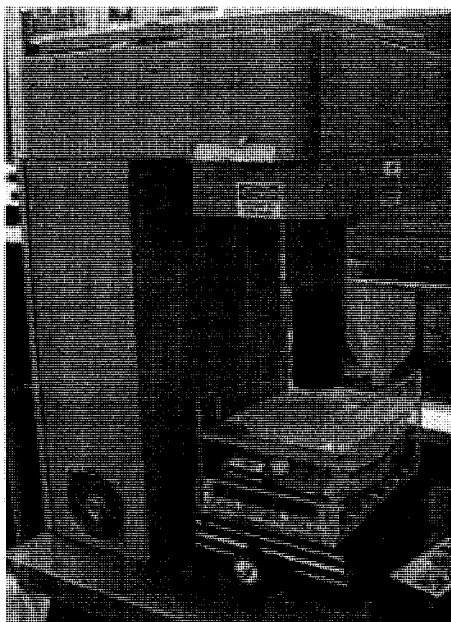


Figure 5.2 View of the collimated beam apparatus

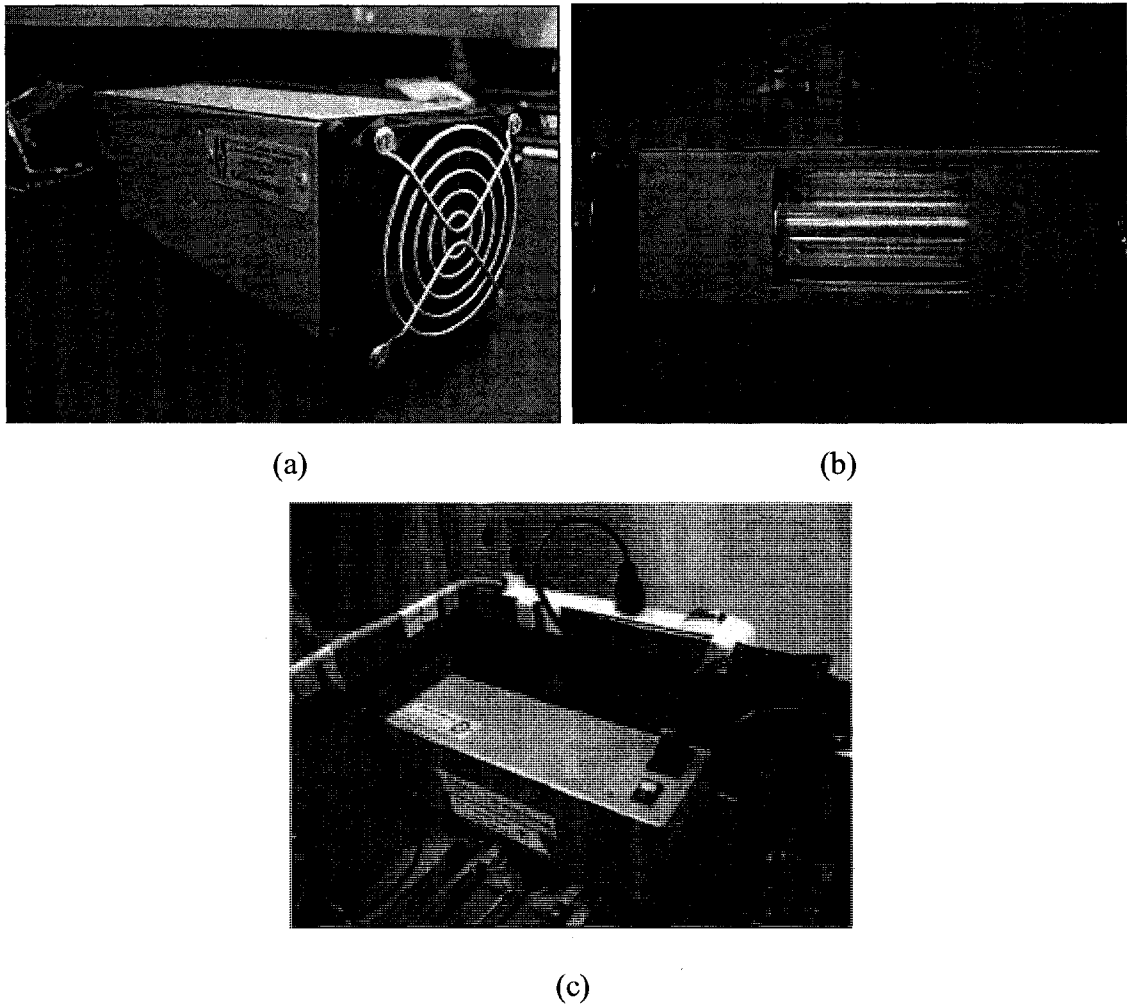


Figure 5.3 KrCl^* excilamp: (a) View; (b) Ignition of the lamp; (c) The lamp housed on the top of the apparatus

5.2.2 The Fluence Determination at the wavelengths of 254 nm and 222 nm

The UV irradiance at the center of the UV beam on the surface of spores sample was measured using a radiometer (International Light, Model: IL 1400A) equipped with a UV detector (International Light, Model: SED240), which was calibrated at 254 nm. For 254 nm UV light emitted by the LP lamp, the readings from the radiometer were the exact

fluence rate, which were used to calculate the average germicidal fluence rate throughout the volume of a spore sample and used to determine the exposure time for the desired fluence, based on the spreadsheet developed by Bolton (2004). For the 222 nm UV light emitted by the KrCl* excilamp, the sensor factor of detector should be taken into account, since the detector is less sensitive at wavelengths below 254 nm. Based on the calibration data of the detector, which are partially tabulated in Table 5.1, the sensitivity ratio of 222 nm to 254 nm was calculated using the interpolation method.

Table 5.1 Calibration data of the detector

Wavelength λ (nm)	Irradiance response y (A cm ² W ⁻¹)
220	3.830E-06
230	5.146E-06
240	6.536E-06
250	7.672E-06
260	7.972E-06

From Table 5.1, the irradiance response at 254 nm (y_{254}) and 222 nm (y_{222}) were determined by Equations [5.1] and [5.2], respectively.

$$[5.1] \quad y_{254} = y_{250} + \frac{y_{260} - y_{250}}{260 - 250} \cdot (254 - 250) = 7.792 \times 10^{-6} \text{ A cm}^2 \text{ W}^{-1}$$

$$[5.2] \quad y_{222} = y_{220} + \frac{y_{230} - y_{220}}{230 - 220} \cdot (222 - 220) = 4.093 \times 10^{-6} \text{ A cm}^2 \text{ W}^{-1}$$

Therefore, the sensitivity ratio of 222 nm to 254 nm was determined by y_{222} divided by y_{254} , which was 0.525. For the fluence rate measurement at 222 nm, the actual fluence rate was the reading of detector divided by the 0.525.

The reflection factor should also be considered. For 254 nm, the reflection factor was 0.975. For 222 nm, it was 0.973. The detailed calculation has been described in Section 3.2.6.

5.2.3 UV Exposure Experiments

A diluted suspension of *B. subtilis* spores at a concentration of approximately 2.5×10^6 CFU mL⁻¹ was used in UV exposure experiments at 254 nm and 222 nm. It was prepared by transferring 2 mL aliquot of spore stock suspension to 500 mL sterile DI water. A sample of 15 mL of this dilute suspension contained in a Petri dish was used in each exposure, and each sample was exposed only once. The absorption coefficient of this diluted suspension at 254 nm or 222 nm was determined by a UV-Vis spectrophotometer (Model: UV-2410 PC, Shimadzu, Japan). The absorption coefficients of different experiment runs at 254 nm and 222 nm ranged from 0.026 to 0.043 cm⁻¹ and from 0.026 to 0.053 cm⁻¹, respectively.

A series of exposure times, which represents the desired fluences obtained by the samples, was carried out in triplicate. For 254 nm, the fluences of 4.4, 8.8, 13.1, 17.5, 26.3, 35.0, 52.6 and 70.1 mJ cm⁻² were performed. For 222 nm, the fluences of 2.9, 5.8, 8.7, 11.7, 14.6, 17.5, 20.4, 23.3, 35.0, 46.6, 69.9 and 93.2 mJ cm⁻² were carried out. The reason that the fluences were not integers is that the new calibration data of the detector of the radiometer were used. Partial data were given in Table 5.1. The initial values of fluences were corrected based on the new calibration.

5.2.4 Inactivation Kinetics

Since both of the fluence-response curves of *B. subtilis* spores at 222 nm and 254 nm showed shoulder regions, the multi-target model was used to predict the log inactivation of *B. subtilis* spores as a function of the fluence at 254 nm and 222 nm. The detailed description of the model has been discussed in Section 4.2.4. In the multi-target model, the parameters k and n_c were determined by the non-linear least-square regression using the MS Excel™ “Solver” tool.

5.3 Results and Discussion

5.3.1 Fluence-response Curves of *B. subtilis* Spores at 254 nm and 222 nm

The data and the calculations of the UV exposure experiments at 254 nm and 222 nm are shown in Tables B7 to B10. Figures 5.4 and 5.5 illustrate the fluence-response curves of *B. subtilis* spores as well as the least-square regression curves at 254 nm and 222 nm, respectively. Tailing regions were observed in the fluence-response curves at high fluences, especially for the wavelength of 222 nm. Since the multi-target model does not accommodate the tailing behaviour, data in the tailing regions were omitted from the least-squares estimation of the parameters k and n_c . Using the MS Excel™ “Solver” tool, the parameters k and n_c in multi-target models were: $k = 0.069 \text{ cm}^2 \text{ mJ}^{-1}$, $n_c = 6$ at 254 nm; $k = 0.122 \text{ cm}^2 \text{ mJ}^{-1}$, $n_c = 4$ at 222 nm. Therefore, the multi-target models, which describe the relationship of the inactivation of spores and the fluences at 254 nm and 222 nm, are

shown in Equations [5.3] and [5.4], respectively.

$$[5.3] \quad \frac{N}{N_0} = 1 - (1 - 10^{-0.069F})^6 \text{ at 254 nm}$$

$$[5.4] \quad \frac{N}{N_0} = 1 - (1 - 10^{-0.122F})^4 \text{ at 222 nm}$$

where, N_0 is the initial concentration of *B. subtilis* spore in a sample before exposure to UV light, CFU mL⁻¹; N is the final concentration of viable spores in the sample after exposure to UV light, CFU mL⁻¹; F is the fluence at 254 nm or 222 nm, mJ cm⁻². From Equations [5.3] and [5.4], the 2 log reduction of *B. subtilis* spores required the fluence of 40.4 mJ cm⁻² at 254 nm and the fluence of 21.6 mJ cm⁻² at 222 nm.

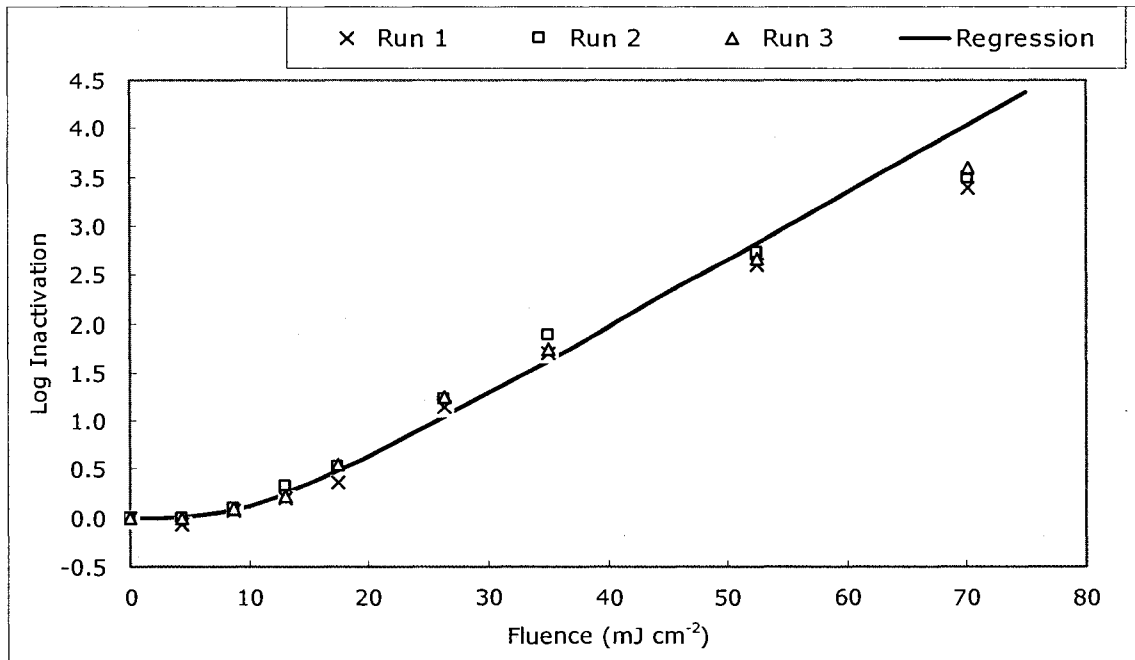


Figure 5.4 Fluence-response curve of *B. subtilis* spores with UV light at 254 nm

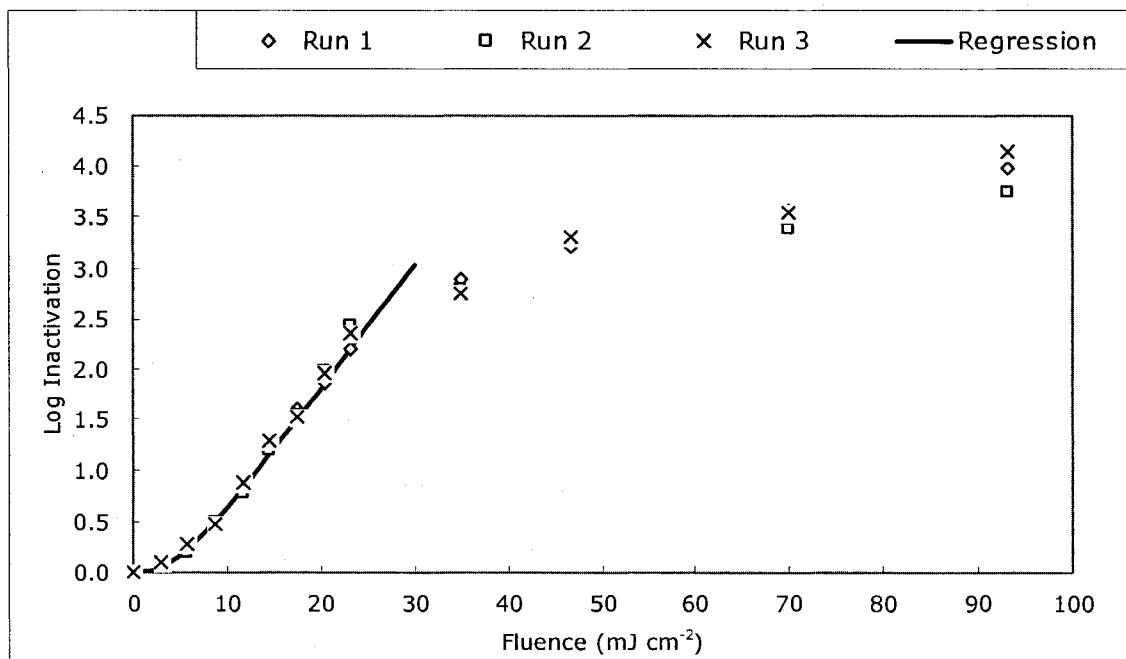


Figure 5.5 Fluence-response curve of *B. subtilis* spores with UV light at 222 nm

According to ÖNORM 2003, which was cited in Sommer *et al.* (2004), the values of k and $\log(n_c)$ at wavelength of 254 nm should be in the following range:

$$[5.5] \quad k = 0.065 \pm 20\% \text{ cm}^2 \text{ mJ}^{-1} \text{ (i.e., } k = 0.052 \text{ to } 0.078 \text{ cm}^2 \text{ mJ}^{-1}\text{)}$$

$$[5.6] \quad \log(n_c) = 0.7 \pm 30\% \text{ [i.e., } \log(n_c) = 0.49 \text{ to } 0.91\text{]}$$

It can be found that the k and n_c values in this research fit into this range very well.

5.3.2 Shoulder and Tailing Regions in the Fluence-response Curves

From Figures 5.4 and 5.5, the shoulder regions were observed at low fluence. The corresponding log inactivations were approximately 0 to 0.3 in both curves. In addition, the tailing regions appeared when the log inactivations were approximately above 3.0 at 254 nm and above 2.5 at 222 nm. According to Mamane-Gravetz and Linden (2005), the

shoulder was probably caused by:

- (1) the smallest fluence required to hit the targets in the double-stranded DNA before the full inactivation of a spore occurs;
- (2) the protection of the protoplasm by the thick spore coat and cortex outside.

However, Riesenman and Nicholson (2000) indicated that the spore coat is not the important determinant of spore resistance to UV light at 254 nm. Proteins are weak absorbers at 254 nm. The photochemical reactions in proteins may be significant when the large microorganisms, such as fungi, protozoa and algae with dimensions of tens or hundred of micrometers, are exposed to 254 nm UV light, since photons at this wavelength may be unable to penetrate far beneath the surface of these microorganisms and cannot induce the photoreaction of DNA (Kallsvaart, 2001). The average size of a spore is approximately 1.5 μm in length and 0.7 μm in diameter with an ellipsoidal shape. The small dimensions allow UV light to penetrate into the spore core, resulting in the photochemical reaction of DNA. However, the absorption of proteins is significant at wavelengths below 240 nm. As a result, the mechanism of disinfection of spores with UV light at 222 nm may be different from that at 254 nm.

- (3) the self-repair capacity of double-stranded DNA. This process may be dependent on the fluence. At a high fluence, this process is probably inhibited.

The probable reasons leading to the tailing of the fluence-response curves are listed as

follows:

- (1) heterogeneity of spore population. Some spores may be more resistant to UV light, and some may be more sensitive.
- (2) heterogeneity of treatment. The water matrix of the sample, such as pH, temperature etc., and the fluence rate throughout the sample may be not uniform. At a high fluence, the inactivated spores may intercept UV light and shield the viable spores. This perhaps results in the decrease of efficiency of UV treatment.
- (3) aggregation of spores and/or association of spores with other particles. The hydrophobicity and the surface charge of spores may cause the attachment or adhesion of spores to other spores or particles.

5.3.3 Comparison of Inactivation Kinetics at 254 nm with Other Research Papers

Two parameters of the multi-target model, k and n_c , at 254 nm were determined to lie in the regular range proposed by ÖNORM 2003. However, a large variation of inactivation kinetics was found from published papers. Table 5.2 shows the different fluence required per log inactivation of *B. subtilis* spores from several papers, as well as from this research.

Table 5.2 Fluence required per log inactivation of *B. subtilis* spores at 254 nm

Reference	Fluence required at 254 nm (mJ cm ⁻²)			<i>k</i>
	1 log	2 log	3 log	(cm ² mJ ⁻¹)
Qualls and Johnson (1983)	12	18	24	0.167
Qualls <i>et al.</i> (1989)	38	49	60	0.091
Chang <i>et al.</i> (1985)	36	48	59	0.087
Uvbiana (2006)	17	28	38	0.095
Mamane-Gravetz and Linden (2005)	13	25	38	0.081
Mamane-Gravetz <i>et al.</i> (2005)	13	21	28	0.127
Mamane and Linden (2006)	24	41	58	0.059
Kang (2008)	30	51	71	0.049
Chen (2007)	20	32	43	0.089
Feng (2007)	19	32	44	0.083
Cabaj <i>et al.</i> (1996)	34	48	64	0.069
Cabaj, <i>et al.</i> (2002)	28	43	57	0.061
Sommer <i>et al.</i> (2004)	30	42	55	0.080
USEPA (2006b)	35	50	62	0.074
Average of above studies	24	37	49	0.086
Percentage error	37%	30%	28%	34%
This research	25	40	55	0.069

From Table 5.2, the percentage error of *k* values from the above studies is 34%, which is fairly large. In fact, the range of *k* proposed by ÖNORM 2003 also has a large percentage error of 20%. The large variation is probably caused by the following reasons:

- (1) Different methods used to measure the fluence rate. Chen (2007) used

ferrioxalate actinometry method to determine the fluence rate, whereas other studies used the radiometry method.

- (2) Different sources of 254 nm UV light. Chen (2007) used 254 nm UV light emitted by a MP lamp, of which other wavelengths were filtered out. Other studies, such as Mamane-Gravetz and Linden (2005), used LP lamps as the light source.
- (3) Different models to express the mathematical relationship between the log inactivation and the fluence. Qualls and Johnson (1983) used a log-linear model without including the shoulder region. However, the model determined by most of the other papers used the multi-target model.
- (4) Different cultivation methods of *B. subtilis* spores. Mamane-Gravetz *et al.* (2005) and Cabaj, *et al.* (2002) used the different cultivation methods, which leads to very distinct results. Mamane-Gravetz *et al.* (2005) reported that the liquid-cultivated spores [used by Cabaj, *et al.* (2002)] were more resistant than the surface spores [used by Mamane-Gravetz *et al.* (2005)] by a factor of 2. Chang *et al.* (1985) indicated that the different types of agar that was used to incubate spores could influence the survival of spores after exposure to UV light.
- (5) Different batches of *B. subtilis* spores. Even using the same cultivation method and the same source of spores, the different batches may cultivate spores with different inactivation behaviours. This was proved by Uvbiana

(2006) and Kang (2008).

5.3.4 Comparison of Disinfection Effects of UV Light at 254 nm, 222 nm and 172 nm

Table 5.3 summarizes the first-order inactivation rate constants of *B. subtilis* spores exposed to UV light at 254 nm, 222 nm and 172 nm, respectively, which were obtained from this research.

Table 5.3 The first-order inactivation rate constants of *B. subtilis* spores at different wavelengths determined in this research

Wavelength λ (nm)	First-order inactivation rate constant k ($\text{cm}^2 \text{mJ}^{-1}$)
254	0.069
222	0.122
172	0.0022

From the above table, it is clear that the inactivation rate constant at 172 nm is far lower than at the other two wavelengths. The mechanism of disinfection by 172 nm VUV light is very different from that by UVC light, which was discussed in Section 4.3.2. The disinfection effect of VUV light on microorganisms indirectly derives from a strong oxidant, hydroxyl radical, generated by VUV photolysis of water. Therefore the inactivation rate constant evaluated by fluence at 172 nm in Table 5.3 is not exact, but it still reflects that the disinfection of microorganisms by AOPs is much less efficient and requires much longer time than the disinfection by UVC exposure. This is consistent with the conclusion obtained in the previous chapter.

From Table 5.3, the inactivation rate constant at 222 nm is about 1.8 times higher than that at 254 nm. It is similar to the results reported by Chen (2007), who found the inactivation rate constant of $0.089 \text{ cm}^2 \text{ mJ}^{-1}$ at 254 nm and $0.176 \text{ cm}^2 \text{ mJ}^{-1}$ at 222 nm, which means the ratio of rate constant at 222 nm to that at 254 nm is about 2.0. The probable reasons of the difference of inactivation rate constants between these two wavelengths will be discussed in the next section.

5.3.5 The Mechanisms of UVC Disinfection of *B. subtilis* Spores

In a *B. subtilis* spore, the absorption of proteins is far less than that of DNA at 254 nm (Setlow, 1960). As a result, almost all irradiance at this wavelength is absorbed by DNA. Although spores cannot constantly repair DNA damage, since enzyme activity in spores is limited without ATP and other nucleoside triphosphates, spores are 10- to 50-fold more resistant to 254 nm UV light than their corresponding growing cells. This is attributed to the unique UV photochemistry of the DNA in spores (Setlow, 1992a; Setlow, 2001).

UV exposure of DNA in growing cells generates a number of DNA lesions, in particular cyclobutane-type dimers between adjacent pyrimidines, primarily thymine dimers as the major photoproduct. In contrast, DNA in spores exposed to UV light generates no detectable thymine dimers, but contains a novel photoproduct, termed spore photoproduct (SP), which has been determined as 5-thyminyl-5,6-dihydrothymine (Setlow, 2001). The formation of SP in spore DNA is the reason for the elevated spore UV resistance.

Although SP is produced rather than cyclobutane dimers after spore DNA was exposed to UV light, SP is potentially a lethal lesion in DNA. Moreover, SP formation as a function of UV fluence is similar to that for thymine dimers (Setlow, 2001). The reason that formation of SP is less lethal than cyclobutane dimers is that spores have at least two repair systems for SP. The first system is nucleotide excision repair (NER), also present in growing cells, which can repair cyclobutane dimers as well. The second repair system is unique to SP in spores called the SP-specific repair system. It is able to monomerize SP to two thymines without DNA backbone cleavage early in spore germination. This process can repair SP extremely rapidly and efficiently. It requires metabolic energy but not light (Setlow, 1992a; Setlow, 1995; Setlow 2001). These two repair systems ensure that SP is repaired in a relatively error-free process, while cyclobutane dimers are always subject to error-prone repair (Ross and Setlow, 2000).

The major reason for SP rather than thymine dimers formation in a spore after UV exposure is the binding of α/β -type small acid-soluble proteins (SASP) to the spore DNA. These proteins convert spore DNA from a B-like conformation to an A-like conformation. A-like DNA, which rarely exists in cells, is a wider right-handed spiral, and is characterized by more base pairs per turn of the helix and a wider minor groove but a narrower and deeper major groove than B-like DNA (Setlow, 1992b). They are sufficient in a spore to saturate the DNA, comprising 4% to 8% of total spore proteins (Setlow, 2001; Setlow and Setlow, 1993a). These proteins are only synthesized within the sporulation in parallel with the acquisition of UV resistance by a developing spore and

change the primary photoproducts of the spore DNA from cyclobutane dimers to SP. Spores of *B. subtilis* mutant that lack α/β -type SASP are much more sensitive to UV light than spores with these proteins (Setlow and Setlow, 1993b; Setlow, 2001). In addition, these proteins only exist in spores. They are rapidly degraded to amino acids early in spore germination (Setlow, 1992a).

Exposure of spore DNA saturated with α/β -type SASP to UV light produces SP rather than thymine dimers. However, the high yield of SP is caused by the presence of pyridine-2,6-dicarboxylic acid or dipicolinic acid (DPA) in the spore core. In contrast, the yield of SP as a function of UV fluence *in vitro* is about 15 fold lower than that found in spores. DPA accounts for about 10% of spore dry weight (Setlow and Setlow, 1993a). It probably chelates with divalent cations, predominantly Ca^{2+} . It is unique to spores, not present in growing cells, and it is acquired by the developing spores very late in sporulation after the synthesis of α/β -type SASP (Setlow, 1995). However, DPA release is one of the earliest events in spore germination before the degradation of SASP (Setlow, 2001). DPA has a significant absorption in the UV region, and it is considered to be a photosensitizer to UV light. It has been suggested that the high SP yield in spores as a function of UV fluence is attributed to the high level of DPA present in the spore core (Douki *et al.*, 2005). Since SP is a potentially lethal photoproduct, spores with increasing DPA have less resistance to UV light (Setlow, 2001). This is proven by the phenomenon that the developing spores and the germinated spores are more resistant to UV light than are the dormant spores (Setlow, 1995). The reason is that DPA accumulation and

excretion are before the synthesis and the degradation of α/β -type SASP in spores, respectively. Douki *et al.* (2005) proposed that the presence of α/β -type SASP did not significantly alter the level of total photoproducts, but did alter the distribution of individual photoproducts (i.e., more SP but almost no cyclobutane dimers). However, in the presence of DPA, they reported a significant increase in the formation of SP in spores, which resulted in the larger total photoproducts. Therefore, DPA plays an important role in the photochemistry of DNA in spores. In addition, Douki *et al.* (2005) proposed that the principal mechanism of this effect of DPA might be a photosensitized triplet energy transfer from the excited DPA to thymine residues.

The higher efficiency of UV inactivation of *B. subtilis* spores at 222 nm than that at 254 nm probably derives from triplet state energy transfer from DPA to thymine bases. Since the absorption coefficient of DPA at 222 nm is over twice that at 254 nm (Miller and Senkfor, 1982), more photons are absorbed by DPA, which therefore results in more photons being transferred to thymine bases in DNA. The higher the photon flux into DNA, the more SP is produced, which causes a higher inactivation of the spores. At the same time, a portion of UV light is absorbed by DNA directly and also results in DNA disruption. Although the absorption coefficient of DNA decreases from 254 nm to 222 nm, the synergistic effect of UV absorption by DNA and triplet state energy transfer from DPA to DNA probably gives rise to the enhanced disinfection effect of UV light at 222 nm.

5.4 Conclusions

In this chapter, the relation between the inactivations of *B. subtilis* spores and their corresponding UV fluences at 254 nm and 222 nm was evaluated. From the fluence-response curves, the first-order inactivation rate constants (k) were 0.069 and 0.122 $\text{cm}^2 \text{mJ}^{-1}$ at 254 nm and 222 nm, respectively. Subsequently, the fluences required by a 2 log inactivation of the spores at these two wavelengths were calculated, which were 40.4 and 21.6 mJ cm^{-2} at 254 nm and 222 nm, respectively.

Shoulder and tailing regions were observed in the fluence-response curves both at 254 nm and 222 nm. The shoulders were primarily caused by the multi-target property of double-stranded DNA of spores and spore self-repair capacity. The tailings probably resulted from the experimental artefacts, such as the heterogeneity of the spore population and the treatment, as well as the presence of the aggregation of spores and/or the association of spores with other particles.

The first-order inactivation rate constant of spores at 254 nm fit into the range proposed by ÖNORM 2003, although a large variation of this value has been observed from different studies. The ratio of the inactivation rate constant at 222 nm to that at 254 nm was about 1.8, which is similar to the result reported by Chen (2007).

From the comparison of disinfection effects of UV light at 254 nm, 222 nm and 172 nm, it is obvious that UV disinfection at 172 nm was the least efficient, while UV disinfection at 222 nm was more efficient than that at 254 nm.

The reason that spores are 10 to 50 times more resistant to 254 nm UV light than their corresponding growing cells is attributed to the unique UV photoproduct of the spore DNA, which is called the spore photoproduct (SP). In contrast, the generation of cyclobutane-type dimers is not detectable in spores exposed to UV light.

Although SP is a potential lethal lesion in DNA and SP formation as a function of UV fluence is similar to that for thymine dimers, the reason that formation of SP is less lethal than cyclobutane dimers is that spores have at least two repair systems for SP. The first system is nucleotide excision repair (NER), also present in growing cells. And the second repair system is unique to SP in spores, which is termed the SP-specific repair system. It can repair SP extremely rapidly and efficiently.

The major reason for SP rather than thymine dimers formation in a spore after UV exposure is the binding of α/β -type small acid-soluble proteins (SASP) to the spore DNA. These proteins only exist in spores. They are only synthesized within the sporulation and rapidly degraded to amino acids early in spore germination.

UV exposure of spore DNA saturated with α/β -type SASP produces SP rather than thymine dimers. However, the yield of SP as a function of UV fluence *in vitro* is about 15 fold lower than that found in spores. The reason is the presence of pyridine-2,6-dicarboxylic acid or dipicolinic acid (DPA) in the spore core, which is considered to be a photosensitizer with UV light. There may be a photosensitized triplet energy transfer from the excited DPA to thymine residues and lead to the formation of SP.

Since SP is a potentially lethal photoproduct, spores with a higher DPA level should result in the lower resistance to UV light.

Triplet state energy transfer from DPA to thymine bases in DNA probably results in the higher efficiency of UV inactivation of *B. subtilis* spores at 222 nm than that at 254 nm. Since DPA with a much higher absorption coefficient at 222 nm, compared with that at 254 nm, absorbs more photons at 222 nm and transfers them to thymine bases, more SP is produced in DNA exposed to 222 nm UV light, which eventually causes the higher inactivation of the spores. In addition, DNA disruption is also caused by the direct absorption of UV light by DNA. These two pathways lead to the enhanced disinfection effect of UV light at 222 nm.

CHAPTER 6

GENERAL CONCLUSIONS AND RECOMMENDATIONS

6.1 General Conclusions

The objectives of this research were to compare the disinfection effects of UV light at 172 nm, 222 nm and 254 nm on *Bacillus subtilis* spores, and to examine the possibility of different disinfection mechanisms at these wavelengths. The fluence rate of 172 nm UV light emitted by a Xe₂^{*} excilamp was determined by an actinometry method using methanol in aqueous solution as an actinometer. The fluence rates at the other two wavelengths, which were emitted by a KrCl^{*} excilamp and a LP mercury lamp, were determined by a calibrated radiometer. All of the three lamps were housed in a collimated beam apparatus. Since the Xe₂^{*} excilamp cannot be used in the presence of air, a special collimated beam apparatus was designed with an atmosphere of ultra high purity nitrogen.

The conclusions that were drawn from the results of this study are as follows:

- (1) Based on the inactivation data of the same batch of *B. subtilis* spores, the first-order inactivation rate constants at 172 nm, 222 nm and 254 nm were 0.0022, 0.122, 0.069 cm² mJ⁻¹, respectively. Therefore, the 2 log reduction of *B. subtilis* spores required the fluences of 909, 21.6 40.4 mJ cm⁻² at 172 nm, 222 nm and 254 nm, respectively. Thus, the disinfection of *B. subtilis* spores

by 172 nm VUV exposure is much less efficient than the other two wavelengths, while the inactivation rate constant of *B. subtilis* spores at 222 nm is higher than that at 254 nm.

- (2) The disinfection efficacy of the VUV light derives from the high oxidation potential of hydroxyl radicals generated by the VUV-initiated photolysis of water. Compared with other studies, the disinfection effect of VUV-initiated treatment is more effective than other AOPs, which means VUV photolysis is a more efficient AOP to generate hydroxyl radicals. However, compared with other disinfection processes, it is not an efficient method used for microorganism inactivation.
- (3) The mechanisms of the disinfection of *B. subtilis* spores by hydroxyl radicals are not clear yet. Perhaps the disinfection is primarily caused by the oxidation and disruption of the cell membrane by hydroxyl radicals. Before destruction of the cell membrane, hydroxyl radicals firstly destroy the outer structure of the spores, which is comprised of the exosporium, the spore coats and the cortex. However, since the primary component of the cortex is primarily constituted of peptidoglycan, hydroxyl radicals may penetrate through it to oxidize the cell membrane without any destruction of the cortex.
- (4) The binding of α/β -type small acid-soluble proteins (SASP) to the spore DNA leads to the formation of SP rather than thymine dimers after UV exposure. Since spores have at least two repair systems for SP, one of which is extremely

rapid and efficient, spores are much more resistant to 254 nm UV light than their corresponding growing cells. In addition, DPA in the spore core, which is considered to be a photosensitizer with UV light, largely promotes the generation of SP.

- (5) Triplet state energy transfer from DPA to thymine bases in DNA is probably the reason for the higher efficiency of UV inactivation of *B. subtilis* spores at 222 nm than that at 254 nm. Since the absorption coefficient of DPA at 222 nm is much higher than that at 254 nm, more photon flux is transferred from DPA to the spore DNA, which gives rise to more SP produced and eventually leads to the higher inactivation of the spores.

6.2 Recommendations

Based on the conclusions stated above, the following recommendations are made for future studies:

- (1) Although the disinfection of *B. subtilis* spores by VUV-initiated treatment is not as efficient as other disinfection processes, it has been shown that the hydroxyl radicals generated by VUV photolysis of water can still inactivate *B. subtilis* spores. This result is valuable, since VUV light can probably be used in the disinfection of water or wastewater with a very low transmittance. At a low transmittance of a solution, UVC light gets attenuated very fast by

absorbing substances in the solution and, therefore, the penetration depth of the light is shallow. This limits the efficiency of UVC to inactivate microorganisms, since the cells that are far from the light sources are probably not exposed to enough fluence and thus survive the UV exposure. In contrast, VUV disinfection relies on hydroxyl radicals, which can reach anywhere in aqueous solution (depending on their life time), regardless of the transmittance of the solution, as long as the mixing is enough. Therefore, VUV light can be potentially used in disinfection of water or wastewater with low transmittance. But a larger scale examination should be carried out for investigation of this application.

- (2) The disinfection efficiency of UV light at 222 nm is higher than that at 254 nm. But this conclusion is based on the disinfection experiments on *B. subtilis* spores. *B. subtilis* spores have unique disinfection mechanisms that are different from other microorganisms, including *Cryptosporidium*, which has been of considerable concern recently, since SP, SASP and DPA only exist in *B. subtilis* spores. Hence, the disinfection behaviour of other microorganisms may be different from that of *B. subtilis* spores. The comparison of the disinfection effect of UV light at 222 and 254 nm needs to be evaluated for other microorganisms. If the conclusion drawn here is also true for other microorganisms, KrCl* excilamps will probably have a good prospect for use in disinfection for water treatment. In this case, KrCl* excilamps, which have

a better effect on microorganisms inactivation than for a low pressure mercury UV lamp, will consume less energy but obtain the same log inactivation.

REFERENCES

- Alapi, T. and Dombi, A. (2007) Direct VUV photolysis of chlorinated methanes and their mixtures in an oxygen stream using an ozone producing low-pressure mercury vapour lamp. *Chemosphere*, 67, 693–701.
- Anagnostopoulos, C., Miliadis, G.E., Aplada-Sarlis, P. and Ziogas, B.N. (2006) Comparison of external and internal standard methods in pesticide residue determination. *Int. J. Environ. Anal. Chem.*, 86(1), 77–82.
- Araya-Hernández C.G. and Morales, R.G.E. (2006) Sulfur aromatic heterocycles: A new kind of solar ultraviolet-B radiation actinometers. *J. Photochem. Photobiol. A: Chem.*, 177, 125–128.
- Azrague, K., Bonnefille, E., Pradines, V., Pimienta, V., Oliveros, E., Maurette, M.-T. and Benoit-Marquié, F. (2005) Hydrogen peroxide evolution during V-UV photolysis of water. *Photochem. Photobiol. Sci.*, 4, 406–408.
- Baum, G. and Oppenländer, T. (1995) Vacuum-UV-oxidation of chloroorganic compounds in an excimer flow through photoreactor. *Chemosphere*, 30(9), 1781–1790.
- Benabbou, A.K., Derriche, Z., Felix, C., Lejeune, P. and Guillard, C. (2007) Photocatalytic inactivation of *Escherichia coli* Effect of concentration of TiO₂ and microorganism, nature, and intensity of UV irradiation. *Appl. Catal. B: Environ.*, 76, 257–263.
- Betancourt, W.Q. and Rose, J.B. (2004) Review: Drinking water treatment processes for

- removal of *Cryptosporidium* and *Giardia*. *Vet. Parasit.*, 126, 219–234.
- Blatchley, III E.R. (1997) Numerical modeling of UV intensity: Application to collimated-beam reactors and continuous-flow systems. *Water Res.*, 31(9), 2205–2218.
- Bohrerova, Z., Shemer, H., Lantis, R., Impellitteri, C.A. and Linden, K.G. (2008) Comparative disinfection efficiency and continuous-wave UV irradiation technologies. *Water Res.*, in press.
- Bolton, J.R. (2000) Calculation of ultraviolet fluence rate distribution in an annular reactor: Significance of refraction and reflection. *Water Res.*, 34(13), 3315–3324.
- Bolton, J. R. (2001) *Ultraviolet Applications Handbook*. Bolton Photosciences Inc. 628 Cheriton Cres. NW, Edmonton, AB, Canada, T6R 2M5.
- Bolton, J.R. (2004) *Germicidal Fluence (UV Dose) Calculations for a Low Pressure UV lamp*. Bolton Photosciences Inc. 628 Cheriton Cres. NW, Edmonton, AB, Canada, T6R 2M5.
- Bolton, J.R. (2006) Protocol for the measurement of irradiance using the ferrioxalate actinometer. Bolton Photosciences Inc. 628 Cheriton Cres. NW, Edmonton, AB, Canada, T6R 2M5.
- Bolton, J.R. and Linden, K.G. (2003) Standardization of methods for fluence (UV dose) determination in bench-scale UV experiments. *J. Environ. Eng.*, 129(3), 209–215.
- Bolton, J.R. and Stefan, M.I. (2002) Fundamental photochemical approach to the concepts of fluence (UV dose) and electrical energy efficiency in photochemical degradation reactions. *Res. Chem. Intermed.*, 28(7–9), 857–870.

- Bolton, J.R. and Stefan, M.I. (2004) Experimental protocol for incident irradiance measurements with KI/KIO₃ actinometry. Bolton Photosciences Inc. 628 Cheriton Cres. NW, Edmonton, AB, Canada, T6R 2M5.
- Boyd, I.W. and Zhang, J.Y. (1997) New large area ultraviolet lamp sources and their applications. Nucl. Instr. and Meth. in Phys. Res. B, 121, 349–356.
- Brandi, R.J., Citroni, M.A., Alfano, O.M. and Cassano, A.E. (2003) Absolute quantum yields in photocatalytic slurry reactors. Chem. Eng. Sci., 58, 979–985.
- Cabaj, A., Sommer, R., Pribl, W. and Halder, T. (2002) The spectral UV sensitivity of microorganisms used in biosimetry. Water Sci. Technol.: Water Supply, 2(3), 175–181.
- Cabaj, A., Sommer, R. and Schoenen, D. (1996) Biosimetry: model calculations for u.v. water disinfection devices with regard to dose distributions. Water Res., 30(4), 1003–1009.
- Cadet, J., Sage, E. and Douki, T. (2005) Ultraviolet radiation-mediated damage to cellular DNA. Mutat. Res., 571, 3–17.
- Campbell, A.T. and Wallis, P. (2002) The effect of UV irradiation on human-derived *Giardia lamblia* cysts. Water Res., 36, 963–969.
- Chang, J.C.H., Ossoff, S.F., Lobe, D.C., Dorfman, M.H., Dumais, C.M., Qualls, R.G. and Johnson, J.D. (1985) UV inactivation of pathogenic and indicator microorganisms. Appl. Environ. Microbiol., 49(6), 1361–1365.
- Chen, P.-J., Linden, K.G., Hinton, D.E., Kashiwada, S., Rosenfeldt, E.J. and Kullman,

- S.W. (2006) Biological assessment of bisphenol A degradation in water following direct photolysis and UV advanced oxidation. *Chemosphere*, 65, 1094–1102.
- Chen, R.Z. (2007) Comparison of action spectra of microorganisms and DNA absorbance spectra for UV disinfection of water, thesis. University of Alberta. 11419 80th Avenue NW, Edmonton, AB, Canada, T6G 0R6.
- Chen, W., Zhang, J., Fang, Q., Hu, K. and Boyd, I.W. (2004) Surface modification of polyimide with excimer UV radiation at wavelength of 126 nm. *Thin Solid Films*, 453–454, 3–6.
- Cho, M., Chung, H., Choi, W. and Yoon, J. (2004) Linear correlation between inactivation of *E. coli* and OH radical concentration in TiO₂ photocatalytic disinfection. *Water Res.*, 38, 1069–1077.
- Cho, M., Chung, H. and Yoon, J. (2002) Effect of pH and importance of ozone initiated radical reactions in inactivating *Bacillus subtilis* spores. *Ozone Sci. Eng.*, 24, 145–150.
- Cho, M., Chung, H. and Yoon, J. (2003) Disinfection of water containing natural organic matter by using ozone-initiated radical reactions. *Appl. Environ. Microbiol.*, 69(4), 2284–2291.
- Cho, M., Kim, J.-H. and Yoon, J. (2006) Investigating synergism during sequential inactivation of *Bacillus subtilis* spores with several disinfectants. *Water Res.*, 40, 2911–2920.
- Choi, H., Stathatos, E. and Dionysiou, D.D. (2007) Photocatalytic TiO₂ films and membranes for the development of efficient wastewater treatment and reuse systems.

- Desalination, 202, 199–206.
- Clauß, M., Mannesmann, R. and Kolch, A. (2005) Photoreactivation of *Escherichia coli* and *Yersinia enterocolitica* after irradiation with a 222 nm excimer lamp compared to a 254 nm low-pressure mercury lamp. *Acta hydrochim. Hydrobiol.*, 33(6), 579–584.
- Craik, S.A., Smith, D.W., Belosevic, M. and Chardrakanth, M. (2002) Use of *Bacillus subtilis* spores for ozonation of *Cryptosporidium parvum* in drinking water treatment. *J. Environ. Eng. Sci.*, 1, 173–186.
- Craik, S.A., Weldon, D., Finch, G.R., Bolton, J.R. and Belosevic, M. (2000) Inactivation of *Cryptosporidium parvum* oocysts using medium- and low-pressure ultraviolet radiation. *Water Res.*, 35(6), 1387–1398.
- Douki, T., Setlow, B. and Setlow, P. (2005) Photosensitization of DNA by dipicolinic acid, a major component of spores of *Bacillus* species. *Photochem. Photobiol. Sci.*, 4, 591–597.
- Dow, S.M., Barbeau, B., Gunten, U., Chandrakanth, M., Amy, G. and Hernandez, M. (2006) The impact of selected water quality parameters on the inactivation of *Bacillus subtilis* spores by monochloramine and ozone. *Water Res.*, 40, 373–382.
- Du, J. and Gebicki, J.M. (2004) Protein are major initial cell targets of hydroxyl radicals. *Int. J. Biochem. Cell Biol.*, 36, 2334–2343.
- Feng, Y. (2007) Photodegradation of free chlorine and the possible application for the validation of ultraviolet (UV) reactors, Ph.D. thesis. University of Alberta, Edmonton, AB, Canada.

- Feng, Y., Smith, D.W. and Bolton, J.R. (2007) Photolysis of aqueous free chlorine species (HOCl and OCl⁻) with 254 nm ultraviolet light. *J. Environ. Eng. Sci.*, 6, 277–284.
- Franke, S., Lange, H., Schoepp, H. and Witzke, H.-D. (2006) Temperature dependence of VUV transmission of synthetic fused silica. *J. Phys. D: Appl. Phys.*, 39, 3042–3046.
- Gellert B. and Kogelschatz U. (1991) Generation of excimer emission in dielectric barrier discharges. *Appl. Phys. B*, 52, 14–21.
- Geng, J., Yu, S.-B., Wan, X., Wang, X.-J., Shen, P., Zhou, P. and Chen, X.-D. (2008) Protective action of bacterial melanin against DNA damage in full UV spectrums by a sensitive plasmid-based noncellular system. *J. Biochem. Biophys. Methods*, *in press*.
- Giese, N. and Darby, J. (2000) Sensitivity of microorganisms to different wavelengths of UV light: Implication on modeling of Medium pressure UV systems. *Water Res.*, 34(16), 4007–4013.
- Guest, R.K. (2004) *Bacillus* spp. Spore production: A short guidance manual. University of Alberta. 11419 80th Avenue NW, Edmonton, AB, Canada, T6G 0R6.
- Gültekin, I. and Ince, N.H. (2007) Synthetic endocrine disruptors in the environment and water remediation by advanced oxidation processes. *J. Environ. Mangmt.*, 85, 816–832.
- Goldstein, S. and Rabani, J. (2008) The ferrioxalate and iodide-iodate actinometers in the UV region. *J. Photochem. Photobiol. A: Chem.*, 193, 50–55.
- Gonzalez, M.G, Oliveros, E., Wörner, M. and Braun, A.M. (2004) Vacuum-ultraviolet photolysis of aqueous reaction systems. *J. Photochem. Photobiol. C: Photochem.*

- Reviews, 5, 225–246.
- Han, W., Zhang, P., Zhu, W., Yin, J. and Li, L. (2004) Photocatalysis of *p*-chlorobenzoic acid in aqueous solution under irradiation of 254 nm and 185 nm UV light. *Water Res.*, 38, 4197–4203.
- Hargreaves, A., Taiwo, F.A., Duggan, O., Kirk, S.H. and Ahmsd, S.I. (2007) Near-ultraviolet photolysis of β -phenylpyruvic acid generates free radicals and results in DNA damage. *J. Photochem. Photobiol. B: Biol.*, 89, 110–116.
- Heit, G., Neuner, A., Saugy, P-Y. and Braun, A.M. (1998) Vacuum-UV actinometry. The quantum yield of the photolysis of water. *J. Phys. Chem. A*, 102(28), 5551–5561.
- Hellma (2007) Material and technical information.
<http://www.hellma-worldwide.com/html/seiten/text;material-and-technical-informatio;283,en.html> (available on Jul. 25, 2007).
- Heraeus (2008) Premium quartz glass products for UV disinfection and UV cleaning applications. <http://www.siltec.ru/leaflets/Premium-series.pdf> (available on Jun. 4, 2008).
- Herrera Melián, J.A., Doña Rodríguez, J.M., Viera Suárez, A., Tello Rendón, E., Valdés do Campo, C., Arana, J. and Pérez Peña, J. (2000) The photocatalytic disinfection of urban waste waters. *Chemosphere*, 41, 323–327.
- Hijnen, W.A.M., Beerendonk, E.F. and Medema, G.J. (2006) Inactivation credit of UV radiation for viruses, bacteria and protozoan (oo)cysts in water: A review. *Water Res.*, 40, 3–22.

- Huibers, P.D.T. (1997) Models for the wavelength dependence of the index of refraction of water. *Appl. Opt.*, 36, 3785–3787.
- Ikematsu, T., Hayashi, N., Ihara, S. Satoh, S. and Yamabe, C. (2004) Advanced oxidation processes (AOPs) assisted by excimer lamp. *Vacuum*, 73, 579–582.
- Jagger, C.J. and Setlow, R.B. (1964) Overlap of photoreactivation and liquid holding recovery in *Escherichia coli* B. *Science, New Series*, 143(3611), 1170–1171.
- Jin, S., Linden, K.G., Ducoste, J. and Liu, D. (2005) Impact of lamp shadowing and reflection on the fluence rate distribution in a multiple low-pressure UV lamp array. *Water Res.*, 39, 2711–2721.
- Jin, S., Mofidi, A.A. and Linden, K.G. (2006) Polychromatic UV fluence measurement using chemical actinometry, biosimetry, and mathematical techniques. *J. Environ. Eng.*, 132(8), 831–841.
- Jung, Y.J., Oh, B.S. and Kang, J-W. (2008) Synergistic effect of sequential or combined use of ozone and UV radiation for the disinfection of *Bacillus subtilis* spores. *Water Res.*, 42, 1613–1621.
- Jungfer, C., Schwartz, T. and Obst, U. (2007) UV-induced dark repair mechanisms in bacteria associated with drinking water. *Water Res.*, 41, 188–196.
- Kalbin, G, Li, S., Olsman, H., Pettersson, M., Engwall, M. and Strid, Å. (2005) Effects of UV-B in biological and chemical systems: Equipment for wavelength dependence determination. *J. Biochem. Biophys. Methods*, 65, 1–12.
- Kallsvaart, B.F. (2001) Photobiological effects of polychromatic medium pressure UV

- lamps. *Water Sci. Tech.*, 43(4), 191–197.
- Kamiya, H., Iwai, S. and Kasai, H. (1998) The (6–4) photoproduct of thymine-thymine induces targeted substitution mutations in mammalian cells. *Nucleic Acids Res.*, 26(11), 2611–2617.
- Kang, H. (2008) Effect of Aggregation on UV inactivation of microorganisms in filtered water, thesis. University of Alberta. 11419 80th Avenue NW, Edmonton, AB, Canada, T6G 0R6.
- Kim, B.R., Anderson, J.E., Mueller, S.A., Gaines, W.A. and Kendall, A.M. (2002) Literature review—efficacy of various disinfectants against *Legionella* in water system. *Water Res.*, 36, 4433–4444.
- Kirschenbaum, D.M. (1972) Atlas of Protein Spectra in the Ultraviolet and Visible Regions, Volume 1. Springer-Verlag.
- Kogelschatz, U. (1992) Silent-discharge driven excimer UV sources and their applications. *Appl. Surf. Sci.*, 54, 410–423.
- Kogelschatz, U., Esrom, H., Zhang, J.-Y. and Boyd, I.W. (2000) High-intensity sources of incoherent UV and VUV excimer radiation for low-temperature materials processing. *Appl. Surf. Sci.*, 168, 29–36.
- Koivunen, J. and Heinonen-Tanski, H. (2005) Inactivation of enteric microorganisms with chemical disinfection, UV irradiation and combined chemical/UV treatments. *Water Res.*, 39, 1519–1526.
- Kovács, G., Fekete, A. Bérces, A. and Rontó, Gy. (2007) The effect of the short

- wavelength ultraviolet radiation. An extension of biological dosimetry to the UV-C range. *J. Photochem. Photobiol. B: Biol.*, 88, 77–82.
- LeClerc, J.E., Borden, A. and Lawrence, C.W. (1991) The thymine-thymine pyrimidine-pyrimidone(6–4) ultraviolet light photoproduct is highly mutagenic and specifically induces 3' thymine-to-cytosine transitions in *Escherichia coli*. *Proc. Natl. Acad. Sci. USA*, 88, 9685–9689.
- Li, Q.-R., Gu, C.-Z., Di, Y., Yin, H. and Zhang, J.Y. (2006) Photodegradation of nitrobenzene using 172 nm excimer UV lamp. *J. Hazard. Mat., B* 133, 68–74.
- Liu C.-Q., Huttall, S.D., Tran, H., Wilkins, M., Streltsov, V.A. and Alderton, M.R. (2007) Construction, crystal structure and application of a recombinant protein that lacks the collagen-like region of BclA from *Bacillus anthracis* spores. *Biotech. Bioeng.*, 99(4), 774–782.
- Macauley, J.J., Qiang, Z., Adams, C.D., Surampalli, R. and Mormile, M.R. (2006) Disinfection of swine wastewater using chlorine, ultraviolet light and ozone. *Water Res.*, 40, 2017–2026.
- Mamane, H. and Linden, K.G. (2006) Impact of particle aggregated microbes on UV disinfection. I: Evaluation of spores – clay aggregates and suspended spores. *J. Environ. Eng.*, 132(6), 596–606.
- Mamane, H., Shemer, H. and Linden, K.G. (2007) Inactivation of *E. coli*, *B. subtilis* spores, and MS2, T4, and T7 phage using UV/H₂O₂ advanced oxidation. *J. Hazard. Mat.*, 146, 479–486.

- Mamane-Gravetz, H. and Linden, K.G. (2004) UV disinfection of indigenous aerobic spores: Implication for UV reactor validation in unfiltered waters. *Water Res.*, 38, 2898–2906.
- Mamane-Gravetz, H. and Linden, K.G. (2005) Relationship between physiochemical properties, aggregation and u.v. inactivation of isolated indigenous spores in water. *J. Appl. Microbiol.*, 98, 351–363.
- Mamane-Gravetz, H., Linden, K.G., Cabaj, A. and Sommer, R. (2005) Spectral sensitivity of *Bacillus subtilis* spores and MS2 coliphage for validation testing of ultraviolet reactors for water disinfection. *Environ. Sci. Technol.*, 39, 7845–7852.
- Maness, P.-C., Smolinski, S., Blake, D.M., Huang, Z., Wolfrum, E.J. and Jacoby, W.A. (1999) Bacterial activity of photocatalytic TiO₂ reaction: toward an understanding of its killing mechanism. *Appl. Environ. Microbiol.*, 65(9), 4094–4098.
- Martins, L.O., Soares, C.M., Pereira, M.M., Teixeira, M., Costa, T., Jones, G.H. and Henriques, A.O. (2002) Molecular and biological characterization of a highly stable bacterial laccase that occurs as a structural component of the *Bacillus subtilis* endospore coat. *J. Biol. Chem.*, 277(21), 18849–18859.
- Matafonova, G., Christofi, N., Batoev, V. and Sosnin E. (2008) Degradation of chlorophenols in aqueous media using UV XeBr excilamps in a flow-through reactor. *Chemosphere*, 70, 1124–1127.
- Mehta, A.S., Saile, E., Zhong, W., Buskas, T., Carlson, R., Kannenberg, E., Reed, Y., Quinn, C.P. and Boons, G.-J. (2006) Synthesis and antigenic analysis of the BclA

- glycoprotein oligosaccharide from the *Bacillus anthracis* exosporium. Chem. Enr. J., 12, 9136–9149.
- Miller, T.L. and Senkfor, S.I. (1982) Spectrofluorometric determination of calcium and lanthanide elements in dilute solution. Anal. Chem., 54(12), 2022–2025.
- Moore, L. and Ferreira, J.T. (2006) Ultraviolet (UV) transmittance characteristics of daily disposable and silicone hydrogel contact lenses. Cont. Lens Anterior Eye, 29, 115–122.
- Nicholson, W.L., Setlow, B. and Setlow, P. (1991) Ultraviolet irradiation of DNA complexed with α/β -type small, acid-soluble proteins from spores of *Bacillus* or *Clostridium* species makes spore photoproduct but not thymine dimers. Proc. Natl. Acad. Sci., USA, 88(19), 8288–8292.
- Oppenländer, T. and Gliese, S. (2000) Mineralization of organic micropollutants (homologous alcohols and phenols) in water by vacuum-UV-oxidation (H_2O -VUV) with an incoherent xenon-excimer lamp at 172 nm. Chemosphere, 40, 15–21.
- Oppenländer, T. and Schwarzwälder, R. (2002) Vacuum-UV Oxidation (H_2O -VUV) with a xenon excimer flow-through lamp at 172 nm: Use of methanol as actinometer for VUV intensity measurement and reference compound for OH-radical competition kinetics in aqueous system. J. Adv. Oxid. Technol., 5(2), 155–163.
- Oppenländer, T., Walddörfer, C., Burgbacher, J., Kiermeier, M., Lachner, K. and Weinschrott, H. (2005) Improved vacuum-UV (VUV)-initiated photomineralization of organic compounds in water with a xenon excimer flow-through photoreactor (Xe_2^* lamp, 172 nm) containing an axially centered ceramic oxygenator. Chemosphere, 60,

302–309.

- Oppenländer, T. and Xu, F. (2008) Temperature effects on the Vacuum-UV (VUV)-initiated oxidation and mineralization of organic compounds in aqueous solution using a xenon excimer flow-through photoreactor at 172 nm. *Ozone Sci. Eng.*, 30, 99–104.
- Otaki, M., Okuda, A., Tajima, K., Iwasaki, T., Kinoshita, S. and Ohgaki, S. (2003) Inactivation differences of microorganisms by low pressure UV and pulsed xenon lamps. *Water Sci. Technol.*, 47(3), 185–190.
- Paleologou, A., Marakas, H., Xekoukoulotakis, N.P., Moya, A., Vergara, Y., Kalogerakis, N., Gikas, P. and Mantzavinos, D. (2007) Disinfection of Water and wastewater by TiO_2 photocatalysis, sonolysis and UV-C irradiation. *Catal. Today*, 129, 136–142.
- Pera-Titus, M., García-Molina, V., Baños, M.A., Giménez, J. and Esplugas, S. (2004) Degradation of chlorophenols by means of advanced oxidation processes: a general review. *Appl. Catal. B: Environ.*, 47, 219–256.
- Periyasamy, S., Gupta, D. and Gulrajani, M.L. (2007) Modification of one side of mulberry silk fabric by monochromatic VUV excimer lamp. *Euro. Polym. J.*, 43, 4573–4581.
- Pozos, N., Scow, K., Wuertz, S. and Darby, J. (2004) UV disinfection in a model distribution system: biofilm growth and microbial community. *Water Res.*, 38, 3083–3091.
- Qualls, R.G., Dorfman, M.H. and Johnson, J.D. (1989) Evaluation of the efficiency of

- ultraviolet disinfection systems. *Water Res.*, 23(3), 317–325.
- Qualls, R.G. and Johnson, J.D. (1983) Bioassay and dose measurement in UV disinfection. *Appl. Environ. Microbiol.*, 45(3), 872–877.
- Quici, N., Litter, M.I., Braun, A.M. and Oliveros, E. (2008) Vacuum-UV-photolysis of aqueous solutions of citric and gallic acids. *J. Photochem. Photobiol. A: Chem*, *in press*.
- Rahn, R.O., Gerstenberg, H.M. and Vavrina, G.A. (2002) Dosimetry of ionizing radiation using an iodide/iodate aqueous solution. *Appl. Rad. Isotopes*, 56, 525–534.
- Rahn, R.O., Stefan, M.I., Bolton, J.R., Goren, E., Shaw, P.-S. and Lykke, K.R. (2003) Technical Note: Quantum yield of the iodide-iodate chemical actinometer: Dependence on wavelength and concentration. *Photochem. Photobiol.*, 78(2), 146–152.
- Rajala-Mustonen, R.L. and Heinonen-Tanski, H. (1995) Effect of advanced oxidation processes on inactivation of coliphages. *Water Sci. Technol.*, 31(5–6), 131–134.
- Riesenman, P.J. and Nicholson, W.L. (2000) Role of the spore coat layers in *Bacillus subtilis* spores resistance to hydrogen peroxide, artificial UV-C, UV-B, and solar UV radiation. *Appl. Environ. Microbiol.*, 66(2), 620–626.
- Rincón, A.-G. and Pulgarin, C. (2004) Bactericidal action of illuminated TiO₂ on pure *Escherichia coli* and natural bacterial consortia: post-irradiation events in the dark and assessment of the effective disinfection time. *Appl. Catal. B: Environ.*, 49, 99–112.
- Rincón, A.-G. and Pulgarin, C. (2005) Use of coaxial photocatalytic reactor (CAPHORE) in the TiO₂ photo-assisted treatment of mixed *E. coli* and *Bacillus* sp. and bacterial

- community present in wastewater. *Catal. Today*, 101, 331–344.
- Rincón, A.-G. and Pulgarin, C. (2006) Comparative evaluation of Fe³⁺ and TiO₂ photoassisted processes in solar photocatalytic disinfection of water. *Appl. Catal. B: Environ.*, 63, 222–231.
- Ross, M.A. and Setlow, P. (2000) The *Bacillus subtilis* HBSu protein modifies the effects of α/β -type small acid-soluble spore proteins on DNA. *J. Bacteriol.*, 182(7), 1942–1948.
- Saito, T., Iwase, T., Horie, J. and Morioka, T. (1992) Mode of photocatalytic bactericidal action of powdered semiconductor TiO₂ on mutants streptococci. *J. Photochem. Photobiol. B: Biol.*, 14, 369–379.
- Sanz, E.N., Dávila, I.S., Balao J.A.A. and Alonso, J.M.Q. (2007) Modeling of reactivation after UV disinfection: Effect of UV-C dose on subsequent photoreactivation and dark repair. *Water Res.*, 41, 3141–3151.
- Setlow, B. and Setlow, P. (1987) Thymine-containing dimers as well as spore photoproducts are found in ultraviolet-irradiated *Bacillus subtilis* spores that lack small acid-soluble proteins. *Proc. Natl. Acad. Sci., USA*, 84(2), 421–423.
- Setlow, B. and Setlow, P. (1993a) Dipicolinic acid greatly enhanced production of spore photoproduct in bacterial spores upon UV irradiation. *Appl. Environ. Microbiol.*, 59(2), 640–643.
- Setlow, B. and Setlow, P. (1993b) Binding of small, acid-soluble spore proteins to DNA plays a significant role in the resistance of *Bacillus subtilis* spores to hydrogen

- peroxide. *Appl. Environ. Microbiol.*, 59(10), 3418–3423.
- Setlow, J.K. (1966) Photoreactivation. *Rad. Res. Suppl.*, 6, 141–155.
- Setlow, P. (1992a) I will survive: protecting and repairing spores DNA. *J. Bacteriol.*, 174(9), 2737–2741.
- Setlow, P. (1992b) DNA in dormant spores of *Bacillus* species is in an A-like conformation. *Mol. Microbiol.*, 6(5), 563–567.
- Setlow, P. (1995) Mechanisms for the prevention of damage to DNA in spores of *Bacillus* species. *Annu. Rev. Microbiol.*, 49, 29–54.
- Setlow, P. (2001) Resistance of spores of *Bacillus* Species to ultraviolet light. *Environ. Molecul. Mutagenes.*, 38, 97–104.
- Setlow, R. (1960) Ultraviolet wave-length-dependent effects on proteins and nucleic acids. *Rad. Res. Suppl.*, 2, 276–289.
- Setlow, R.B. (1974) The wavelengths in sunlight effective in producing skin cancer: A theoretical analysis. *Proc. Natl. Acad. Sci., USA*, 71(9), 3363–3366.
- Setlow, R.B. (2002) Reflection in mutation research: Shedding light on proteins, nucleic acids, cells, human and fish. *Mut. Res.*, 551, 1–14.
- Setlow, R.B. and Carrier, W.L. (1964) The disappearance of thymine dimers from DNA: An error-correcting mechanism. *Proc. Natl. Acad. Sci., USA*, 51(2), 226–231.
- Setlow, R.B. and Setlow, J.K. (1962) Evidence that Ultraviolet-induced thymine dimers in DNA cause biological damage. *Proc. Natl. Acad. Sci., USA*, 48(7), 1250–1257.
- Setlow, R.B., Swenson, P.A. and Carrier, W.L. (1963) Thymine dimers and inhibition of

- DNA synthesis by ultraviolet irradiation of cells. *Science, New Series*, 142(3598), 1461–1466.
- Severin, B.F., Suidan, M.T. and Engelbrecht, R.S. (1983) Kinetic modeling of u.v. disinfection of water. *Water Res.*, 17(11), 1669–1678.
- Sharrer, M.J. and Summerfelt, S.T. (2007) Ozonation followed by ultraviolet irradiation provides effective bacteria inactivation in a freshwater recirculating system. *Aquacult. Eng.* 37, 180–191.
- Siede, W., Kow, Y.W. and Doetsch, P.W. (2006) *DNA Damage Recognition*. Taylor & Francis Group, New York.
- Skurat, V. (2003) Vacuum ultraviolet photochemistry of polymers. *Nucl. Instr. and Meth. in Phys. Res. B*, 208, 27–34.
- Sommer, R., Cabaj, A., Haider, T. and Hirschmann, G. (2004) UV drinking water disinfection – requirements, testing and surveillance: exemplified by the Austrian National Standards M 5873-1 and 5873-2. *IUVA News*, 6(4), 27–35.
- Sommer, R., Cabaj, A., Sandu, T. and Lhostky, M. (1999) Measurement of UV radiation using suspensions of microorganisms. *J. Photochem. Photobiol. B: Biol.*, 53, 1–6.
- Sommer, R., Pribil, W., Pflieger, S., Haider, T., Werderitsch, M. and Gehringer, P. (2004) Microbicidal efficacy of an advanced oxidation process using ozone/hydrogen peroxide in water treatment. *Water Sci. Technol.*, 50(1), 159–164.
- Son, H., Cho, M., Kim, J., Oh, B., Chung, H. and Yoon, J. (2005) Enhanced disinfection efficiency of mechanically mixed oxidants with free chlorine. *Water Res.*, 39, 721–727.

- Sosnin, E.A., Lavrent'eva, L.V., Erofeev, M.V., Masterova, Y.V., Kuznetzova, E.N. and Tarasenko, V.F. (2004) A new bactericidal UV light sources – excilamps. Proc. of SPIE, 5483, 317–322.
- Sosnin, E.A., Oppenländer, T. and Tarasenko, V.F. (2006) Application of capacitive and barrier discharge excilamps in photoscience. J. Photochem. Photobiol. C: Photochem. Reviews, 7, 145–163.
- Summerfelt, S.T. (2003) Ozonation and UV irradiation — an introduction and examples of current applications. Aquacult. Eng., 28, 21–36.
- Sun, D.D., Tay, J.H. and Tan, K.M. (2003) Photocatalytic degradation of *E. coliform* in water. Water Res., 37, 3452–3462.
- Sunada, K., Watanabe, T. and Hashimoto, K. (2003) Studies on photokilling of bacteria on TiO₂ thin film. J. Photochem. Photobiol. A: Chem., 156, 227–233.
- Tarasenko, V.F., Lomaev, M.I., Panchenko, A.N., Skakun, V.S. and Sosnin, E.A. (1998) UV and VUV efficient excilamps. SPIE, 3343, 732–741.
- Tchobanoglous, G., Burton, F.L. and Stensel, H.D. (2003) Wastewater Engineering, Treatment and Reuse, 4th edition. The McGraw-Hill Companies, Inc., New York.
- Trombert, A., Irazoqui, H., Martín, C. and Zalazar, F. (2007) Evaluation of UV-C induced changes in *Escherichia coli* DNA using repetitive extragenic palindromic-polymerase chain reaction (REP-PCR). J. Photochem. Photobiol. B: Biol., 89, 44–49.
- US Environmental Protection Agency (USEPA) (1996). Ultraviolet light disinfection technology in drinking water application: An overview. Washington, DC, USA.

<http://yosemite.epa.gov/water/owrccatalog.nsf/e673c95b11602f2385256ae1007279fe/5a79cc8e73c4bfla85256b060072561b!OpenDocument> (available on May. 6, 2008).

US Environmental Protection Agency (USEPA) (1998) Handbook on Advanced Photochemical Oxidation Processes. Cincinnati, Ohio 45266.

US Environmental Protection Agency (USEPA) (2006a) National Primary Drinking Water Regulations: Long Term 2 Enhanced Surface Water Treatment Rule; Final Rule. Federal Register, 71(3), 653–702.

US Environmental Protection Agency (USEPA) (2006b) UV Disinfection Guidance Manual for the Final LT2ESWTR. Washington, DC 20460.

Uvbiama, R.D. (2006) The effect of upstream treatment processes on UV inactivation of microorganisms in filtered drinking water, thesis. University of Alberta. 11419 80th Avenue NW, Edmonton, AB, Canada, T6G 0R6.

Waller, L.N., Fox, N., Fox, K.F., Fox, A. and Price, R.L. (2004) Ruthenium red staining for ultrastructural visualization of a glycoprotein layer surrounding the spore of *Bacillus anthracis* and *Bacillus subtilis*. J. Microbiol. Methods, 58, 23–30.

Wang, T., MacGregor, S.J., Anderson, J.G. and Woolsey, G.A. (2005) Pulsed ultra-violet inactivation spectrum of *Escherichia coli*. Water Res., 39, 2921–2925.

Watts, R.J., Kong, S., Orr, M.P., Miller, G.C. and Henry, B.E. (1995) Photocatalytic inactivation of coliform bacteria and viruses in secondary wastewater effluent. Water Res., 29(1), 95–100.

- Zhang, J.-Y., Boyd, I.W. and Esrom, H. (1996) UV intensity measurement for a novel 222 nm excimer lamp using chemical actinometer. *Appl. Surf. Sci.*, 109 / 110, 482–486.
- Zhang, J.-Y., Esrom, H. and Boyd, I.W. (1999) UV intensity measurement of 308 nm excimer lamp using chemical actinometer. *Appl. Surf. Sci.*, 138–139, 315–319.
- Zhang, J.Y., Esrom, H., Kogelschatz, U. and Emig, G. (1993) Large area photochemical dry etching of polyimide with excimer UV lamps. *Appl. Surf. Sci.*, 69, 299–304.
- Zhang, J.-Y., Windall, G. and Boyd, I.W. (2002) UV curing of optical fibre coating using excimer lamps. *Appl. Surf. Sci.*, 186, 568–572.
- Zimmer, J.L., Slawson, R.M. and Huck, P.M. (2003) Inactivation and potential repair of *Cryptosporidium parvum* following low- and medium-pressure ultraviolet irradiation. *Water Res.*, 37, 3517–3523.
- Zhu, Z. and Kelley, M.J. (2005) Grafting onto poly(ethylene terephthalate) driven by 172 nm UV light. *Appl. Surf. Sci.*, 252, 303–310.

APPENDIX A

DETAILED EXPERIMENTAL METHODS

Appendix A-1 *Bacillus subtilis* Spore Production, Purification and Enumeration

1. Spores Production

- (1) First, the *B. subtilis* pre-culture was performed by scratching an isolated *B. subtilis* colony from a streaked plate, and aseptically inoculating the isolate into a disposable test tube (16 mm × 150 mm, borosilicate glass, Fisher Scientific Co., Canada), which contained 8 mL of sterile pre-culture media (sterilized at 121°C for 15 min in an autoclave). The pre-culture media consisted of 8 g L⁻¹ nutrient broth (Difco™, Becton, Dickinson and Company, NJ), 0.25 g L⁻¹ MgSO₄·7H₂O (Fisher Scientific Co., Canada), and 1.00 g L⁻¹ KCl (Fisher Scientific Co., Canada). The mixture of the *B. subtilis* isolate and the pre-culture media, which was contained in the test tube, was incubated at 37°C on an incubator shaker (Model innova 4080, New Brunswick Scientific Co., Inc) for about 12 h at 180 rpm. The culture should be in the log phase growth.
- (2) Modified Shaeffer Media was prepared in two steps. First, a spore production media that contained 8 g L nutrient broth, 0.25 g L⁻¹ MgSO₄·7H₂O and 1.00 g L⁻¹ KCl was prepared and adjusted to pH = 8.0 and sterilized by the autoclave. Second,

a solution containing 1 mM FeSO₄, 10 mM MnCl₂, and 1 M CaCl₂ was sterilized by the filter (0.22 μm, Millipore, Billerica, MA) and was added 1 mL/1000 mL to the spore production media. The final concentration of the nutrients in the modified Shaeffer Media was 1 μM FeSO₄, 10 μM MnCl₂, and 1 mM CaCl₂.

- (3) The modified Shaeffer Media, which contained in a baffled shake flask, was aseptically inoculated with the log phase growth *B. subtilis* culture at a dilution of approximately 1 in 1000 by volume. The flask was shaken on the incubator shaker at 200 rpm and incubated at 37°C for 5 days. After such a long period of time for incubation, the sporulation should be complete and the spores should be produced.

2. Spores Purification

- (1) The culture was harvested by centrifugation (Sorvall RC-5B Refrigerated Superspeed Centrifuge, Mandel Scientific Company Ltd.) at 7500 rpm for 20 min at 4°C. The supernatant was removed and the pellet was re-suspended with sterile DI water and centrifuged again. This process was repeated until the supernatant was clear and the pellet became almost white.
- (2) The pellet was re-suspended again in sterile DI water and heated at 80°C in a water bath for 20 min to kill any remaining vegetative cells.
- (3) The spore suspension was centrifuged again at 7500 rpm for 20 min, and re-suspended in a 50% ethanol solution, and finally refrigerated at 4°C for long-term storage.

3. Spores Enumeration

The pour plate method was used to enumerate spores. It was done by adding an aliquot spore sample to a plate (i.e., a Petri dish) and then adding adequate molten nutrient agar to the sample. The Petri dish was subsequently incubated at 37°C. The detailed procedure is shown below:

- (1) Sufficient number of 1.6% molten nutrient agar tubes was prepared first. This was complete as described by the following steps. First, weigh out and transfer 8 g nutrient broth (Difco™, Becton, Dickinson and Company, NJ.) and 16 g agar (Granulated molecular genetic, Fisher Scientific Co., Canada) per litre DI water into a clean Erlenmeyer flask. Immerse a magnetic stir bar in it. Second, heat the agar solution until it boils. Third, transfer approximate 15 mL molten agar into each of test tubes, which have been placed onto a test tubes rack beforehand. Fourth, autoclave agar at 121°C for 15 min for sterilization. Finally, place the tubes in the water bath at 50°C for future use within one week.
- (2) Sufficient number of 9.0 mL DI water tubes was subsequently prepared. DI water was transferred by 10 mL sterile disposable serological pipettes (Fisher Scientific Co., Canada). These test tubes were then autoclaved for later use to dilute spore samples.
- (3) The spore stock suspension or samples exposed to UV light were thoroughly mixed, which ensure that the no spores settled at the bottom.

- (4) A serial dilution began with a 1 mL aliquot of the well-mixed spore suspension being transferred into the first tube containing 9 mL of sterile DI water. For the spore suspensions before UV exposure and the treated samples, which were contained in the glass Petri dishes (the inner diameter = 5.8 cm), 1 mL sterile disposable serological pipettes (Fisher Scientific Co., Canada) was used to transfer 1 mL aliquot. However for the samples in the cuvettes, 1 mL glass syringe was used to transfer the same volume of the samples. Subsequently, this 10^{-1} diluted sample was vortex mixed completely. And then 1 mL aliquot of this sample was transferred into a second 9 mL dilution blank to yield 10 mL of 10^{-2} diluted sample and so on through the dilution series.
- (5) To prepare a plate, 1 mL aliquot of the desired diluted sample was aseptically transferred into a sterile disposable plastic Petri dish (100 mm × 15 mm, Fisher Scientific Co., Canada), then one nutrient agar tube containing approximate 15 mL nutrient agar was poured into the dish. The contents of the dish was carefully but completely mixed by tilting the dish back-and-forth and side-to-side 10 to 20 times. The lid of the dish should cover the bottom as soon as the transfer was finished.
- (6) The solidified agar plates were incubated at 37°C for 40 h and the colony forming units (CFU) in the region of 30 to 300 in a plate were counted. All enumerations at the proper dilution were carried out in triplicate.

APPENDIX B

RAW DATA AND CALCULATIONS

Appendix B-1 Raw Data and Relative Calculations of Exposure Experiments on Rhodamine B Solutions and Methanol Solutions

Table B.1 Raw data and calculations for the exposure experiments on Rhodamine B solutions in the first collimated beam apparatus

Run 1						
Exposure time (min)	Absorbance @ 554 nm			Average A	Std dev	$\ln(A_t/A_0)^a$
0	2.130	2.123	2.152	2.135	0.015	0.000
1	1.995	1.991	1.997	1.994	0.003	-0.068
2	1.865	1.875	1.886	1.875	0.011	-0.130
3	1.797	1.790	1.800	1.796	0.005	-0.173
4	1.728	1.715	1.720	1.721	0.007	-0.216
5	1.642	1.644	1.667	1.651	0.014	-0.257
6	1.553	1.530	1.530	1.538	0.013	-0.328
7	1.571	1.557	1.559	1.562	0.008	-0.312
8	1.509	1.520	1.513	1.514	0.006	-0.344
9	1.505	1.503	1.510	1.506	0.004	-0.349
10	1.402	1.395	1.401	1.399	0.004	-0.422

Run 2

Exposure time (min)	Absorbance @ 554 nm			Average A	Std dev	$\ln(A/A_0)^a$
0	2.102	2.097	2.098	2.099	0.003	0.000
1	2.059	2.059	2.056	2.058	0.002	-0.020
2	1.830	1.840	1.852	1.841	0.011	-0.131
3	1.771	1.771	1.773	1.772	0.001	-0.170
4	1.722	1.718	1.719	1.720	0.002	-0.199
5	1.563	1.554	1.572	1.563	0.009	-0.295
6	1.544	1.544	1.540	1.543	0.002	-0.308
7	1.533	1.520	1.517	1.523	0.009	-0.321
8	1.457	1.462	1.454	1.458	0.004	-0.365
9	1.361	1.368	1.367	1.365	0.004	-0.430
10	1.350	1.351	1.347	1.349	0.002	-0.442

Run 3

Exposure time (min)	Absorbance @ 554 nm			Average A	Std dev	$\ln(A/A_0)^a$
0	2.083	2.083	2.087	2.084	0.002	0.000
1	1.984	1.998	1.990	1.991	0.007	-0.046
2	1.822	1.813	1.814	1.816	0.005	-0.138
3	1.689	1.679	1.675	1.681	0.007	-0.215
4	1.675	1.670	1.667	1.671	0.004	-0.221
5	1.638	1.631	1.619	1.629	0.010	-0.246
6	1.524	1.502	1.503	1.510	0.012	-0.323
7	1.350	1.343	1.338	1.344	0.006	-0.439
8	1.432	1.429	1.429	1.430	0.002	-0.377
9	1.292	1.286	1.281	1.286	0.006	-0.483
10	1.296	1.294	1.304	1.298	0.005	-0.474

Overall analysis of the three runs

Exposure time (min)	$\ln(A_t/A_0)$ of 1st run	$\ln(A_t/A_0)$ of and run	$\ln(A_t/A_0)$ of 3rd run	Overall average	Overall std dev
0	0.000	0.000	0.000	0.000	0.000
1	-0.068	-0.020	-0.046	-0.045	0.024
2	-0.130	-0.131	-0.138	-0.133	0.004
3	-0.173	-0.170	-0.215	-0.186	0.025
4	-0.216	-0.199	-0.221	-0.212	0.011
5	-0.257	-0.295	-0.246	-0.266	0.026
6	-0.328	-0.308	-0.323	-0.320	0.010
7	-0.312	-0.321	-0.439	-0.357	0.071
8	-0.344	-0.365	-0.377	-0.362	0.017
9	-0.349	-0.430	-0.483	-0.421	0.067
10	-0.422	-0.442	-0.474	-0.446	0.026

^a A_0 stands for the initial absorbance of a Rhodamine B solution at a concentration of 10 mg L⁻¹. In this case, A_0 is the absorbance at the exposure time = 0 min of each run. A_t means the absorbance of a sample exposed to the UV light for a certain length of time.

Table B.2 Raw data and calculations for the exposure experiments on Rhodamine B solutions in the second collimated beam apparatus

Run 1 (cuvette #1)						
Exposure time (min)	Absorbance @ 554 nm			Average A	Std dev	$\ln(A_t/A_0)$
0	2.115	2.119	2.117	2.117	0.002	0.000
5	1.696	1.690	1.684	1.690	0.006	-0.225
10	1.304	1.302	1.301	1.302	0.002	-0.486
15	0.979	0.976	0.976	0.977	0.002	-0.773
20	0.718	0.716	0.715	0.716	0.002	-1.084

Run 2 (cuvette #2)						
Exposure time (min)	Absorbance @ 554 nm			Average A	Std dev	$\ln(A_t/A_0)$
0	2.125	2.123	2.123	2.124	0.001	0.000
5	1.713	1.708	1.704	1.708	0.005	-0.218
10	1.323	1.322	1.321	1.322	0.001	-0.474
15	0.997	0.996	0.995	0.996	0.001	-0.757
20	0.738	0.738	0.737	0.738	0.001	-1.057

Overall analysis of the two runs

Exposure time (min)	$\ln(A_t/A_0)$ of Run 1	$\ln(A_t/A_0)$ of Run 2	Overall average	Std dev
0	0.000	0.000	0.000	0.000
5	-0.225	-0.218	-0.221	0.005
10	-0.486	-0.474	-0.480	0.008
15	-0.773	-0.757	-0.765	0.011
20	-1.084	-1.057	-1.071	0.019

Table B.3 Raw data and calculations for the calibration curves of methanol solutions used for GC analyses

Run 1										In each run		
Concentration of MeOH solution = 5.015 mM, $C_{\text{MeOH}}/C_{\text{standard}}^a = 1.010$										Average of $A_{\text{MeOH}}/A_{\text{standard}}$ of 3 injections	Std dev of 3 injections	Percentage error of 3 injections
	1st injection			2nd injection			3rd injection					
	Retention time(min)	Peak area	$A_{\text{MeOH}}/$ A_{standard}^b	Retention time(min)	Peak area	$A_{\text{MeOH}}/$ A_{standard}^b	Retention time(min)	Peak area	$A_{\text{MeOH}}/$ A_{standard}^b			
MeOH	0.670	5183	0.357	0.669	5152	0.351	0.674	5736	0.353	0.354	0.003	0.94%
1,4-dioxane	1.123	14503		1.123	14684		1.129	16252				
Concentration of MeOH solution = 10.03 mM, $C_{\text{MeOH}}/C_{\text{standard}}^a = 2.020$										Average of $A_{\text{MeOH}}/A_{\text{standard}}$ of 3 injections	Std dev of 3 injections	Percentage error of 3 injections
	1st injection			2nd injection			3rd injection					
	Retention time(min)	Peak area	$A_{\text{MeOH}}/$ A_{standard}^b	Retention time(min)	Peak area	$A_{\text{MeOH}}/$ A_{standard}^b	Retention time(min)	Peak area	$A_{\text{MeOH}}/$ A_{standard}^b			
MeOH	0.673	10539	0.706	0.668	10928	0.715	0.673	11239	0.697	0.706	0.009	1.25%
1,4-dioxane	1.127	14919		1.122	15291		1.128	16123				
Concentration of MeOH solution = 15.04 mM, $C_{\text{MeOH}}/C_{\text{standard}}^a = 3.028$										Average of $A_{\text{MeOH}}/A_{\text{standard}}$ of 3 injections	Std dev of 3 injections	Percentage error of 3 injections
	1st injection			2nd injection			3rd injection					
	Retention time(min)	Peak area	$A_{\text{MeOH}}/$ A_{standard}^b	Retention time(min)	Peak area	$A_{\text{MeOH}}/$ A_{standard}^b	Retention time(min)	Peak area	$A_{\text{MeOH}}/$ A_{standard}^b			
MeOH	0.674	16720	1.038	0.673	15455	1.039	0.674	17188	1.039	1.039	0.001	0.06%
1,4-dioxane	1.129	16108		1.127	14876		1.129	16540				
Concentration of MeOH solution = 20.06 mM, $C_{\text{MeOH}}/C_{\text{standard}}^a = 4.039$										Average of $A_{\text{MeOH}}/A_{\text{standard}}$ of 3 injections	Std dev of 3 injections	Percentage error of 3 injections
	1st injection			2nd injection			3rd injection					
	Retention time(min)	Peak area	$A_{\text{MeOH}}/$ A_{standard}^b	Retention time(min)	Peak area	$A_{\text{MeOH}}/$ A_{standard}^b	Retention time(min)	Peak area	$A_{\text{MeOH}}/$ A_{standard}^b			
MeOH	0.675	22722	1.418	0.676	21673	1.427	0.669	23149	1.435	1.427	0.008	0.59%
1,4-dioxane	1.130	16024		1.131	15186		1.122	16135				

Run 2

Concentration of MeOH solution = 5.015 mM, $C_{\text{MeOH}}/C_{\text{standard}}^a = 1.010$										In each run		
	1st injection			2nd injection			3rd injection			Average of $A_{\text{MeOH}}/A_{\text{standard}}$ of 3 injections	Std dev of 3 injections	Percentage error of 3 injections
	Retention time(min)	Peak area	$A_{\text{MeOH}}/$ A_{standard}^b	Retention time(min)	Peak area	$A_{\text{MeOH}}/$ A_{standard}^b	Retention time(min)	Peak area	$A_{\text{MeOH}}/$ A_{standard}^b			
MeOH	0.674	5316	0.355	0.669	5002	0.355	0.668	5071	0.355	0.355	0.000	0.10%
1,4-dioxane	1.127	14993		1.121	14082		1.121	14280				
Concentration of MeOH solution = 10.03 mM, $C_{\text{MeOH}}/C_{\text{standard}}^a = 2.020$												
	1st injection			2nd injection			3rd injection			Average of $A_{\text{MeOH}}/A_{\text{standard}}$ of 3 injections	Std dev of 3 injections	Percentage error of 3 injections
	Retention time(min)	Peak area	$A_{\text{MeOH}}/$ A_{standard}^b	Retention time(min)	Peak area	$A_{\text{MeOH}}/$ A_{standard}^b	Retention time(min)	Peak area	$A_{\text{MeOH}}/$ A_{standard}^b			
MeOH	0.669	8933	0.688	0.668	9486	0.688	0.669	10799	0.699	0.691	0.007	0.96%
1,4-dioxane	1.121	12991		1.121	13796		1.122	15446				
Concentration of MeOH solution = 15.04 mM, $C_{\text{MeOH}}/C_{\text{standard}}^a = 3.028$												
	1st injection			2nd injection			3rd injection			Average of $A_{\text{MeOH}}/A_{\text{standard}}$ of 3 injections	Std dev of 3 injections	Percentage error of 3 injections
	Retention time(min)	Peak area	$A_{\text{MeOH}}/$ A_{standard}^b	Retention time(min)	Peak area	$A_{\text{MeOH}}/$ A_{standard}^b	Retention time(min)	Peak area	$A_{\text{MeOH}}/$ A_{standard}^b			
MeOH	0.673	16119	1.076	0.673	16394	1.081	0.674	16320	1.078	1.078	0.003	0.26%
1,4-dioxane	1.127	14985		1.127	15161		1.128	15136				
Concentration of MeOH solution = 20.06 mM, $C_{\text{MeOH}}/C_{\text{standard}}^a = 4.039$												
	1st injection			2nd injection			3rd injection			Average of $A_{\text{MeOH}}/A_{\text{standard}}$ of 3 injections	Std dev of 3 injections	Percentage error of 3 injections
	Retention time(min)	Peak area	$A_{\text{MeOH}}/$ A_{standard}^b	Retention time(min)	Peak area	$A_{\text{MeOH}}/$ A_{standard}^b	Retention time(min)	Peak area	$A_{\text{MeOH}}/$ A_{standard}^b			
MeOH	0.678	19539	1.463	1.675	21341	1.447	0.673	23406	1.457	1.456	0.008	0.56%
1,4-dioxane	1.131	13352		1.129	14745		1.128	16062				

Run 3

Concentration of MeOH solution = 5.015 mM, $C_{\text{MeOH}}/C_{\text{standard}}^a = 1.010$										In each run		
	1st injection			2nd injection			3rd injection			Average of $A_{\text{MeOH}}/A_{\text{standard}}^b$ of 3 injections	Std dev of 3 injections	Percentage error of 3 injections
	Retention time(min)	Peak area	$A_{\text{MeOH}}/$ A_{standard}^b	Retention time(min)	Peak area	$A_{\text{MeOH}}/$ A_{standard}^b	Retention time(min)	Peak area	$A_{\text{MeOH}}/$ A_{standard}^b			
MeOH	0.675	6265	0.355	0.669	5435	0.351	0.675	6377	0.360	0.355	0.004	1.17%
1,4-dioxane	1.129	17651		1.123	15473		1.130	17735				
Concentration of MeOH solution = 10.03 mM, $C_{\text{MeOH}}/C_{\text{standard}}^a = 2.020$												
	1st injection			2nd injection			3rd injection			Average of $A_{\text{MeOH}}/A_{\text{standard}}^b$ of 3 injections	Std dev of 3 injections	Percentage error of 3 injections
	Retention time(min)	Peak area	$A_{\text{MeOH}}/$ A_{standard}^b	Retention time(min)	Peak area	$A_{\text{MeOH}}/$ A_{standard}^b	Retention time(min)	Peak area	$A_{\text{MeOH}}/$ A_{standard}^b			
MeOH	0.670	11308	0.707	0.674	10517	0.690	0.671	11870	0.708	0.702	0.010	1.46%
1,4-dioxane	1.123	15985		1.127	15239		1.125	16760				
Concentration of MeOH solution = 15.04 mM, $C_{\text{MeOH}}/C_{\text{standard}}^a = 3.028$												
	1st injection			2nd injection			3rd injection			Average of $A_{\text{MeOH}}/A_{\text{standard}}^b$ of 3 injections	Std dev of 3 injections	Percentage error of 3 injections
	Retention time(min)	Peak area	$A_{\text{MeOH}}/$ A_{standard}^b	Retention time(min)	Peak area	$A_{\text{MeOH}}/$ A_{standard}^b	Retention time(min)	Peak area	$A_{\text{MeOH}}/$ A_{standard}^b			
MeOH	0.674	16927	1.051	0.673	16562	1.061	0.669	16478	1.053	1.055	0.005	0.49%
1,4-dioxane	1.129	16101		1.128	15608		1.123	15645				
Concentration of MeOH solution = 20.06 mM, $C_{\text{MeOH}}/C_{\text{standard}}^a = 4.039$												
	1st injection			2nd injection			3rd injection			Average of $A_{\text{MeOH}}/A_{\text{standard}}^b$ of 3 injections	Std dev of 3 injections	Percentage error of 3 injections
	Retention time(min)	Peak area	$A_{\text{MeOH}}/$ A_{standard}^b	Retention time(min)	Peak area	$A_{\text{MeOH}}/$ A_{standard}^b	Retention time(min)	Peak area	$A_{\text{MeOH}}/$ A_{standard}^b			
MeOH	0.669	23375	1.488	0.676	23777	1.477	0.669	22504	1.476	1.480	0.007	0.46%
1,4-dioxane	1.123	15707		1.130	16094		1.123	15249				

Overall analysis of the three runs

Concentration of methanol solution	Average of $A_{\text{MeOH}}/A_{\text{standard}}$ of 1st run	Average of $A_{\text{MeOH}}/A_{\text{standard}}$ of 2nd run	Average of $A_{\text{MeOH}}/A_{\text{standard}}$ of 3rd run	Overall average of 3 runs	Std dev of 3 runs	Percentage error of 3 runs
5.015 mM	0.354	0.355	0.355	0.355	0.001	0.23%
10.03 mM	0.706	0.691	0.702	0.700	0.008	1.08%
15.04 mM	1.039	1.078	1.055	1.057	0.020	1.89%
20.06 mM	1.427	1.456	1.480	1.454	0.027	1.85%

^a $C_{\text{MeOH}}/C_{\text{standard}}$ is a ratio of the concentration of a methanol solution to that of the 1,4-dioxane solution (the internal standard for GC analyses) in a mixture that was prepared by mixing 1 mL of a methanol solution at a know concentration (5.015, 10.03, 15.04 or 20.06 mM) with 0.5 mL of the 1,4-dioxane solution at 9.933 mM.

^b $A_{\text{MeOH}}/A_{\text{standard}}$ is a ratio of a peak area of methanol to that of 1,4-dioxane in a mixture counted from a chromatogram of GC. The numbers of A_{MeOH} and A_{standard} are shown in the previous column of this table.

Table B.4 Raw data and calculations for the concentrations of methanol solutions exposed to the VUV light

Run 1													
0.5 h exposure time													
Before exposure for 0.5 h (the concentration of the stock solution) ^a													
	1st injection			2nd injection			3rd injection			Average $A_{\text{MeOH}}/A_{\text{standard}}$ of 3 injections	Average MeOH conc. (mM) ^d	Std dev of $A_{\text{MeOH}}/A_{\text{standard}}$ of 3 injections	Percentage error of 3 injections
	Retention time(min)	Peak area	$A_{\text{MeOH}}/A_{\text{standard}}$	Retention time(min)	Peak area	$A_{\text{MeOH}}/A_{\text{standard}}$	Retention time(min)	Peak area	$A_{\text{MeOH}}/A_{\text{standard}}$				
MeOH	0.686	9622	1.117	0.678	16774	1.139	0.680	18913	1.140	1.132	15.83	0.013	1.17%
1,4-dioxane	1.145	8617		1.138	14732		1.140	16584					
cuvette #1 after exposure for 0.5 h (blank) ^b													
	1st injection			2nd injection			3rd injection			Average $A_{\text{MeOH}}/A_{\text{standard}}$ of 3 injections	Average MeOH conc. (mM) ^d	Std dev of $A_{\text{MeOH}}/A_{\text{standard}}$ of 3 injections	Percentage error of 3 injections
	Retention time(min)	Peak area	$A_{\text{MeOH}}/A_{\text{standard}}$	Retention time(min)	Peak area	$A_{\text{MeOH}}/A_{\text{standard}}$	Retention time(min)	Peak area	$A_{\text{MeOH}}/A_{\text{standard}}$				
MeOH	0.682	10650	0.986	0.682	10511	1.000	0.676	9051	1.000	0.995	13.96	0.008	0.81%
1,4-dioxane	1.140	10800		1.140	10507		1.133	9054					
cuvette #2 after exposure for 0.5 h ^c													
	1st injection			2nd injection			3rd injection			Average $A_{\text{MeOH}}/A_{\text{standard}}$ of 3 injections	Average MeOH conc. (mM) ^d	Std dev of $A_{\text{MeOH}}/A_{\text{standard}}$ of 3 injections	Percentage error of 3 injections
	Retention time(min)	Peak area	$A_{\text{MeOH}}/A_{\text{standard}}$	Retention time(min)	Peak area	$A_{\text{MeOH}}/A_{\text{standard}}$	Retention time(min)	Peak area	$A_{\text{MeOH}}/A_{\text{standard}}$				
MeOH	0.682	10309	0.848	0.680	14982	0.884	0.682	9336	0.831	0.854	12.03	0.027	3.15%
1,4-dioxane	1.141	12154		1.140	16951		1.140	11234					

1 h exposure time										Average $A_{\text{MeOH}}/A_{\text{standard}}$ of 3 injections	Average MeOH conc. (mM) ^d	Std dev of $A_{\text{MeOH}}/A_{\text{standard}}$ of 3 injections	Percentage error of 3 injections
Before exposure for 1 h (the concentration of the stock solution) ^a													
	1st injection			2nd injection			3rd injection						
	Retention time(min)	Peak area	$A_{\text{MeOH}}/A_{\text{standard}}$	Retention time(min)	Peak area	$A_{\text{MeOH}}/A_{\text{standard}}$	Retention time(min)	Peak area	$A_{\text{MeOH}}/A_{\text{standard}}$				
MeOH	0.670	18701	1.152	0.673	13781	1.086	0.673	14819	1.102	1.113	15.57	0.034	3.07%
1,4-dioxane	1.125	16237		1.125	12687		1.126	13449					
cuvette #1 after exposure for 1 h (blank) ^b													
	1st injection			2nd injection			3rd injection						
	Retention time(min)	Peak area	$A_{\text{MeOH}}/A_{\text{standard}}$	Retention time(min)	Peak area	$A_{\text{MeOH}}/A_{\text{standard}}$	Retention time(min)	Peak area	$A_{\text{MeOH}}/A_{\text{standard}}$				
MeOH	0.669	16029	1.026	0.670	15882	1.029	0.675	18702	1.040	1.032	14.46	0.007	0.70%
1,4-dioxane	1.123	15620		1.123	15428		1.130	17982					
cuvette #2 after exposure for 1 h ^c													
	1st injection			2nd injection			3rd injection						
	Retention time(min)	Peak area	$A_{\text{MeOH}}/A_{\text{standard}}$	Retention time(min)	Peak area	$A_{\text{MeOH}}/A_{\text{standard}}$	Retention time(min)	Peak area	$A_{\text{MeOH}}/A_{\text{standard}}$				
MeOH	0.671	13893	0.778	0.670	12877	0.773	0.673	7845	0.751	0.767	10.83	0.015	1.91%
1,4-dioxane	1.125	17853		1.123	16667		1.125	10453					
1.5 h exposure time													
Before exposure for 1.5 h (the concentration of the stock solution) ^a													
	1st injection			2nd injection			3rd injection						
	Retention time(min)	Peak area	$A_{\text{MeOH}}/A_{\text{standard}}$	Retention time(min)	Peak area	$A_{\text{MeOH}}/A_{\text{standard}}$	Retention time(min)	Peak area	$A_{\text{MeOH}}/A_{\text{standard}}$				
MeOH	0.669	17675	1.120	0.668	16593	1.125	0.672	18806	1.128	1.124	15.73	0.004	0.37%
1,4-dioxane	1.122	15782		1.121	14749		1.125	16669					

cuvette #1 after exposure for 1.5 h (blank)^b										Average $A_{\text{MeOH}}/A_{\text{standard}}$ of 3 injections	Average MeOH conc. (mM) ^d	Std dev of $A_{\text{MeOH}}/A_{\text{standard}}$ of 3 injections	Percentage error of 3 injections
1st injection			2nd injection			3rd injection							
	Retention time(min)	Peak area	$A_{\text{MeOH}}/A_{\text{standard}}$	Retention time(min)	Peak area	$A_{\text{MeOH}}/A_{\text{standard}}$	Retention time(min)	Peak area	$A_{\text{MeOH}}/A_{\text{standard}}$				
MeOH	0.668	14971	1.028	0.674	15158	1.028	0.673	14851	1.031	1.029	14.42	0.002	0.15%
1,4-dioxane	1.120	14561		1.128	14739		1.126	14404					
cuvette #2 after exposure for 1.5 h^c													
1st injection			2nd injection			3rd injection							
	Retention time(min)	Peak area	$A_{\text{MeOH}}/A_{\text{standard}}$	Retention time(min)	Peak area	$A_{\text{MeOH}}/A_{\text{standard}}$	Retention time(min)	Peak area	$A_{\text{MeOH}}/A_{\text{standard}}$				
MeOH	0.669	10114	0.633	0.669	9440	0.637	0.670	10854	0.635	0.635	9.03	0.002	0.32%
1,4-dioxane	1.121	15967		1.121	14808		1.124	17083					
2 h exposure time													
Before exposure for 2 h (the concentration of the stock solution)^a													
1st injection			2nd injection			3rd injection							
	Retention time(min)	Peak area	$A_{\text{MeOH}}/A_{\text{standard}}$	Retention time(min)	Peak area	$A_{\text{MeOH}}/A_{\text{standard}}$	Retention time(min)	Peak area	$A_{\text{MeOH}}/A_{\text{standard}}$				
MeOH	0.673	16182	1.125	0.673	12104	1.118	0.674	10643	1.089	1.111	15.54	0.019	1.74%
1,4-dioxane	1.126	14381		1.125	10825		1.126	9775					
cuvette #1 after exposure for 2 h (blank)^b													
1st injection			2nd injection			3rd injection							
	Retention time(min)	Peak area	$A_{\text{MeOH}}/A_{\text{standard}}$	Retention time(min)	Peak area	$A_{\text{MeOH}}/A_{\text{standard}}$	Retention time(min)	Peak area	$A_{\text{MeOH}}/A_{\text{standard}}$				
MeOH	0.668	15445	1.018	0.668	14566	1.023	0.669	15701	1.004	1.015	14.23	0.010	0.99%
1,4-dioxane	1.120	15170		1.120	14235		1.122	15641					

cuvette #2 after exposure for 2 h ^c										Average $A_{\text{MeOH}}/A_{\text{standard}}$ of 3 injections	Average MeOH conc. (mM) ^d	Std dev of $A_{\text{MeOH}}/A_{\text{standard}}$ of 3 injections	Percentage error of 3 injections
1st injection			2nd injection			3rd injection							
	Retention time(min)	Peak area	$A_{\text{MeOH}}/A_{\text{standard}}$	Retention time(min)	Peak area	$A_{\text{MeOH}}/A_{\text{standard}}$	Retention time(min)	Peak area	$A_{\text{MeOH}}/A_{\text{standard}}$				
MeOH	0.667	7265	0.525	0.673	6630	0.526	0.673	8828	0.535	0.529	7.57	0.005	0.99%
1,4-dioxane	1.119	13826		1.125	12608		1.127	16509					
2.5 h exposure time													
Before exposure for 2.5 h (the concentration of the stock solution) ^a													
1st injection			2nd injection			3rd injection							
	Retention time(min)	Peak area	$A_{\text{MeOH}}/A_{\text{standard}}$	Retention time(min)	Peak area	$A_{\text{MeOH}}/A_{\text{standard}}$	Retention time(min)	Peak area	$A_{\text{MeOH}}/A_{\text{standard}}$				
MeOH	0.674	18721	1.171	0.674	16845	1.118	0.674	16491	1.128	1.139	15.93	0.028	2.49%
1,4-dioxane	1.132	15985		1.131	15069		1.131	14620					
cuvette #1 after exposure for 2.5 h (blank) ^b													
1st injection			2nd injection			3rd injection							
	Retention time(min)	Peak area	$A_{\text{MeOH}}/A_{\text{standard}}$	Retention time(min)	Peak area	$A_{\text{MeOH}}/A_{\text{standard}}$	Retention time(min)	Peak area	$A_{\text{MeOH}}/A_{\text{standard}}$				
MeOH	0.674	16525	1.051	0.679	16355	1.057	0.675	17073	1.048	1.052	14.73	0.005	0.43%
1,4-dioxane	1.131	15723		1.137	15477		1.133	16294					
cuvette #2 after exposure for 2.5 h ^c													
1st injection			2nd injection			3rd injection							
	Retention time(min)	Peak area	$A_{\text{MeOH}}/A_{\text{standard}}$	Retention time(min)	Peak area	$A_{\text{MeOH}}/A_{\text{standard}}$	Retention time(min)	Peak area	$A_{\text{MeOH}}/A_{\text{standard}}$				
MeOH	0.679	5769	0.428	0.675	6860	0.439	0.678	5582	0.429	0.432	6.24	0.006	1.32%
1,4-dioxane	1.136	13473		1.132	15640		1.135	12999					

Run 2

0.5 h exposure time

Before exposure for 0.5 h (the concentration of the stock solution)^a

1st injection		2nd injection		3rd injection		Average $A_{\text{MeOH}}/A_{\text{standard}}$ of 3 injections	Average MeOH conc. (mM) ^d	Std dev of $A_{\text{MeOH}}/A_{\text{standard}}$ of 3 injections	Percentage error of 3 injections				
Retention Peak time(min)	Peak area	Retention Peak time(min)	Peak area	Retention Peak time(min)	Peak area								
MeOH	0.674	20061	1.133	0.678	17446	1.120	0.678	16459	1.112	1.122	15.69	0.010	0.93%
1,4-dioxane	1.131	17707		1.135	15573		1.134	14799					

cuvette #1 after exposure for 0.5 h (blank)^b

1st injection		2nd injection		3rd injection		Average $A_{\text{MeOH}}/A_{\text{standard}}$ of 3 injections	Average MeOH conc. (mM) ^d	Std dev of $A_{\text{MeOH}}/A_{\text{standard}}$ of 3 injections	Percentage error of 3 injections				
Retention Peak time(min)	Peak area	Retention Peak time(min)	Peak area	Retention Peak time(min)	Peak area								
MeOH	0.672	14773	1.000	0.678	17405	1.025	0.678	16799	0.990	1.005	14.09	0.018	1.82%
1,4-dioxane	1.127	14768		1.135	16975		1.135	16953					

cuvette #2 after exposure for 0.5 h^c

1st injection		2nd injection		3rd injection		Average $A_{\text{MeOH}}/A_{\text{standard}}$ of 3 injections	Average MeOH conc. (mM) ^d	Std dev of $A_{\text{MeOH}}/A_{\text{standard}}$ of 3 injections	Percentage error of 3 injections				
Retention Peak time(min)	Peak area	Retention Peak time(min)	Peak area	Retention Peak time(min)	Peak area								
MeOH	0.677	13428	0.811	0.673	13426	0.827	0.674	13659	0.817	0.819	11.54	0.008	1.00%
1,4-dioxane	1.134	16557		1.129	16228		1.130	16709					

1 h exposure time										Average $A_{\text{MeOH}}/A_{\text{standard}}$ of 3 injections	Average MeOH conc. (mM) ^d	Std dev of $A_{\text{MeOH}}/A_{\text{standard}}$ of 3 injections	Percentage error of 3 injections
Before exposure for 1 h (the concentration of the stock solution) ^a													
	1st injection			2nd injection			3rd injection						
	Retention time(min)	Peak area	$A_{\text{MeOH}}/A_{\text{standard}}$	Retention time(min)	Peak area	$A_{\text{MeOH}}/A_{\text{standard}}$	Retention time(min)	Peak area	$A_{\text{MeOH}}/A_{\text{standard}}$				
MeOH	0.675	18495	1.127	0.674	18053	1.124	0.676	19175	1.127				
1,4-dioxane	1.132	16409		1.132	16056		1.133	17013					
cuvette #1 after exposure for 1 h (blank) ^b													
	1st injection			2nd injection			3rd injection						
	Retention time(min)	Peak area	$A_{\text{MeOH}}/A_{\text{standard}}$	Retention time(min)	Peak area	$A_{\text{MeOH}}/A_{\text{standard}}$	Retention time(min)	Peak area	$A_{\text{MeOH}}/A_{\text{standard}}$				
MeOH	0.676	18003	1.068	0.674	16145	1.040	0.679	15057	1.027	1.045	14.64	0.021	1.98%
1,4-dioxane	1.133	16858		1.132	15519		1.137	14656					
cuvette #2 after exposure for 1 h ^c													
	1st injection			2nd injection			3rd injection						
	Retention time(min)	Peak area	$A_{\text{MeOH}}/A_{\text{standard}}$	Retention time(min)	Peak area	$A_{\text{MeOH}}/A_{\text{standard}}$	Retention time(min)	Peak area	$A_{\text{MeOH}}/A_{\text{standard}}$				
MeOH	0.676	12038	0.696	0.676	12316	0.700	0.678	9884	0.676	0.691	9.78	0.013	1.82%
1,4-dioxane	1.134	17302		1.133	17602		1.136	14617					
1.5 h exposure time													
Before exposure for 1.5 h (the concentration of the stock solution) ^a													
	1st injection			2nd injection			3rd injection						
	Retention time(min)	Peak area	$A_{\text{MeOH}}/A_{\text{standard}}$	Retention time(min)	Peak area	$A_{\text{MeOH}}/A_{\text{standard}}$	Retention time(min)	Peak area	$A_{\text{MeOH}}/A_{\text{standard}}$				
MeOH	0.674	17298	1.116	0.677	20493	1.133	0.680	19722	1.144	1.131	15.82	0.014	1.25%
1,4-dioxane	1.131	15499		1.135	18090		1.139	17238					

cuvette #1 after exposure for 1.5 h (blank)^b										Average $A_{\text{MeOH}}/A_{\text{standard}}$ of 3 injections	Average MeOH conc. (mM) ^d	Std dev of $A_{\text{MeOH}}/A_{\text{standard}}$ of 3 injections	Percentage error of 3 injections
1st injection			2nd injection			3rd injection							
Retention time(min)	Peak area	$A_{\text{MeOH}}/A_{\text{standard}}$	Retention time(min)	Peak area	$A_{\text{MeOH}}/A_{\text{standard}}$	Retention time(min)	Peak area	$A_{\text{MeOH}}/A_{\text{standard}}$					
MeOH	0.675	16730	1.033	0.674	15405	1.024	0.674	15469	1.017	1.024	14.36	0.008	0.79%
1,4-dioxane	1.132	16197		1.131	15049		1.131	15215					
cuvette #2 after exposure for 1.5 h^c										0.577	8.22	0.001	0.25%
1st injection			2nd injection			3rd injection							
Retention time(min)	Peak area	$A_{\text{MeOH}}/A_{\text{standard}}$	Retention time(min)	Peak area	$A_{\text{MeOH}}/A_{\text{standard}}$	Retention time(min)	Peak area	$A_{\text{MeOH}}/A_{\text{standard}}$					
MeOH	0.675	9554	0.576	0.680	9903	0.578	0.675	9349	0.576				
1,4-dioxane	1.133	16573		1.138	17122		1.132	16244					
2 h exposure time													
Before exposure for 2 h (the concentration of the stock solution)^a													
1st injection			2nd injection			3rd injection			1.121	15.68	0.009	0.76%	
Retention time(min)	Peak area	$A_{\text{MeOH}}/A_{\text{standard}}$	Retention time(min)	Peak area	$A_{\text{MeOH}}/A_{\text{standard}}$	Retention time(min)	Peak area	$A_{\text{MeOH}}/A_{\text{standard}}$					
MeOH	0.676	10257	1.111	0.682	19527	1.125	0.677	17519	1.126				
1,4-dioxane	1.133	9231		1.141	17351		1.135	15554					
cuvette #1 after exposure for 2 h (blank)^b													
1st injection			2nd injection			3rd injection			0.989	13.88	0.004	0.37%	
Retention time(min)	Peak area	$A_{\text{MeOH}}/A_{\text{standard}}$	Retention time(min)	Peak area	$A_{\text{MeOH}}/A_{\text{standard}}$	Retention time(min)	Peak area	$A_{\text{MeOH}}/A_{\text{standard}}$					
MeOH	0.678	16239	0.990	0.678	17797	0.985	0.679	17525	0.993				
1,4-dioxane	1.137	16400		1.138	18062		1.138	17657					

cuvette #2 after exposure for 2 h ^c										Average $A_{\text{MeOH}}/A_{\text{standard}}$ of 3 injections	Average MeOH conc. (mM) ^d	Std dev of $A_{\text{MeOH}}/A_{\text{standard}}$ of 3 injections	Percentage error of 3 injections
1st injection			2nd injection			3rd injection							
	Retention time(min)	Peak area	$A_{\text{MeOH}}/A_{\text{standard}}$	Retention time(min)	Peak area	$A_{\text{MeOH}}/A_{\text{standard}}$	Retention time(min)	Peak area	$A_{\text{MeOH}}/A_{\text{standard}}$				
MeOH	0.678	7809	0.503	0.678	8183	0.511	0.683	7486	0.488	0.501	7.18	0.011	2.27%
1,4-dioxane	1.136	15537		1.136	16018		1.141	15327					
2.5 h exposure time													
Before exposure for 2.5 h (the concentration of the stock solution) ^a													
1st injection			2nd injection			3rd injection							
	Retention time(min)	Peak area	$A_{\text{MeOH}}/A_{\text{standard}}$	Retention time(min)	Peak area	$A_{\text{MeOH}}/A_{\text{standard}}$	Retention time(min)	Peak area	$A_{\text{MeOH}}/A_{\text{standard}}$				
MeOH	0.677	18198	1.128	0.677	18150	1.116	0.680	17276	1.099	1.114	15.59	0.014	1.30%
1,4-dioxane	1.135	16131		1.136	16269		1.140	15716					
cuvette #1 after exposure for 2.5 h (blank) ^b													
1st injection			2nd injection			3rd injection							
	Retention time(min)	Peak area	$A_{\text{MeOH}}/A_{\text{standard}}$	Retention time(min)	Peak area	$A_{\text{MeOH}}/A_{\text{standard}}$	Retention time(min)	Peak area	$A_{\text{MeOH}}/A_{\text{standard}}$				
MeOH	0.680	11680	0.877	0.677	14237	1.912	0.682	16688	0.920	0.903	12.69	0.023	2.51%
1,4-dioxane	1.138	13313		1.135	15613		1.142	18136					
cuvette #2 after exposure for 2.5 h ^c													
1st injection			2nd injection			3rd injection							
	Retention time(min)	Peak area	$A_{\text{MeOH}}/A_{\text{standard}}$	Retention time(min)	Peak area	$A_{\text{MeOH}}/A_{\text{standard}}$	Retention time(min)	Peak area	$A_{\text{MeOH}}/A_{\text{standard}}$				
MeOH	0.682	4379	0.317	0.677	5314	0.331	0.678	5301	0.328	0.325	4.78	0.007	2.25%
1,4-dioxane	1.140	13804		1.135	16039		1.136	16179					

^aThe concentration of the stock solution was first analyzed by GC. The theoretical concentration was 15.04 mM. But it probably

changed due to the evaporation, during transferring solutions to be treated from it.

^{b, c}Cuvette #1 was exposed by UV with cuvette #2 simultaneously. The difference was that cuvette #1 was always covered by an aluminum foil as a blank run, but the sample in cuvette #2 was actually exposed to UV.

^dThe average methanol concentration of each sample was determined by the mathematical model shown in Equation [3.16]: $C_{\text{MeOH}} / C_{\text{standard}} = 2.7582 \times A_{\text{MeOH}} / A_{\text{standard}} + 0.065$. The value of $A_{\text{MeOH}} / A_{\text{standard}}$ used in this model was the average value of $A_{\text{MeOH}} / A_{\text{standard}}$ of 3 injections for each sample. Since 1 mL of methanol sample was analyzed by GC mixed with 0.5 mL 1,4-dioxane solution at 9.933 mM, the methanol and 1,4-dioxane solution were diluted by each other in the mixture. The concentration of methanol in the mixture were only 2/3 of that in the actual methanol sample, at the same time, the concentration of 1,4-dioxane in the mixture was 1/3 of 9.933 mM. Therefore, the actual concentration of a treated methanol sample was determined by Equation [3.17]: $C_{\text{MeOH}} = (2.7582 \times A_{\text{MeOH}} / A_{\text{standard}} + 0.065) \times (9.933 \times 1/3) / (2/3)$.

Table B.5 Calculations for the rate of methanol degradation versus UV exposure time

Run 1						
Time (T) (h)	Stock solution conc. (mM) ^a	Concentration of cuvette #1 covered by Al foil (blank) (mM)	Concentration of Cuvette #2 exposed to UV (mM)	Corrected conc. of cuvette #2 plus blank factor (mM) ^b	Pure degradation in cuvette #2 (mM) ^c	
0	15.72 ^d			15.72 ^e		
0.5	15.83	13.96	12.03	13.90	1.82	
1	15.57	14.46	10.83	11.94	3.78	
1.5	15.73	14.42	9.03	10.34	5.38	
2	15.54	14.23	7.57	8.88	6.84	
2.5	15.93	14.73	6.24	7.44	8.28	

Std dev of stock solution conc.^f = 0.17
 Percentage error of stock solution conc. = 1.06%

Run 2

Time (<i>T</i>) (h)	Stock solution conc. (mM) ^a	Concentration of cuvette #1 covered by Al foil (blank) (mM)	Concentration of Cuvette #2 exposed to UV (mM)	Corrected conc. of cuvette #2 plus blank factor (mM) ^b	Pure degradation in cuvette #2 (mM) ^c
0	15.71 ^d			15.71 ^e	
0.5	15.69	14.09	11.54	13.14	2.57
1	15.75	14.64	9.78	10.89	4.82
1.5	15.82	14.36	8.22	9.68	6.03
2	15.68	13.88	7.18	8.98	6.73
2.5	15.59	12.69	4.78	7.68	8.03

Std dev of stock solution conc.^f = 0.09

Percentage error of stock solution conc. = 0.55%

Overall analysis of the two runs

Time (<i>T</i>) (h)	Average of the corrected concentrations of cuvette #2 of duplicate runs (mM)	Std dev of the corrected concentrations of cuvette #2 of duplicate runs (mM)	Percentage error of the corrected concentrations of cuvette #2 of duplicate runs (mM)
0	15.72	0.01	0.06%
0.5	13.52	0.54	3.97%
1	11.42	0.74	6.50%
1.5	10.01	0.47	4.66%
2	8.93	0.07	0.79%
2.5	7.56	0.17	2.24%

Zero-order reaction rate constant (mM h⁻¹)

Run 1	Run 2	Average	Std dev	Percentage error
3.32	3.08	3.20	0.17	5.36%

^aThe values of this column are from the initial concentrations of stock solution measured before each exposure experiment, which have been shown in Table B.4.

^bThe values of this column was calculated by: “Concentration of Cuvette #2 exposed to UV” + “Stock solution conc.” – “Concentration of cuvette #1 covered by Al foil (blank)” at the same exposure time (T).

^cThe pure degradation in cuvettes #2 at a certain exposure time (T) was calculated by the difference of the “stock solution conc.” at time = 0 h and the “corrected conc. of cuvette #2 plus blank factor” at the exposure time (T).

^dThe concentration of stock solution at time = 0 h was the average value of the initial concentrations of the stock solution analyzed every time before exposure experiments.

^eThe corrected concentration of cuvette #2 at time = 0 h was considered to be the same as the concentration of stock solution at time = 0 h, since no irradiance has treated the sample at this time.

^fThis value is calculated from the standard deviation of the initial concentrations of stock solutions measured before each experiment for exposure time from 0.5 h to 2.5 h.

Appendix B-2 CFU Enumeration of *Bacillus subtilis* Spores

Table B.6 CFU enumeration of *B. subtilis* spores exposed to the VUV light at 172 nm

	Exposure time (min)	Fluence (mJ cm ⁻²)	Dilution	CFU counts			Geometric mean	<i>N</i> (CFU mL ⁻¹)	Log inactivation
Run 1	0 ^a	0	10 ⁻⁵	27	40	42	35.7	3.57E+06	
	5	200.7	10 ⁻⁴	122	99	114	111.2	1.11E+06	0.507
Run 2	0 ^a	0	10 ⁻⁵	48	54	45	48.9	4.89E+06	
	5	200.7	10 ⁻⁴	118	119	104	113.5	1.13E+06	0.636
Run 3	0 ^a	0	10 ⁻⁵	30	38	46	37.4	3.74E+06	
	5	200.7	10 ⁻⁴	141	150	147	146.0	1.46E+06	0.409
Run 1	0 ^a	0	10 ⁻⁴	307	292	280	292.8	2.93E+06	
	10	401.4	10 ⁻⁴	44	32	35	36.7	3.67E+05	0.902
Run 2	0 ^a	0	10 ⁻⁵	33	38	33	34.6	3.46E+06	
	10	401.4	10 ⁻⁴	42	38	33	37.5	3.75E+05	0.965
Run 3	0 ^a	0	10 ⁻⁵	37	38	34	36.3	3.63E+06	
	10	401.4	10 ⁻⁴	39	38	36	37.6	3.76E+05	0.985
Run 1	0 ^a	0	10 ⁻⁵	41	32	38	36.8	3.68E+06	
	15	602.1	10 ⁻³	224	234	202	219.6	2.20E+05	1.223
Run 2	0 ^a	0	10 ⁻⁵	41	41	35	38.9	3.89E+06	
	15	602.1	10 ⁻³	212	196	219	208.8	2.09E+05	1.270
Run 3	0 ^a	0	10 ⁻⁵	37	34	38	36.3	3.63E+06	
	15	602.1	10 ⁻³	238	226	221	228.2	2.28E+05	1.202
Run 1	0 ^a	0	10 ⁻⁵	44	39	42	41.6	4.16E+06	
	30	1204.2	10 ⁻²	229	236	233	232.6	2.33E+04	2.252
Run 2	0 ^a	0	10 ⁻⁵	37	39	37	37.7	3.77E+06	
	30	1204.2	10 ⁻²	242	213	250	234.4	2.34E+04	2.207
Run 3	0 ^a	0	10 ⁻⁴	216	224	211	216.9	2.17E+06	
	30	1204.2	10 ⁻²	136	125	130	130.3	1.30E+04	2.223
Run 1	0 ^a	0	10 ⁻⁵	41	34	45	39.7	3.97E+06	
	60	2408.4	10 ⁻¹	213	227	215	218.2	2.18E+03	3.260
Run 2	0 ^a	0	10 ⁻⁵	31	30	36	32.2	3.22E+06	
	60	2408.4	10 ⁻¹	135	150	152	145.5	1.45E+03	3.346
Run 3	0 ^a	0	10 ⁻⁵	36	31	34	33.6	3.36E+06	
	60	2408.4	10 ⁻¹	158	149	154	153.6	1.53E+03	3.342

Overall analysis

Exposure time (min)	Fluence (mJ cm ⁻²)	Average log inactivation ^b	Standard deviation ^b	Percentage error ^b
10	401.4	0.951	0.043	4.53%
15	602.1	1.232	0.035	2.81%
30	1204.2	2.227	0.023	1.02%
60	2408.4	3.316	0.048	1.46%

^aThis value derived from cuvette #1, which was covered by aluminum foil.

^bThis value was calculated based on triplicate runs for each exposure time.

Table B.7 CFU enumeration of *B. subtilis* spores exposed to the UV light at 254 nm

	Fluence	Dilution	CFU counts			Geometric	<i>N</i>	Log inactivation	<i>N/N</i> ₀
	(mJ cm ⁻²)		mean	(CFU mL ⁻¹)	log(<i>N</i> ₀ / <i>N</i>)				
Run 1	0.0	10 ⁻⁴	221	209	250	226.0	2.26E+06	0.000	1.00E+00
	4.4	10 ⁻⁴	292	252	266	269.5	2.69E+06	-0.076	1.19E+00
	8.8	10 ⁻⁴	188	205	176	189.3	1.89E+06	0.078	8.36E-01
	13.1	10 ⁻⁴	150	133	150	144.1	1.44E+06	0.196	6.37E-01
	17.5	10 ⁻⁴	102	100	94	98.6	9.86E+05	0.360	4.36E-01
	26.3	10 ⁻³	167	161	155	160.9	1.61E+05	1.147	7.12E-02
	35.0	10 ⁻³	51	37	50	45.5	4.55E+04	1.696	2.01E-02
	52.6	10 ⁻²	48	53	67	55.4	5.54E+03	2.611	2.45E-03
	70.1	10 ⁻¹	75	95	110	92.2	9.22E+02	3.389	4.08E-04
Run 2	0.0	10 ⁻⁴	242	218	245	234.7	2.35E+06	0.000	1.00E+00
	4.4	10 ⁻⁴	237	240	238	238.3	2.38E+06	-0.006	1.01E+00
	8.8	10 ⁻⁴	193	171	198	187.0	1.87E+06	0.099	7.96E-01
	13.1	10 ⁻⁴	109	107	122	112.5	1.12E+06	0.322	4.77E-01
	17.5	10 ⁻⁴	75	57	75	68.4	6.84E+05	0.536	2.91E-01
	26.3	10 ⁻³	141	130	146	138.8	1.39E+05	1.228	5.91E-02
	35.0	10 ⁻³	28	32	32	30.6	3.06E+04	1.885	1.30E-02
	52.6	10 ⁻²	42	45	46	44.3	4.43E+03	2.725	1.89E-03
	70.1	10 ⁻¹	65	77	89	76.4	7.64E+02	3.488	3.25E-04
Run 3	0.0	10 ⁻⁴	237	236	242	238.3	2.38E+06	0.000	1.00E+00
	4.4	10 ⁻⁴	239	230	257	241.7	2.42E+06	-0.007	1.02E+00
	8.8	10 ⁻⁴	182	193	195	189.9	1.90E+06	0.098	7.98E-01
	13.1	10 ⁻⁴	140	151	132	140.8	1.41E+06	0.227	5.92E-01
	17.5	10 ⁻⁴	72	59	74	68.0	6.80E+05	0.544	2.86E-01
	26.3	10 ⁻³	136	135	140	137.0	1.37E+05	1.240	5.76E-02
	35.0	10 ⁻³	43	46	41	43.3	4.33E+04	1.740	1.82E-02
	52.6	10 ⁻²	49	50	52	50.3	5.03E+03	2.675	2.11E-03
	70.1	10 ⁻¹	63	64	54	60.2	6.02E+02	3.597	2.53E-04

Overall analysis of the three runs

Fluence (mJ cm ⁻²)	Run 1 log(N ₀ /N)	Run 2 log(N ₀ /N)	Run 3 log(N ₀ /N)	Geometric mean of log(N ₀ /N)	Std dev	Percentage error
4.4	-0.076	-0.006	-0.007	-0.029	0.040	-135.77%
8.8	0.078	0.099	0.098	0.092	0.012	13.19%
13.1	0.196	0.322	0.227	0.248	0.066	26.42%
17.5	0.360	0.536	0.544	0.480	0.104	21.64%
26.3	1.147	1.228	1.225	1.200	0.046	3.81%
35.0	1.696	1.885	1.740	1.774	0.099	5.58%
52.6	2.611	2.725	2.675	2.670	0.057	2.14%
70.1	3.389	3.488	3.597	3.491	0.104	2.97%

Table B.8 Calculations of non-linear least-square regression for disinfection data at

254 nm

Fluence (mJ cm ⁻²)	Average N ₀ /N of the three runs (Y)	Estimate (Ŷ)	Y - Ŷ	(Y - Ŷ) ²
0.0	1.00E+00	1.00E+00	0.00E+00	0.00E+00
5.8	8.10E-01	8.27E-01	-1.69E-02	2.86E-04
8.7	5.69E-01	5.57E-01	1.20E-02	1.45E-04
11.7	3.38E-01	3.25E-01	1.29E-02	1.66E-04
14.6	6.27E-02	9.12E-02	-2.85E-02	8.14E-04
17.5	1.71E-02	2.34E-02	-6.31E-03	3.98E-05
20.4	2.15E-03	1.47E-03	6.79E-04	4.61E-07
23.3	3.29E-04	9.15E-05	2.37E-04	5.62E-08
			sum	1.45E-03

$k = 0.069$
 $n_c = 6$

Table B.9 CFU enumeration of *B. subtilis* spores exposed to the UV light at 222 nm

	Fluence (mJ cm ⁻²)	Dilution	CFU counts			Geometric mean	<i>N</i> (CFU mL ⁻¹)	Log inactivation log(<i>N</i> ₀ / <i>N</i>)	<i>N</i> / <i>N</i> ₀
Run 1	0.0	10 ⁻⁴	286	292	302	293.3	2.93E+06	0.000	1.00E+00
	2.9	10 ⁻⁴	227	234	236	232.3	2.32E+06	0.101	7.92E-01
	8.7	10 ⁻⁴	81	107	92	92.7	9.27E+05	0.500	3.16E-01
	14.6	10 ⁻³	165	171	160	165.3	1.65E+05	1.249	5.63E-02
	20.4	10 ⁻³	42	38	41	40.3	4.03E+04	1.862	1.38E-02
	0.0	10 ⁻⁴	253	239	232	241.2	2.41E+06	0.000	1.00E+00
	5.8	10 ⁻⁴	153	146	142	146.9	1.47E+06	0.215	6.10E-01
	11.7	10 ⁻⁴	42	36	41	39.6	3.96E+05	0.784	1.64E-01
	17.5	10 ⁻³	65	62	54	60.1	6.01E+04	1.603	2.49E-02
	23.3	10 ⁻²	155	167	144	155.0	1.55E+04	2.192	6.43E-03
	35.0	10 ⁻²	29	39	26	30.9	3.09E+03	2.892	1.28E-03
	46.6	10 ⁻¹	145	155	152	150.6	1.51E+03	3.203	6.27E-04
	69.9	10 ⁻¹	64	62	74	66.5	6.65E+02	3.559	2.76E-04
	93.2	10 ⁰	240	251	257	249.2	2.49E+02	3.986	1.03E-04
Run 2	0.0	10 ⁻⁴	293	289	273	284.9	2.85E+06	0.000	1.00E+00
	2.9	10 ⁻⁴	249	225	253	242.0	2.42E+06	0.071	8.49E-01
	8.7	10 ⁻⁴	90	100	80	89.6	8.96E+05	0.503	3.14E-01
	14.6	10 ⁻³	187	192	173	183.8	1.84E+05	1.190	6.46E-02
	20.4	10 ⁻³	41	26	26	30.3	3.03E+04	1.973	1.06E-02
	0.0	10 ⁻⁴	252	263	275	263.2	2.63E+06	0.000	1.00E+00
	5.8	10 ⁻⁴	158	168	174	166.5	1.67E+06	0.197	6.35E-01
	11.7	10 ⁻⁴	39	46	50	44.8	4.48E+05	0.769	1.70E-01
	17.5	10 ⁻³	68	75	78	73.5	7.35E+04	1.554	2.79E-02
	23.3	10 ⁻²	93	93	108	97.8	9.78E+03	2.430	3.72E-03
	35.0	10 ⁻²	47	39	42	42.5	4.25E+03	2.792	1.62E-03
	46.6	10 ⁻¹	139	144	136	139.6	1.40E+03	3.274	5.32E-04
	69.9	10 ⁻¹	101	104	119	107.7	1.08E+03	3.387	4.11E-04
	93.2	10 ⁻¹	43	53	47	47.5	4.75E+02	3.743	1.81E-04
Run 3	0.0	10 ⁻⁴	275	291	298	287.8	2.88E+06	0.000	1.00E+00
	2.9	10 ⁻⁴	234	223	230	229.0	2.29E+06	0.100	7.95E-01
	5.8	10 ⁻⁴	165	163	139	155.2	1.55E+06	0.269	5.38E-01
	8.7	10 ⁻⁴	84	104	102	96.2	9.62E+05	0.476	3.34E-01
	11.7	10 ⁻⁴	34	40	41	38.2	3.82E+05	0.877	1.33E-01
	14.6	10 ⁻³	157	156	137	149.7	1.50E+05	1.283	5.21E-02
	17.5	10 ⁻³	83	94	81	85.8	8.58E+04	1.526	2.98E-02
	20.4	10 ⁻³	33	28	35	31.9	3.19E+04	1.956	1.11E-02
	23.3	10 ⁻²	128	114	137	126.0	1.26E+04	2.359	4.38E-03

35.0	10 ⁻²	52	53	46	50.2	5.02E+03	2.759	1.74E-03
46.6	10 ⁻¹	153	131	138	140.4	1.40E+03	3.313	4.86E-04
69.9	10 ⁻¹	71	96	77	80.7	8.07E+02	3.553	2.80E-04
93.2	10 ⁰	194	228	204	208.2	2.08E+02	4.141	7.22E-05

Overall analysis of the three runs

Fluence (mJ cm ⁻²)	Run 1 log(N ₀ /N)	Run 2 log(N ₀ /N)	Run 3 log(N ₀ /N)	Geometric mean of log(N ₀ /N)	Std dev	Percentage error
2.9	0.101	0.071	0.100	0.091	0.017	18.78%
5.8	0.215	0.197	0.269	0.227	0.037	16.50%
8.7	0.500	0.503	0.476	0.493	0.014	2.94%
11.7	0.784	0.769	0.877	0.810	0.059	7.25%
14.6	1.249	1.190	1.283	1.241	0.047	3.80%
17.5	1.603	1.554	1.526	1.561	0.039	2.51%
20.4	1.862	1.973	1.956	1.930	0.060	3.11%
23.3	2.192	2.430	2.359	2.327	0.122	5.25%
35.0	2.892	2.792	2.759	2.814	0.069	2.47%
46.6	3.203	3.274	3.313	3.263	0.056	1.71%
69.9	3.559	3.387	3.553	3.499	0.098	2.80%
93.2	3.986	3.743	4.141	3.957	0.201	5.07%

Table B.10 Calculations of non-linear least-square regression for disinfection data at

222 nm

Fluence (mJ cm ⁻²)	Average N ₀ /N of the three runs (Y)	Estimate (Ŷ)	Y - Ŷ	(Y - Ŷ) ²
0.0	1.00E+00	1.00E+00	0.00E+00	0.00E+00
5.8	5.94E-01	5.98E-01	-3.75E-03	1.41E-05
8.7	3.22E-01	3.15E-01	6.10E-03	3.73E-05
11.7	1.56E-01	1.51E-01	4.95E-03	2.45E-05
14.6	5.77E-02	6.90E-02	-1.14E-02	1.30E-04
17.5	2.76E-02	3.10E-02	-3.45E-03	1.19E-05
20.4	1.18E-02	1.38E-02	-1.99E-03	3.95E-06
23.3	4.84E-03	6.13E-03	-1.29E-03	1.65E-06
			sum	2.23E-04

$k = 0.122$
 $n_c = 4$

